

April 2021

Mechanical Design and Analysis: High-Precision Microcontact Printhead for Roll-to-Roll Printing of Flexible Electronics

Mehdi Riza
University of Massachusetts Amherst

Follow this and additional works at: https://scholarworks.umass.edu/masters_theses_2



Part of the [Manufacturing Commons](#)

Recommended Citation

Riza, Mehdi, "Mechanical Design and Analysis: High-Precision Microcontact Printhead for Roll-to-Roll Printing of Flexible Electronics" (2021). *Masters Theses*. 1022.
<https://doi.org/10.7275/20198295> https://scholarworks.umass.edu/masters_theses_2/1022

This Open Access Thesis is brought to you for free and open access by the Dissertations and Theses at ScholarWorks@UMass Amherst. It has been accepted for inclusion in Masters Theses by an authorized administrator of ScholarWorks@UMass Amherst. For more information, please contact scholarworks@library.umass.edu.

*Mechanical Design & Analysis:
High-Precision Microcontact Printhead
for Roll-to-Roll Printing of Flexible
Electronics*

A THESIS PRESENTED
BY
MEHDI N. RIZA

FEBRUARY 2021

Submitted to The Graduate School of The
University of Massachusetts Amherst
In Partial Fulfillment of the Requirements for The Degree of

MASTER OF SCIENCE IN MECHANICAL ENGINEERING

Department of Mechanical and Industrial Engineering

© Copyright by Mehdi N. Riza 2021

All Rights Reserved

Mechanical Design & Analysis: High-Precision Microcontact Printhead for Roll-to-Roll Printing of Flexible Electronics

THESIS
BY
MEHDI N. RIZA

Approved by:

DocuSigned by:
Xian Du
454CC89855C64E1...

Dr. Xian Du, Chair

DocuSigned by:
Ian Grosse
CA05FF478397420...

Dr. Ian Grosse, Member

DocuSigned by:
Frank Sup
C7BB100453AC44B...

Dr. Frank Sup, Member

DocuSigned by:
Sundar Krishnamurthy
3F8496455D304DC...

Dr. Sundar Krishnamurthy,
Department Head
Department of Mechanical and Industrial Engineering
UMASS Amherst

Acknowledgements

I would like to thank my thesis supervisor Dr. Xian Du for giving me the opportunity to conduct research and mechanical design for the R2R system under development in the Intelligent Sensing Laboratory. Additionally, I would like to express gratitude to Dr. Du for providing a half Research Assistantship financial support. Likewise, the Department of Mechanical and Industrial Engineering is acknowledged for providing a half Teaching Assistant support for Spring 2020 semester. Further thank you to Dr. Ian Grosse and Dr. Frank Sup who have graciously found time to be on my thesis committee. The support from my fellow lab members Dr. Henry Yao and Mr. Jingyang Yan is greatly appreciated, as is the assistance from Mr. Richard Winn and Mr. Colby Norwood in the MIE building's machine workshop. This design would not have been possible without their contributions in fabricating several of the key components and supervising me while I worked on additional parts. During my undergraduate studies in Electrical & Electronic Engineering at University College Cork (UCC), Ireland, I was given funded research opportunities in mechanical design for optical and biomedical applications by faculty members Dr. Guangbo Hao and Dr. Pdraig Cantillon-Murphy, respectively. I thank both these UCC faculty members for their encouragements that allowed me to transition to the exciting field of mechanical engineering design. My stay in Amherst was made very enjoyable and fulfilling by Coach Rocky Snow, and I thank him for selecting me for the joint UMass/Westover ARB boxing team and having me compete in collegiate and club boxing tournaments at interesting locations around the US. Finally, I owe thanks to my family members in Cork, Ireland, for their encouragement and support, especially during the current COVID-19 pandemic uncertain times.

ABSTRACT

MECHANICAL DESIGN & ANALYSIS: HIGH PRECISION MICROCONTACT PRINthead FOR ROLL-TO-ROLL PRINTING OF FLEXIBLE ELECTRONICS

FEBRUARY 2021

MEHDI N. RIZA, B.E., UNIVERSITY COLLEGE CORK

M.S. M.E., UNIVERSITY OF MASSACHUSETTS AMHERST

Directed by: Professor Xian Du

Flexible electronics have demonstrated potential in a wide range of applications including wearable sensors, photovoltaics, medical devices and more, due to their properties of extreme adaptability while also being lightweight and highly robust. The main challenge standing in the way of progress in this field is the difficulty of large-scale manufacturing of these flexible electronics compared to their rigid counterparts. Microcontact printing is a form of soft lithography in which an elastomeric stamp is used to transfer sub-micron scale surface patterns onto a flexible substrate via ink monolayers. The integration of microcontact printing into a roll-to-roll (R2R) system will enable continuous printing of flexible electronics and scale it up for massive manufacturing.

The proposed thesis outlines a novel mechanical design for a microcontact printer which utilizes flexural motion stages with integrated position and force sensors to control the print process on a R2R system. The printhead is designed to fit the available space on the pre-installed UMass Amherst Intelligent Sensing Laboratory test table and breadboard. The R2R system includes motorized rollers for winding/unwinding the PET (polyethylene terephthalate) web substrate, and idler rollers for guiding a web through the print system. As the central element to this design, two matching plate flexures are designed on the two ends of the printer roller to control the tilting and positioning of the print roller. Flexure mechanisms rely on bending and torsion of flexible elements: this allows them to achieve much

higher precision in positioning compared to conventional mechanisms which rely on surface interaction between multiple moving parts. The print resolution target for this design is 500 nm (linewidth), based on current state-of-the-art designs [1, 2].

In the initial version of the printhead design, a total of 33 parts are custom fabricated for assembly and installation in the R2R system lab setup. These include everything from the components of the print roller, specially adapted air-bearing mounts, support structures, and connectors. The design and fabrication process for every component is outlined here along with the functionality, as every component was designed with the system objectives and constraints in mind. Using SolidWorks simulation, FEA (finite element analysis) is performed for every part of the assembly that is subjected to stress in the real system, so that predictions can be made about the displacement of the motion stages and the frequency of vibration. These predictions are evaluated by comparison with the experimental results from tests conducted on the real system hardware and used to assess the quality of the fabricated assembly.

The work performed in this thesis enables advancements in the assembly of an updated, optimized R2R system and has led to an experimentally functioning lab setup that is ripe for further improvements. Completion and calibration of this augmented R2R system will, in future, enable UMass Amherst in-house production of large-area flexible electronics which may be used in a wide range of applications, including medical sensors, solar cells, displays, and more. In addition to microcontact printing, this R2R system may also be applied to nanoimprint lithography, another contact-based print method, or integrated with inkjet printing, a non-contact method.

Table of Contents

Acknowledgements.....	iv
Abstract	v
List of Tables.....	ix
List of Figures.....	x
List of Abbreviations	xiv
1 INTRODUCTION	1
1.01 Motivation	1
1.02 Objectives in the Context of R2R System Requirements	2
2 BACKGROUND & PRIOR ART	5
2.01 Flexible Electronics in the World	5
2.02 Synopsis of Different Print Methods on Flexible Substrates	9
2.03 Related Projects in the Field	12
MIT projects 2008 - 2018.....	12
University of Hong Kong project 2015.....	14
2.04 Table of Pros & Cons of Past Design Approaches.....	16
3 DESIGN ENGINEERING	18
3.01 Design Objectives and Constraints	18
3.02 Advantages of Compliant Mechanisms	21
3.03 Basic Design Elements.....	23
3.04 Print & Impression Roller Design.....	25
3.05 Advanced 2 DOF Flexure Design	28
3.06 Actuation	32
3.07 Load Simulation & Calculations	34
4 COMPONENTS FABRICATION AND ASSEMBLY	38

4.01	Fabrication of Flexures	38
4.02	Roller Fabrication, Assembly, and Smoothing	39
4.03	Air Bearings for Frictionless Rotation	41
4.04	Assembly & Alignment of R2R Components	43
4.05	Actuator Setup & Linkages.....	47
4.06	Sensors for Precision Control	51
4.07	ASSEMBLY DRAWING WITH LABELLED COMPONENTS.....	54
5	EXPERIMENTAL TESTING AND RESULTS.....	56
5.01	R2R Setup in Lab.....	56
5.02	Dynamics Data from R2R Setup	57
5.03	Positioning & Force Control/Sensor Operation	59
5.04	Engineering Problems Encountered & Solutions	62
5.05	Work on PDMS stamp / Validation of Test Prints.....	65
6	IMPROVED DESIGN WORK	66
6.01	Optimized Flexure Assembly	66
6.02	Redesigned Lightweight & Transparent Rollers	70
6.03	Cylindrical PDMS Stamp Fabrication	71
7	CONCLUDING DISCUSSION	75
7.01.	Synopsis of Work/Accomplishments.....	75
7.02.	Unresolved Issues.....	75
7.03.	Conclusion	77
	References	79

List of Tables

Table 1. Overview of print methods that have been used to fabricate flexible electronics (part 1)	10
Table 2. Overview of print methods that have been used to fabricate flexible electronics (part 2)	11
Table 3. Visual summary of design innovations and drawbacks for the most significant projects, previously discussed	17
Table 4. List of all system components shown in Figure 39, with material info and fabrication tolerances provided.	55

List of Figures

Figure 1. Hand-drawing of a printed circuit in 1960. Early methods used stencils and a light board [5].....	1
Figure 2. Examples of commercial grade solar PV panels fabricated via inkjet printing [10].....	6
Figure 3. NASA–ISRO Synthetic Aperture Radar [14].....	7
Figure 4. A patient monitoring device which transmits blood pressure readings, etc. [18]	8
Figure 5. Design drawings from 2008 MIT Project by Adam Stagnaro [41].....	12
Figure 6. Visual explanation of self-assembly process of thiol ink on gold surface [41]	13
Figure 7. Flexures for microcontact print roller by the CUHK group; R2R setup shown right [1]	15
Figure 8. (a) PDMS stamp, bonded to glass cylinder; (b) Gold electrodes printed using the CUHK R2R printer; (c) SEM images of print results showing 300 nm linewidth [46]	16
Figure 9. Initial assembly of R2R setup in IALS Intelligent Sensing Lab [48]......	18
Figure 10. Axes of alignment for impression (1) and print (2) rollers.....	19
Figure 11. Simple visualization of mechanical backlash in a traditional geared mechanism	21
Figure 12. Comparison of a normal stapler with one built using compliant mechanisms [53]	22
Figure 13. DOFs and Degree of Constraint (DOC) for the desired print roller control mechanism.....	23
Figure 14. Illustration of stiffness in two types of parallelogram (a.k.a P-joint) flexure mechanisms	24
Figure 15. SolidWorks drawings of the printhead roller assemblies, showing outer diameters.....	25
Figure 16. CAD model of pre-built speed encoder	26
Figure 17. Bisymmetrical 2 DOF flexure with highlighted elements	28
Figure 18. How to calculate stiffness in 3 DOFs for simple sheet flexure.....	29
Figure 19. An early design concept for the flexure positioning stage, showing the print roller and air bearing connection.	30
Figure 20. First prototype of new 2 DOF flexure design, showing three different views.....	31

Figure 21. Specifications and diagram of the two H2W actuators (dimensions given in mm and in). Red – larger actuator; blue – smaller actuator. Source company: H2W Technologies.	33
Figure 22. Mesh used for FEA of the flexure prototype mechanism.	34
Figure 23. Five modes of vibration for the flexure. Modes (1) and (2) are intended DOFs of the mechanism.	35
Figure 24. FEA result showing three modes of vibration of print roller system; ROM exaggerated.	37
Figure 25. Print and impression roller parts prior to completion.	41
Figure 26. Technical drawing of the air bushing. Dimensions in inches. Source company: New Way Air Bearings.	42
Figure 27. CAD drawing of custom mount designed to house the air bushing for the print roller.	42
Figure 28. Brass air fittings and T-connectors ordered from same company.	43
Figure 29. SolidWorks 3D model of the entire R2R assembly, minus the PDMS stamp.	44
Figure 30. RollCheck® MINI devices for alignment of rollers. Each device is mounted using elastic belts. Source company: Seiffert Industrial. [56]	45
Figure 31. Impression roller frame assembly.	46
Figure 32. Horizontal actuator mount & connection.	47
Figure 33. Aluminum plates designed to connect large VCA to table breadboard.	48
Figure 34. The two pieces of the vertical VCA and motion stage connection assembly.	49
Figure 35. Capacitive sensor probe with 6 mm detection range. Source company: Micro-Epsilon America, LP.	51
Figure 36. Sliding clamp mounts for the vertical (left) and horizontal (right) capacitive sensors.	52
Figure 37. View of the printhead mechanism showing vertical capacitive sensor position (sensor is circled).	53

Figure 38. Load cell for tension measurement, featuring flanged shaft connection. Source company: MAGPOWR. Model: TS-25-FC EC12.	53
Figure 39. Assembly drawing of R2R system, components labelled below.....	54
Figure 40. Microcontact printhead design (left) and real setup (right) but without vertical actuators, encoder, or web.....	56
Figure 41. R2R setup in action: running web tension experiment. Note that lower right idler roller has been swapped for tension measuring roller.....	57
Figure 42. Vibration experiments on single flexure mechanism.	58
Figure 43. Circuit model and equations for the VCA.	60
Figure 44. Simplified model of the print roller mechanism. The purple text indicates the force generated by the VCAs.....	61
Figure 45. Plots from load cell calibration experiment. Tables display force data from both sides' VCAs.61	
Figure 46. SolidWorks drawing of unused asset – roller alignment post.	63
Figure 47. Sketch of improved mount for small VCA.....	64
Figure 48. Compression testing procedure for PDMS stamp pieces (cut from larger stamp).....	65
Figure 49. Method for applying force to a parallelogram joint with minimal parasitic rotation. [59].....	66
Figure 50. New flexure design, 2 pieces, polycarbonate	67
Figure 51. FEA simulated actuation force resulting in translation in horizontal and vertical DOFs.	68
Figure 52. New printhead mechanism assembly design, front and back, featuring capacitive sensors and VCA connectors built into mechanism. Nuts/bolts omitted from drawing.	69
Figure 53. Same scale comparison between versions of printhead mechanism, including actuation and sensing components.	69
Figure 54. Desired cylindrical PDMS stamp with outward facing pattern.....	71

Figure 55. Diagram showing fabrication of patterned master cylinder, which is used in the mold to create a PDMS stamp of uniform thickness..... 72

Figure 56. Sketch from notes about idea for reversing/unwrapping PDMS stamp..... 73

Figure 57. Alternative method of using the R2R system to invert the stamp from the master. 74

List of Abbreviations

3D	3 Dimensional
CAD	Computer Aided Design
CNC	Computer Numerical Control (machining method)
DOC	Degree of Constraint
DOF	Degree of Freedom
FEA	Finite Element Analysis
IALS	Institute for Applied Life Sciences
IC	Integrated Circuits
μ CP	Microcontact Printing
MEMS	Micro-electromechanical systems
MIT	Massachusetts Institute of Technology
NIL	Nanoimprint Lithography
OD	Outer diameter (referring to tube structure)
PCB	Printed Circuit Board
PDMS	Polydimethylsiloxane (soft polymer)
PET	Polyethylene terephthalate (thermoplastic polymer)
PHM	Personalized Health Monitoring
PV	Photovoltaic
R2R	Roll-to-roll
ROM	Range of Motion
SAM	Self-assembled monolayer
UMass Amherst	University of Massachusetts at Amherst
VCA	Voice Coil Actuator

1.01 Motivation

Ever since its invention in 1936, the Printed Circuit Board (PCB) has been constantly evolving in its mechanical properties and means of fabrication [3]. From the early days of through-hole design followed by the development of surface-mount technology and other advanced lithographic production methods, each evolution has greatly improved the versatility and manufacturability of these devices [4]. Given that the PCB is the centerpiece of all consumer electronics, it goes without saying that efforts to manufacture this technology in versions that are more adaptable to fit all kinds of environments will be highly profitable and pave the way for groundbreaking innovations/devices in a wide range of fields.

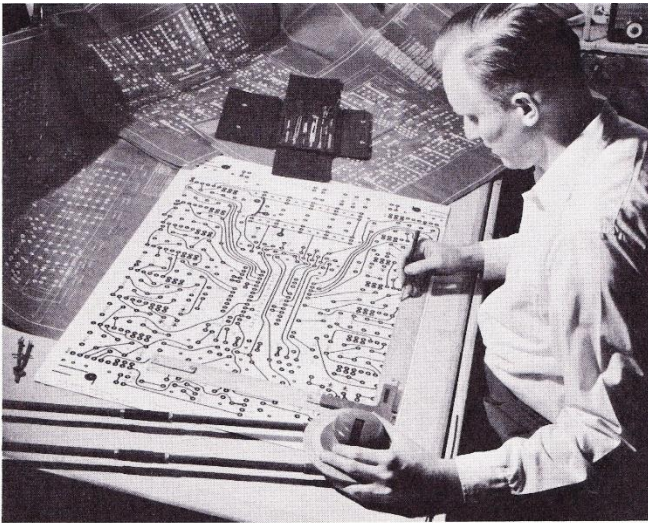


Figure 1. Hand-drawing of a printed circuit in 1960. Early methods used stencils and a light board [5]

Flexible electronics, an area of study originating soon after the introduction of the first PCBs, is currently among the fastest growing research areas in global technology. This term refers to circuits that have been mounted onto flexible substrates, allowing them to be contorted and wrapped around different shapes while maintaining functionality. One can imagine the numerous advantages of having

elastic electronic structures, as such designs would not only be adaptable but lightweight and highly robust as well. Examples of successful implementation of these flex circuits can be found in cameras, automobiles, satellites, and numerous other applications for which flexibility and/or space are constraints. The main challenge standing in the way of progress in this field is the high cost and difficulty of large-scale manufacturing of these flexible electronics compared to standard ones. [6, 7]

Due to the compliance requirement of the substrate, flexible electronics cannot be fabricated via conventional means used to manufacture integrated circuits on semiconductor substrates. However, they can be “printed” onto the desired material surface via precise application of conductive ink. This can be accomplished using contact or non-contact methods depending on the desired application, as will be described in the *Background & Prior Art* chapter of this report. The aim of this project is to build and test a functional roll-to-roll (R2R) machine capable of high-precision, large area, microcontact printing (μ CP) of flexible electronics.

1.02 Objectives in the Context of R2R System Requirements

As one might imagine, constructing a complete R2R system for μ CP is a complex and multifaceted task. It involves high-accuracy sensing, actuation, closed-loop control, precision design & fabrication, and real-time monitoring. In keeping with the author’s area of study, this thesis will primarily be focusing on the mechanical aspects of R2R system design. The most cutting-edge methods of precision engineering shall be applied in the mechanical design of this system and its specific components to achieve the desired high-accuracy results.

The primary task of this thesis is designing the microcontact *printhead* of the system. This is the component that imprints the desired ink micropattern onto the flexible substrate – it does this via direct

application of a precisely defined contact force between the stamp and the web. The stamp, also made from an elastomeric material, is generated using a mold so that the desired micropattern is already on its surface. Accurate alignment of the stamp with the web is crucial to successful printing.

Listed, the thesis objectives for the finalized design are as follows:

- 1)** The printhead must be compatible with the current lab setup. This includes a 24"×36" (surface area) granite table which is mounted on an adjustable 28" tall support frame which contains room for electrical connections, air pumps, controllers, linear amplifiers, and supplementary equipment. On top of the table is a vertically standing steel backboard 36"×36", which has a grid pattern of ¼" diameter through holes (for attachments), sixteen 4" diameter through holes for larger mounts, and a steel supporting frame. Two idler(passive) rollers and two motorized rollers are already connected to the backboard and will serve as key components of the completed R2R system. Therefore, the printhead should be mounted on the table and interface with the web and the pre-installed rollers.
- 2)** Printhead and stamp must be capable of large area printing. Generally, the definition of "large area" is relative to the scale (linewidth) of the pattern being generated. In device fabrication, this term is used to contrast with the area-minimizing technology of integrated Si chips. Typical large-area device applications are photovoltaics and medical sensor arrays [8]. In this thesis, large area will be defined by the ability to print onto a 4.0" wide PET (polyethylene terephthalate) web which is compatible with the pre-installed roller setup.
- 3)** The printing force, also referred to as the contact force, must be controlled so that its variation during the print process stays within a specific tolerance range. Too little force and there will be insufficient ink transfer to the substrate; too much force and the elastic micropattern on the

stamp will collapse. Feedback control should be used to maintain the contact force in the acceptable region. The precise level of contact force control that is desired for this microcontact print system is based on the results from previous research studies by MIT and the Chinese University of Hong Kong (CUHK). This is discussed in further detail in *Chapter 4.06 – Sensors for Precision Control* about the systems sensing components.

- 4) The microcontact printhead must be designed for minimal assembly. This will reduce the amount of calibration necessary, facilitate (re)construction of the design, and improve repeatability of performance. A versatile design that relies on uncluttered assemblies, robust mechanisms and structures may be easily replicated/implemented in other laboratories and provide consistent results.

These objectives are outlined in detail in *Chapter 3.01 – Design Objectives and Constraints* of this document, where it is explained how these initial parameters are used to plan the design of the printhead mechanisms and assembly.

2.01 Flexible Electronics in the World

Consider the ubiquity of electronic circuitry in the modern industrialized world. The rapid miniaturization of transistors and other key components (see Moore's Law: source [9]) has enabled the development of increasingly complex electronics. Now consider that less than 30 years ago, much of the electronics available today would have been impossible even to manufacture due to the limitations in semiconductor device fabrication; even though many of the concepts had already been envisioned as early as 1965 [9].

Currently the world is entering a new, similar phase with flexible electronics. As new methods of advanced fabrication are developed and improved, large-scale printing of ICs (integrated circuits) on elastomeric substrates will make flexible electronics common and affordable in the global market [6, 7]. The following paragraphs present some of the key areas in which there is the greatest potential for flexible electronics to make a large contribution.

With the global push towards clean energy, solar radiation has been identified as the most energy-dense renewable resource and the most promising for fulfilling growing demands for electricity. Photovoltaic (PV) cells directly convert this radiation into electricity; and the cost to manufacture and install PV panels on buildings, vehicles, and other fixtures has been steadily decreasing due to advances in technology. If PV panels can be successfully incorporated onto flexible thin films, then this opens a whole host of new applications for the technology. [10, 11, 12]

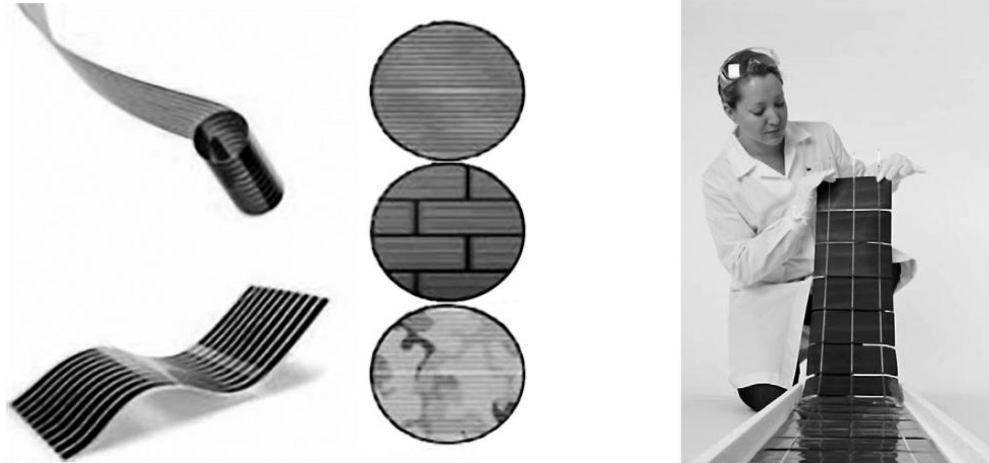


Figure 2. Examples of commercial grade solar PV panels fabricated via inkjet printing [10]

Flexible PV cells could be integrated into fabrics on buildings, clothing, tents, sails, glass, etc. Significant progress has already been made in developing these devices experimentally using inkjet and R2R printing, as is shown in Figure 2 [12, 11]. As these modules become commercially available worldwide, it is speculated that the cost of solar electricity will go down and PV generated power will finally be competitive with coal-fired electricity. [10]

Space exploration is another field in which there is great interest in manufacturing large area flexible electronics [13]. On spacecraft there are many types of externally deployed electronic structures including telescopes, radar, solar sails (relevant to previous point), and balloon-like reflectors. It is desirable for these structures to be kept as lightweight and large-area as possible, which means that flexible electronics have a large advantage over conventional metallic constructions. These mechanisms also require the ability to fold up for storage and fold out for large-area deployment; which is another obvious reason why flexible electronics would be preferential to rigidly constructed apparatus [13]. The following image, Figure 3, shows a NASA-ISRO (joint US and India) satellite with synthetic aperture radar deployed, showing how a thin membrane can be expanded to encompass a greater surface area than the carrier module [14].

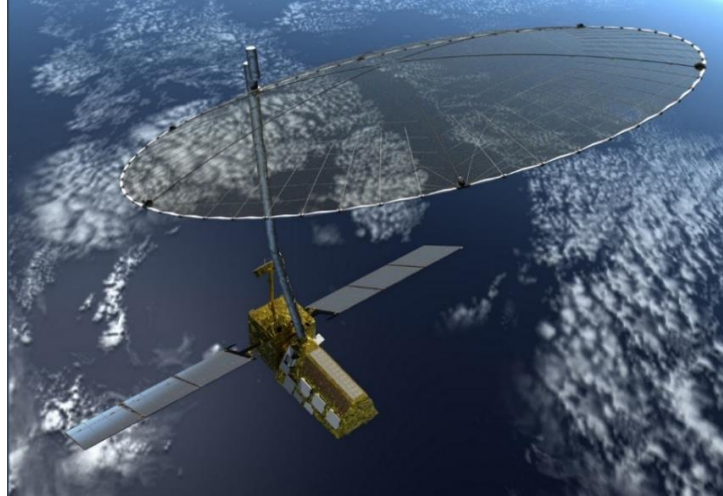


Figure 3. NASA-ISRO Synthetic Aperture Radar [14]

Flexible polymeric membranes can be deployed via inflation, thermal expansion, and rigidizing, which gives more options for control and reduces the complexity of the assembly. The difficulties with this kind of technology are related to the high robustness and reliability requirements for the sensors and the thin membrane, along with the difficulty in fabrication of the large area structures. [13]

Lastly, and most relevant to the research in Life Science Laboratories at UMass Amherst, is the area of wearable electronic devices. Eyeglasses and ear-trumpets (archaic hearing aids) are excellent examples of time-tested, highly functional wearable devices that have aided humans for centuries. Founded on simple material properties and ergonomic principles, these devices are examples of passive technological aids that greatly enhanced the quality of life of the wearer while minimizing obstruction into daily activities. In recent years, the development of new additive manufacturing methods, especially R2R flexible electronics printing technologies, and the miniaturization of computational platforms have unlocked the potential for wearable medical technology that fulfills considerably more advanced functions.

Researchers and engineers around the world have already developed prototypes of different wearable electronic devices which incorporate sensors, microfluidics, and even haptic feedback for

personalized user applications. As with any emergent technology, developing intelligent fabrication methods is essential to reduce the cost of these products and maximize the accessibility to the public. R2R allows large-scale manufacturing of these and other kinds of flexible wearable devices [15, 16, 17].



Figure 4. A patient monitoring device which transmits blood pressure readings, etc. [18]

Among the primary applications of wearable electronics is Personalized Health Monitoring (PHM) [18, 19]. PHM is a growing field in the medical community that is intended to address the needs of patients requiring regular monitoring of biodata from a distance. Successful efforts have been made in recent years to solve this problem using wearable electronic sensors/devices. The most effective designs utilize flexible electronics: sensor arrays mounted on polymer substrates that can be wrapped on the skin. This differentiates them from the bulky, unwieldy designs such as the one shown in Figure 4.

Wearable devices can be of immense help in PHM applications, ranging from the vitals monitoring of patients, hospital/home care treatment, and even providing functions that improve the daily lives of individual wearers. Given the current COVID-19 pandemic with social distancing regulations and the elderly finding themselves cocooning and in isolation, such wearable health monitoring devices have taken on a new sense of urgency. To increase the portability of these devices and make them self-sustained, there have even been efforts in self-powering these wearable devices using integrated

photovoltaics [20, 21] or triboelectric processes [22, 23]. The latter refers to a form of contact electrification resulting from – in this case – friction between sheets of different materials.

While flexible designs are immensely useful due to their inherent advantages in conformability, comfort, and lightweight structures, the challenge lies in finding effective ways to manufacture these devices on a mass scale. As stated in the introduction of this paper, R2R printing promises high-throughput, high-fidelity fabrication via multiple different methods of imprinting conductive patterns on the substrate. The following section will summarize the most effective print methods, along with their respective advantages and disadvantages.

2.02 Synopsis of Different Print Methods on Flexible Substrates

While the work in this thesis is focused specifically on designing a microcontact printer (μ CP) on R2R, it is important for the reader to keep in mind that μ CP is only one of several viable approaches for ink pattern deposition on flexible substrates. Table 1 and Table 2 have been provided on the following pages to summarize the key points of each approach. Note that all the methods listed here have proven to be implementable on R2R systems, albeit with varying degrees of compatibility. [24]

		PRINT METHODS	
		Non-contact Deposition	Screen Printing
MECHANISM		<p>Non-contact methods: rely on deposition of conductive ink droplets/particles onto substrate to form desired pattern/circuit. The key design approaches are outlined here, including inkjet, laser direct writing, and aerosol. These differ in their means of depositing the ink particles, as shown below.</p>	<p>Screen printing relies on ink transmission through a form of stencil. This is typically a plate with a screen mesh and a mask to control the pattern. Mask/stencil are low cost fabrics or stainless-steel mesh.</p>
DIAGRAM		<p>The diagram shows three non-contact deposition methods: 1. Laser Direct Writing: A red cone labeled 'Transfer Laser' is directed at a 'Thin source film' on a 'Transparent carrier', which is positioned above a 'Receiving substrate'. 2. Aerosol printing: A container of ink is shown with 'Gas' entering from the sides, creating a spray of ink particles that fall onto a 'Substrate'. 3. Inkjet printing: A 'Piezo Crystal' is shown driving ink droplets onto a 'Substrate'.</p>	<p>The diagram illustrates the screen printing process. It shows a 'Mask' and 'Ink' being pushed through a screen by a 'Squeegee'. The 'Squeegee angle' and 'Clearance' between the squeegee and the screen are indicated. The ink is deposited onto a 'Substrate'.</p>
ADVANTAGES		<p>Versatile choice of inks/substrates; can print on top of prefabricated flexible circuits – good for layered device design; reconfigurable print pattern (versus having to fabricate a new stamp or mask). Possible to integrate inkjet into R2R system. If conductive inks are used, wet-etching step is unnecessary.</p>	<p>Mask and screen are easily scaleable to large area; capable of low-temperature processing – this reduces the cost greatly; The transparent mask allows easy alignment on the substrate.</p>
DRAWBACKS		<p>Lower throughput (slower) compared to contact-based methods; energy inefficient; high temperatures involved.</p> <p>Resolution is limited by droplet size – advanced systems are more costly and use more energy.</p>	<p>Lower resolution patterns compared to lithography, etc. – limited by screen mesh; ink residue must be cleaned at intervals.</p> <p>Speed/throughput is comparable to inkjet, less than lithography/gravure/flexography.</p>
REFS		[16, 17, 25, 12, 24, 26], drawings: [24]	[27, 28, 29, 11, 30, 31], drawings: [28]

Table 1. Overview of print methods that have been used to fabricate flexible electronics (part 1)

		PRINT METHODS		
		Soft Lithography (μ CP, NIL)	Gravure	Flexography
MECHANISM		Soft lithographic techniques use pre-patterned elastomeric stamps that are wetted with alkanethiol ink. The ink pattern is transferred onto the substrate through contact/compression. Includes μ CP and nanoimprint lithography (NIL), which are two different contact-based print methods.	R2R method: ink is applied directly to an engraved (gravure) cylinder and is then transferred to the substrate web via contact, backed by an impression roller.	Inverse mechanism to gravure – prints out negative pattern. Ink from the ink bath is collected by a cylinder called the anilox roller. From the anilox roller, a patterned flexible relief plate is used to transfer ink to the substrate, instead of using an engraved cylinder.
DIAGRAM				
ADVANTAGES		Bulk-scaling potential using R2R system; potentially very high speed in ft/s; print resolution very high (sub- μ m possible with NIL); energy efficient process.	High throughput using R2R; High resolution (10s of μ m); very high precision for ink thickness (μ m) due to doctoring.	More versatile material options for substrate and ink than gravure (e.g. CNT ink); R2R compatible with high throughput.
DRAWBACKS		Requires complex feedback control system to manage print forces and alignment at the microscale. Limited ink material choices for wetting PDMS stamp (alkanethiols). Development and wrap up of cylindrical stamp for R2R is a challenge.	High initial cost and lead time for setting up gravure cylinder, which also requires replacement. Limited substrate options – works better for porous substrates.	Limitations for large area of high-throughput flexo-plate; nanoporous stamps are difficult to fabricate. Halo effect (patterns with excessive ink) commonly observed due to compression of plate, limiting resolution.
REFS		[15, 16, 32, 33, 34, 35, 36], drawings: [35]	[29, 37, 31, 38], drawings: [38]	[39, 37, 24, 40], drawings: [40]

Table 2. Overview of print methods that have been used to fabricate flexible electronics (part 2)

2.03 Related Projects in the Field

MIT projects 2008 - 2018

Researchers at the Massachusetts Institute of Technology (MIT) have done pioneering work on realizing effective microcontact printing via roll-to-roll since 2008. The first of these projects, done by a team supervised by Dr. David E. Hardt, successfully demonstrated the capability of a very high throughput prototype R2R machine employing μ CP. Their machine was able to print at 400 feet per minute while maintaining high quality: the coefficient of variance for their printed sample patterns was approximately 0.5%, and the pattern resolution was within 66 μ m. The schematic and CAD drawing of their print mechanism is shown below. [41, 42]

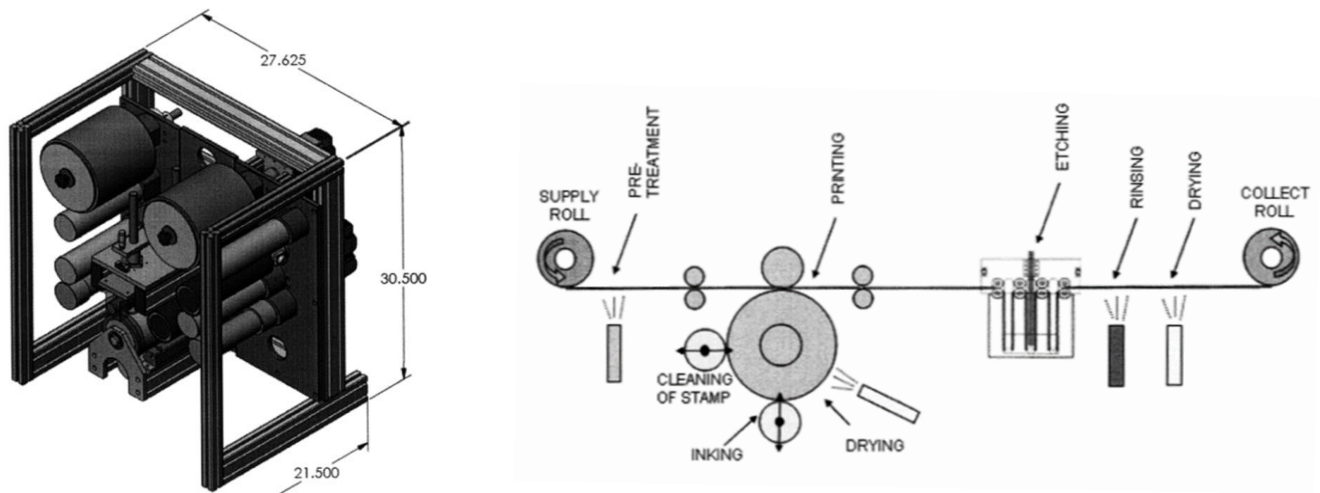


Figure 5. Design drawings from 2008 MIT Project by Adam Stagnaro [41]

As shown in Figure 5, the two large rollers are for wrapping/unwrapping while the remaining rollers are used for web guidance. The printhead did not use actuation for controlling the print pressure or positional alignment. However, the design has a limitation in that it could only be used to print octadecanethiols (an organic ink) onto gold coated substrates. The thiol ink reacts with the gold substrate to create a partially hydrophobic, partially hydrophilic coating – this is called a self-assembled monolayer

(SAM) – that resists wet etching. When etchants are applied to the web in a later stage of the R2R process, the gold pattern underneath the SAM are protected while the remainder is removed. [36, 1, 41]

The self-assembly characteristics of this inking process means that a uniform pattern (deviation of less than 100 μm) may be generated on the gold surface without requiring precise control of the contact pressure (see Figure 6). This phenomenon – resulting from molecular processes – is highly useful for ensuring print pattern quality, but it has no effect when other print media are used. However, the use of gold-coated PET substrates and alkanethiol inks is conventionally used for μCP due to these inks' absorption compatibility with the elastomeric PDMS stamps [36].

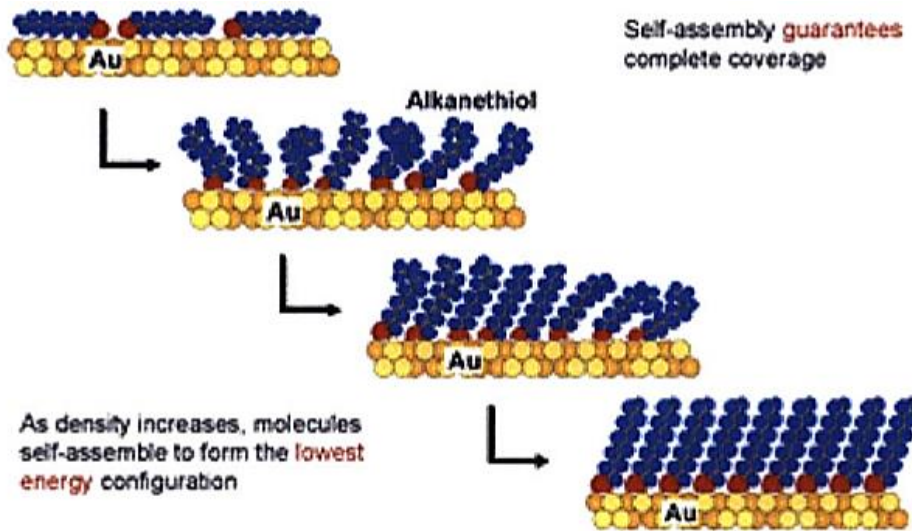


Figure 6. Visual explanation of self-assembly process of thiol ink on gold surface [41]

The 2008 MIT group's design yielded impressive results: high speed (400 feet/min) and satisfactory print quality (66 μm) on the flexible gold-PET substrate. Over the next 10 years, subsequent groups from the same lab (under supervision of Dr. David E. Hardt) aimed to improve on this system's print quality and design flexibility [42, 35, 43, 44, 45, 2]. In the process, the R2R system at MIT was redesigned three times, incorporating more sensors and actuation. Although these projects were not without performance issues and limitations, the work done by these groups is extensive as it includes

hardware design, open-loop control schemes, analysis of stamp microfeature behavior, continuous inking systems, fabrication of cylindrical PDMS stamp, and discussion of many other complex design problems.

These designs from MIT have had an important influence on the ongoing R2R system work in the Intelligent Sensing Laboratory at UMass Amherst supervised by Dr. Xian Du – especially given Dr. Du’s MIT-Singapore Alliance PhD degree and further MIT postdoctoral background. Although the scope of this thesis is limited to the mechanical design and fabrication concerns of μ CP printing on R2R, further references to the MIT project designs (particularly those by Libert [45] and Bageant [2]) are made in *Chapter 3: Design Engineering*. In addition, the inspiration in this thesis for the idea to generate a cylindrical PDMS stamp comes from the project by Petrzelka [35], although a novel technique is proposed for the stamp fabrication method (see *Chapter 6.03*).

University of Hong Kong project 2015

In 2015, a group of researchers from the Chinese University of Hong Kong (CUHK) conducted a project with the goal of developing a R2R microcontact printer capable of generating sub-micrometer resolution patterns on gold-coated PET substrate. This project was running concurrently with some of the later (earlier-discussed) MIT work, and the CUHK researchers were influenced by the results of those projects. In turn, the CUHK project had an influence on the mechanical design of the system proposed in this thesis. [1, 46]

The printer designed by the CUHK group consists of a motorized unwinding/rewinding module, web guide mechanism, and a core positioning stage which precisely controls the print roller. The web guide mechanism is set up as a series of idler rollers which constrain the web and keep it aligned laterally (shown in Figure 7). The most unique aspect of this design is the positioning stage: this is made up of two parallel plate flexures, each one connected to the ends of the print roller shaft via air bushings. This

configuration is reminiscent of the 2012 MIT design by Petrezelka [35], however the flexures used here are more complex and have an extra degree of freedom (each allows motion in two dimensions). Using these flexure mechanisms – along with actuation, sensory feedback, and web tension control – enables precise real-time active control of the contact (print) pressure and alignment. [46]

Flexures, also known as compliant mechanisms, utilize the inherent elasticity of certain materials and structures to transmit force/movement over short ranges with nanometer-scale repeatability [47]. As these are an important design feature, the properties of these mechanisms will be further explored in *Chapter 3*. The 2 DOF (degree of freedom) flexures used by the CUHK designers are shown here, in Figure 7. Flexures for microcontact print roller by the CUHK group; R2R setup shown right Figure 7.

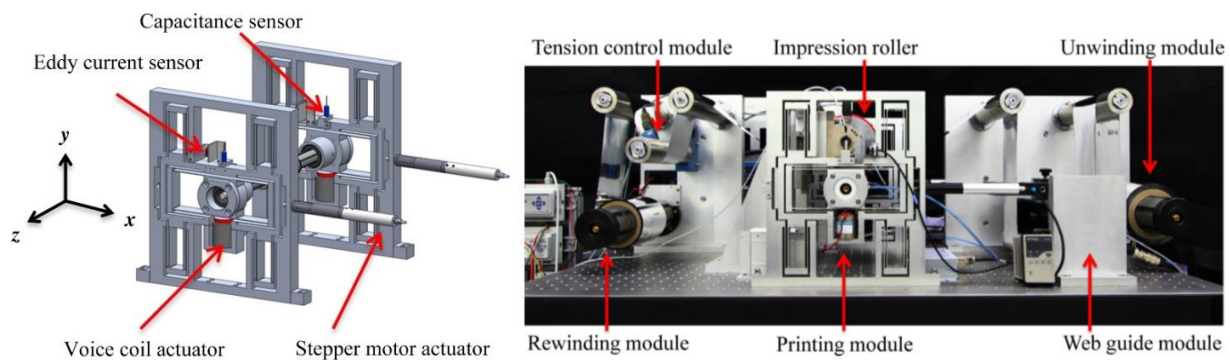


Figure 7. Flexures for microcontact print roller by the CUHK group; R2R setup shown right [1]

With the aid of cascaded and motion decoupled control, the CUHK microcontact R2R printer was able to achieve extraordinary printing results, surpassing those of previously developed designs. The reported precision is ± 200 nm motion control and ± 0.05 N contact force control, measured using feedback from capacitive displacement sensors and load cells, respectively. The resolution of the printer, as demonstrated by test prints (see Figure 8), is estimated at ~ 100 nm. [1, 46]

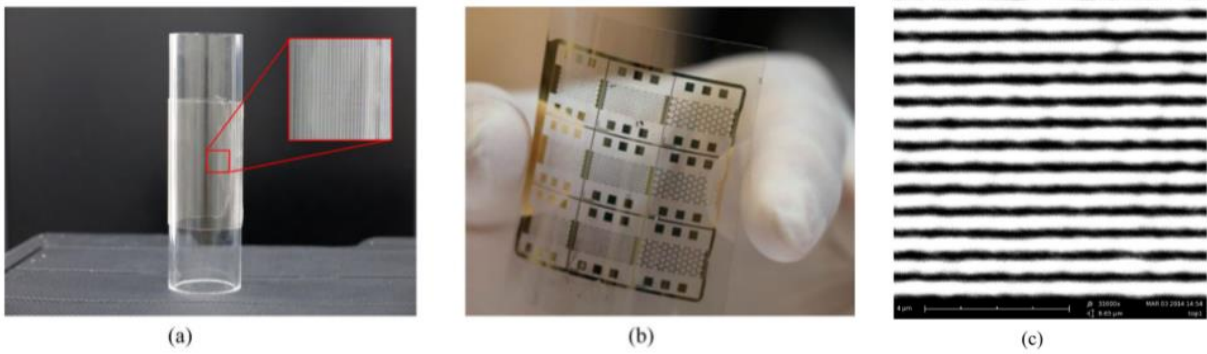


Figure 8. (a) PDMS stamp, bonded to glass cylinder; (b) Gold electrodes printed using the CUHK R2R printer; (c) SEM images of print results showing 300 nm linewidth [46]

2.04 Table of Pros & Cons of Past Design Approaches

	INNOVATIONS	SHORTCOMINGS	IMAGE OF EXPERIMENTAL SET-UP
2008 MIT design by Stagnaro	<ul style="list-style-type: none"> + Successfully adapted μCP to R2R system. + Very high speed (8 inches per second). + Achieved patterning of etch-resistant SAM with 66 μm resolution; though not continuous 	<ul style="list-style-type: none"> – No control of contact pressure between stamp and substrate. – Difficulties with accurate stamp alignment. – Problem with air trapping when running at high speeds. 	<p>A photograph of a roll-to-roll printing machine with two large white rollers and a central printing mechanism, mounted on a metal frame.</p>
2012 MIT design by Petrzelka	<ul style="list-style-type: none"> + Flexural bearing allows precisely repeatable vertical motion of print roller. + Air bushings ensure frictionless rotation of print roller 	<ul style="list-style-type: none"> – Limited motion range and degrees of freedom for print roller mechanism – Can only compensate for errors with very long spatial wavelengths 	<p>A photograph of a more complex roll-to-roll printing machine with multiple rollers and a central printing mechanism, with a 100 mm scale bar in the top left corner.</p>

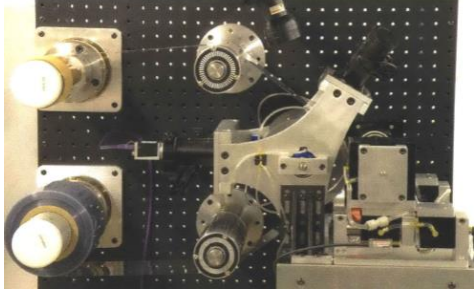
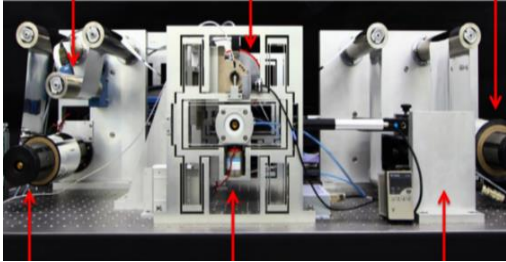
<p>2014 MIT design by Libert</p>	<ul style="list-style-type: none"> + Glass impression roller and camera setup allows real-time monitoring of prints. + Real-time visual feedback factors into control scheme. 	<ul style="list-style-type: none"> – Control not optimized for system dynamics, including inertia of rollers, etc. – Lacks displacement sensors for positioning control: these may aid print resolution more so than visual feedback. 	
<p>2015 CUHK precision flexure-based design</p>	<ul style="list-style-type: none"> + Setup isolated from ground vibrations of >40 nm using table. + Combines feedback from web tension, contact force, and positioning sensors. + Uniform contact force control within ± 0.05 N 	<ul style="list-style-type: none"> – Design lacks continuous inking module; the stamp must be removed and replenished with ink every few days. – Small area stamp (print roller diameter 1.0") has limited usefulness in printing of complex micro circuitry. 	

Table 3. Visual summary of design innovations and drawbacks for the most significant projects, previously discussed

3.01 Design Objectives and Constraints

The objectives for this microcontact printhead design have been outlined previously in *Chapter 1.02*. To recap, the design must be (1) compatible with the current Intelligent Sensing Lab R2R setup, (2) suited for continuous large-area printing, (3) capable of controlling the contact force and position, and (4) designed for minimal assembly. Out of these, point (1) is the most stringent requirement. From the beginning of the project, any design that could not adhere to the spatial, geometric, or equipment constraints of the pre-installed lab table had to be immediately discarded.

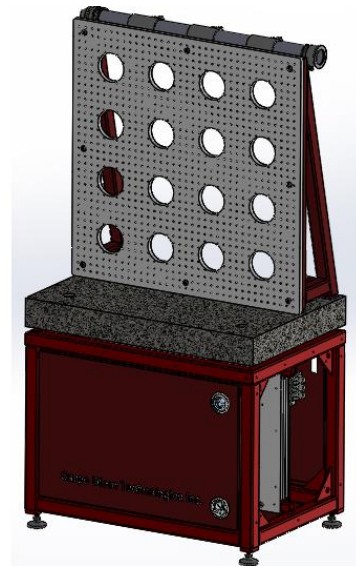
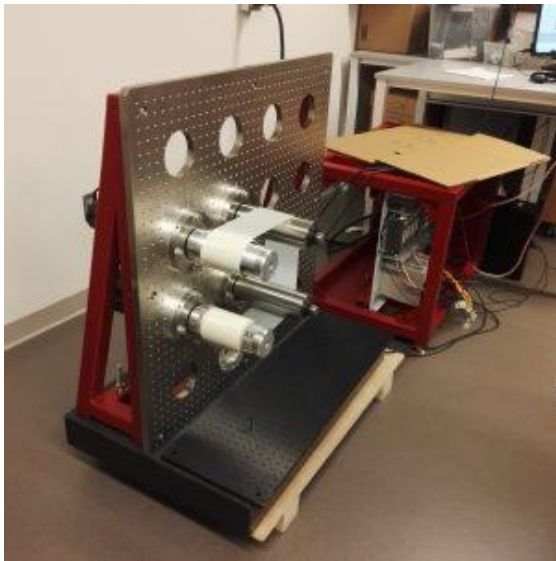


Figure 9. Initial assembly of R2R setup in IALS Intelligent Sensing Lab [48]. Frame components supplied by Carpe Diem Technologies, Inc. CAD model shown on the right.

The initial R2R setup was installed in Summer 2018 before the beginning of this thesis work. Significant elements include a smooth granite block measuring 36"×24"×4" on which is placed two aluminum breadboards for attaching the R2R components. The standing breadboard measures 36"×36"×0.75" and is primarily used for mounting the rollers, hence the sixteen large diameter holes. The lower breadboard measuring 36"×12"×0.25" is mounted to the granite block via precise threaded

connections. It is this component that imposes the tightest restrictions on the printhead assembly as it constrains the width of the print roller system (including the end-control mechanisms) to no more than 12 inches, the width of the bottom breadboard. As an additional constraint, the pre-installed rollers on the standing breadboard must align well with the printhead setup on the table.

The microcontact printhead operates by compressing the ink coated PDMS stamp against the PET web substrate. Recall the details of this process from *Chapter 2.02 – Synopsis of Different Print Methods on Flexible Substrates*. To accomplish this in a continuously running R2R system, the stamp support and the backing structures must be cylindrical in shape and rotationally mobile – these are known as the *Print Roller* and *Impression Roller*, respectively. These features were previously described and illustrated in the Gravure section of Table 2 in *Chapter 2.02*, and they also apply to μ CP R2R systems. The print quality of the μ CP printhead is directly linked to the system’s ability to maintain the alignment between the print and impression rollers in real time during operation.

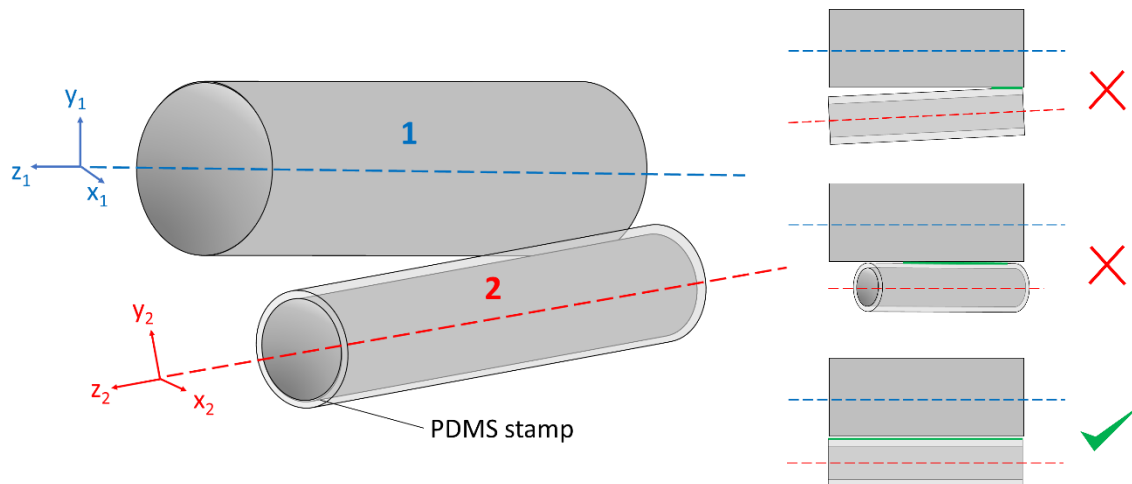


Figure 10. Axes of alignment for impression (1) and print (2) rollers; right side sketch shows the two dimensions of misalignment compared to the proper alignment, from the top view.

The difference in alignment between the two rollers is illustrated in Figure 10. Because at least one of the rollers (in this case the print roll) must be mobile to allow engagement/disengagement of the system and real-time control of the contact pressure on the stamp, this means that it is inevitable that

there will be dynamic changes in the roller alignment while the web is running. This is due to a multitude of factors such as non-concentricity of the rollers, errors in setup and calibration, and asymmetries in the fabricated components. Even with all these factors minimized in an optimal design, the presence of small errors necessitates real-time dynamic control of the print roller alignment so that the stamp maintains the desired position/pressure of contact with the substrate. This accounts for point (3) on the list of design requirements for the system – the need for contact force and positioning control.

Requirement (2), the need for the printhead to be suitable for continuous large-area printing, imposes another constraint on the design, albeit one that is simpler to implement. The axial length of the print and impression rollers must be greater than the width of the 4.0" PET web that is used in the current R2R system. Since the horizontal (table mounted) breadboard has a width of 12.0", this leaves more than sufficient room to attach the printhead of the required breadth.

The final requirement (4) for minimal assembly is aimed at maximizing precision, repeatability, and ease of calibration while also minimizing the effects of mechanical backlash (explained further in the following section), asymmetries in fabricated components, and human error involved in the physical setup of the device on the lab table . This final design principle is employed in tandem with the other 3 requirements to develop a model that most effectively fulfills the desired purpose.

Now that all the objectives and constraints of the system have been established, as well as the initial parameters, we may generate a design for the mechanisms that are needed for the printhead. In this instance where positioning accuracy and repeatable precision are of paramount importance for a stable printer, we elect to use flexures a.k.a. compliant mechanisms to precisely guide (and constrain) the motion of the ends of the print roller.

3.02 Advantages of Compliant Mechanisms

This thesis is not a review of compliant mechanisms in precision machine technology, but nevertheless it is necessary to briefly summarize the fundamentals of flexures for the reader to understand the reasoning behind this design. The most important benefit of using flexure mechanisms for these kind of applications is high precision in positioning, due to the absence of mechanical backlash [49]. Backlash is a form of deadband in mechanical systems with moving parts. Since there must always be gaps between moving parts to allow them to move, this means that there is a certain distance or angle by which one part must be moved before it applies force/displacement to the next part in sequence. In geared systems such as in Figure 11, the consequences of this means it is impossible to attain precision to a degree finer than is allowed by the inherent backlash of a system. [50]

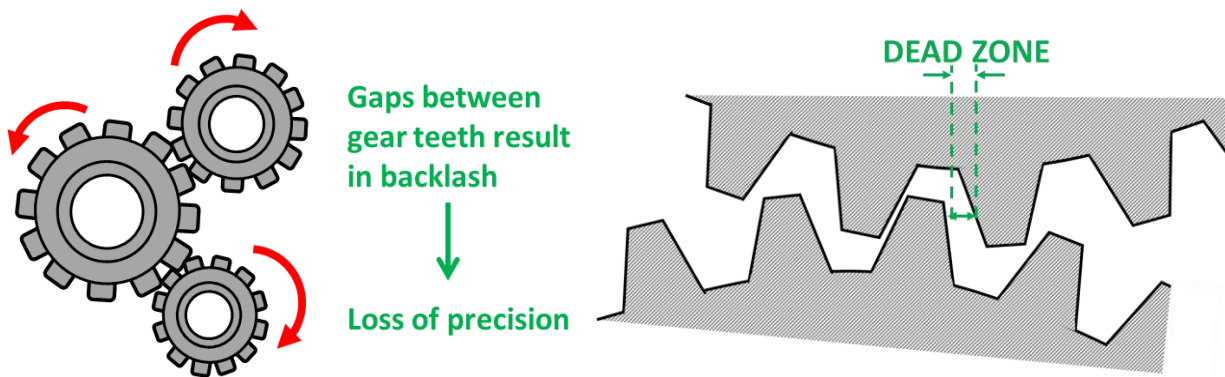


Figure 11. Simple visualization of mechanical backlash in a traditional geared mechanism

Another key feature of compliant mechanisms is that they are monolithic. While this property limits the range of motion (ROM), which is one of the main downsides of using compliant mechanisms versus multi-part assemblies [51, 52], it does also confer a number of different advantages, for instance:

- No friction-induced wear and tear, and therefore no need for lubrication of components. [52]
- Monolithic build means complex assembly is not required – see Figure 12.

- Flexures can be fabricated through well-established machining techniques such as water jet cutting, CNC milling, wire electrical discharge machining, etc. [51]

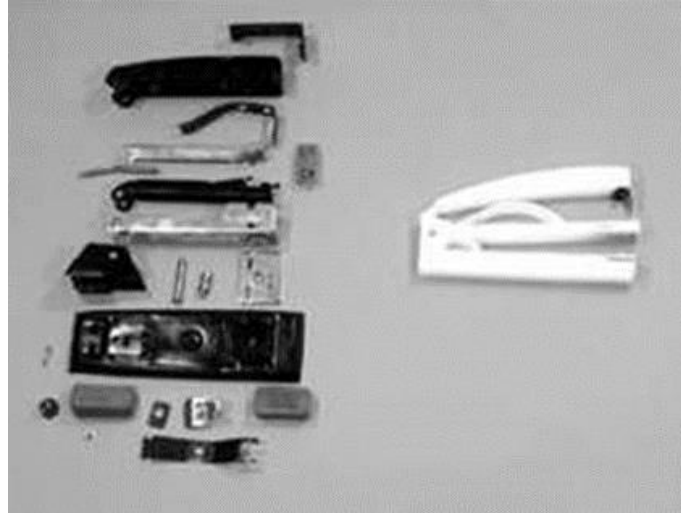


Figure 12. Comparison of a normal stapler with one built using compliant mechanisms [53]

For these reasons and others, flexure mechanisms are often preferred over traditional ones when the required ROM is small [52]. This is often the case in precision motion/positioning stages, metrology instruments, medical devices, MEMS/NEMS, energy harvesting, and other applications where ROM is not as important as positioning accuracy [51, 54]. The mechanism needed for controlling the print roller in our microcontact printhead fits the same profile: the ROM need only be large enough to allow the print and impression rollers to be brought into contact, separate, and make sub-millimeter adjustments to the positioning while in contact (to vary the pressure on the stamp). If the initial setup and calibration is performed successfully, minimal motion will be required during the continuous operation of the printer, as it will only be making small corrections to the positioning of each end of the roller. Using flexures also fulfills the requirement for minimal assembly mentioned in the previous section, making both fabrication and installation of the device that much easier.

3.03 Basic Design Elements

The shape of a compliant mechanism and the elastic properties of its material dictate the ROM available. It is crucial that the mechanism can move freely in specific directions while being constrained in other directions, because parasitic (a.k.a. undesired) motion introduces nonlinearities in the stiffness behavior and makes the system more difficult to control [47, 52]. Design of the flexure mechanism requires the use of SolidWorks CAD software, as well as knowledge of the basic principles of motion and vibration involved with compliant beam structures. Other factors such as ergonomics, cost, and reliability must also be considered – however they are something of a lesser focus here in designing the initial prototype which must be completed early for experimentation.



Figure 13. DOFs and Degree of Constraint (DOC) for the desired print roller control mechanism.

In Figure 10 from the earlier Section 3.01, we saw how the endpoints of each roller in the printhead may be represented by 3D Cartesian coordinates. If axial movement of the shaft is constrained, then each endpoint can only move in 2D space, i.e. in the radial plane of the shaft where it connects to the flexure motion stage. This is shown more clearly in Figure 13. For the print roller to be able to move with the desired DOFs and DOCs, the endpoints of its shaft must be connected to a motion stage which is compliant in the x-y directions while remaining stiff in the z direction.

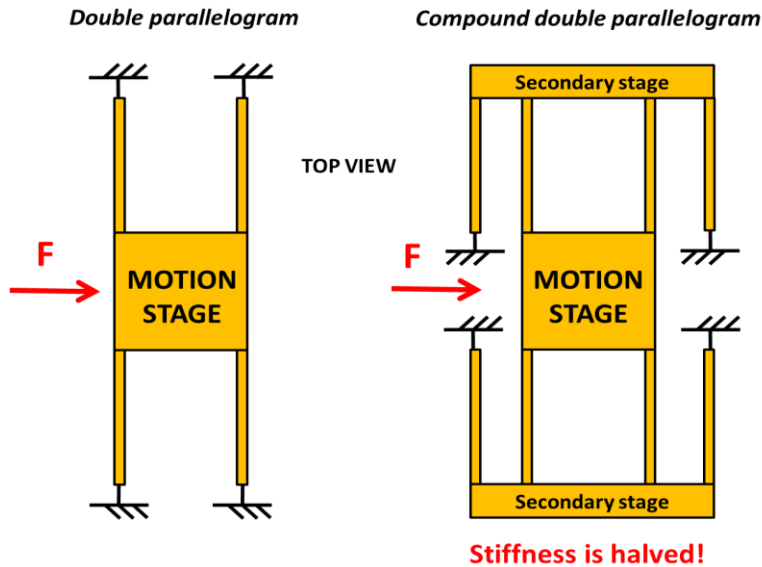


Figure 14. Illustration of stiffness in two types of parallelogram (a.k.a P-joint) flexure mechanisms

The above figure, Figure 14, illustrates the principle of a highly useful flexure mechanism known as the parallelogram joint (a.k.a. the P-joint) which is used to generate 1D linear translational motion – exactly the kind that is needed in our system. Recall that the compound double P-joint mechanism was used in the CUHK group’s flexure design [1], shown in Figure 7, albeit for a significantly smaller area print roller. The P-joint can be represented as a mass-spring system on rails (constrained) for the calculations of the static force behavior, and to a lesser degree, the vibrational behavior as well. Hooke’s Law linear relation between force, stiffness (spring constant), and displacement applies here. This makes it possible to calculate the exact displacement for a given amount of force applied, which is precisely repeatable if the force does not exceed the yield or fatigue limit of the structure/material.

A 2 DOF flexure is required for our positioning stage to which each end of the print roller shaft is mounted. This may be accomplished by a clever design that overlays multiple sets of translational joints; a concept which is elaborated on further in *Section 3.05 – Advanced 2 DOF Flexure Design*.

3.04 Print & Impression Roller Design

As the only printhead components that directly contact the PDMS stamp and PET substrate, respectively, the design of the print and impression rollers must be carefully considered. Recall from *Chapter 2.04* that previous microcontact print rollers were cylinders of uniform diameter on which the PDMS stamp was wrapped. In the case of the CUHK model, the roller shaft is a one-inch diameter steel shaft, the ends of which are mounted in air bushings and connected to the flexure motion stages. Using a simple steel shaft as the roller is effective because of its simplicity, however it does have several drawbacks.

It poses a limitation on the diameter of the roller and by extension, the area of the stamp, because the ends of the shaft must fit into the air bushings. Large (over 1.0" diameter) air bushings are increasingly expensive and require heavier mounting blocks, which must be installed into the flexures. If the motion stage is too heavy, it will negatively impact the dynamic performance of the system, making it slow to respond to control signals. Also, it creates a difficulty in aligning the stamp on the roller because there are no distinct features on a smooth cylinder that may be used for registration, apart from the end faces. For these reasons, we elect to design unique roller assemblies for our machine.

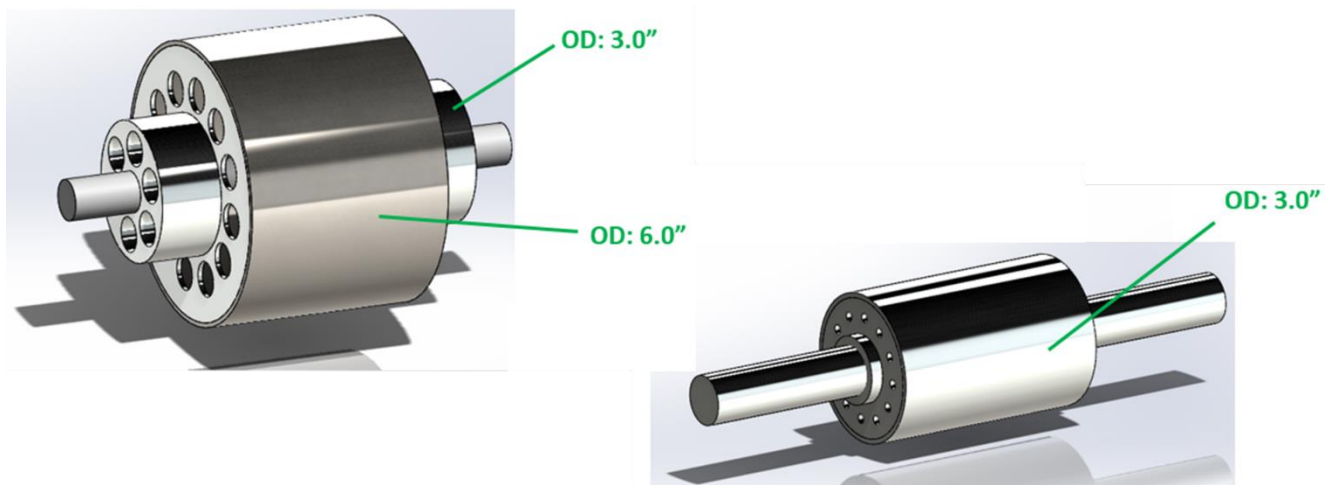


Figure 15. SolidWorks drawings of the printhead roller assemblies, showing outer diameters.

Figure 15 shows the CAD models of the two rollers in this thesis design, with the impression roller on the left and the smaller print roller on the right. The print roller is designed with the same outer diameter (3.0") as the pre-purchased idler and motor rollers that were already present in the lab setup. Using the formula $\pi R^2 L$ for the surface area of a cylinder, it can be demonstrated that the area of the stamp increases by a factor of 9 compared to the 1.0" single diameter shaft. This vast increase in stamp surface area is highly conducive to our goal of achieving large area R2R μ CP and represents a step-up from previously attempted systems described in *Chapter 2*.

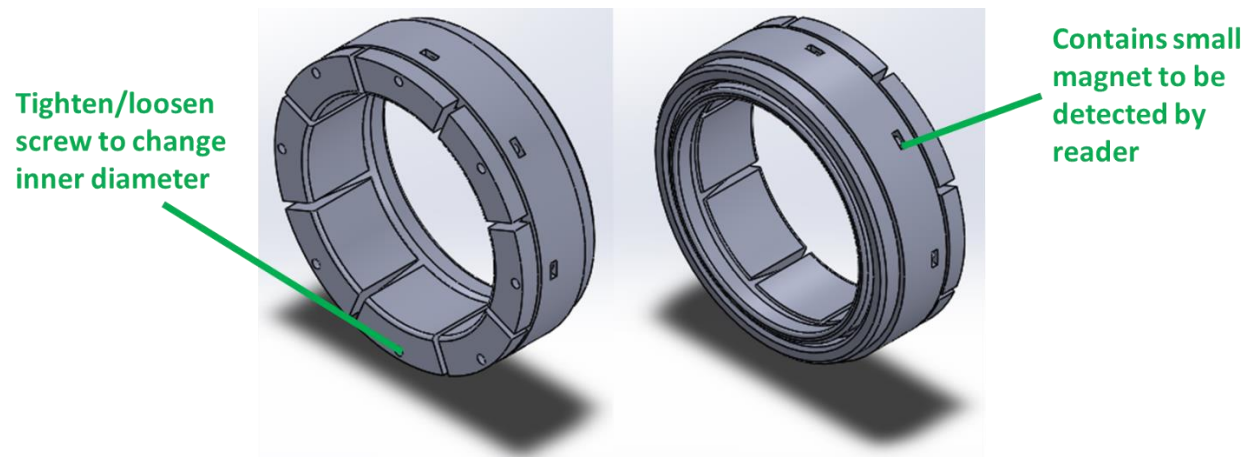


Figure 16. CAD model of pre-built speed encoder designed to fit on approximately 3.0" diameter rollers [55].

The print roller is an assembly of 4 components, all stainless steel: the inner shaft (1.0" diam.), the outer cylinder, and the two positioning disks. A dowel pin inserted into a threaded hole in each disk is used to secure the outer cylinder in place and prevent sliding. The disks must be connected onto the large cylinder via welding. The impression roller is assembled from 6 components: it has the same structure as the print roller assembly but with an additional two hubs (3.0" diam.), which form an extra "step" in diameter. The reason for adding this feature is so that the speed reader a.k.a. encoder ring, shown in Figure 16, may be placed on the impression roller and used to gather data on the printing angular velocity. This ring was previously designed (3D printed) to be tightened onto the other rollers in the system which have outer diameters (ODs) of 3.0", thus the reason for the step size [55].

Both rollers are designed to be as lightweight as possible given the dense material (stainless steel). Heavier rollers have more rotational inertia, which means the web tension in the system needs to be higher to control the speed and positioning accuracy. And as stated earlier, heavier weight on the motion stage worsens the dynamic performance in terms of bandwidth i.e. response time. To save weight, the wall thickness of the cylinders is limited to 0.1". FEA (finite element analysis) in simulation was performed using SolidWorks to ensure that these hollow cylinders would not deform under load. Additionally, the hub and disk components contain symmetrical hole patterns which cuts out a substantial chunk of material. The only parts of the roller that are solid throughout are the thin shafts, which could not be purchased hollow and it was not worth modifying them further, in the interest of time.

When accounting for the volume and density of all parts, the total weights of each are calculated to be 1.935 kg (4.27 lbs) for the print roller, and 3.630 kg (8.00 lbs) for the impression roller. The weight of the 1.0" shaft by itself is 1.205 kg; this means that with only a 60% increase in weight we get a 900% increase in surface area for the print roller.

The impression roller is designed with a larger diameter than the print roller for two reasons. First, when the impression roller is large relative to the print roller it has an effect that is like roll-to-plate printing. This is beneficial because the flatter the contact, the less spatial variation in contact pressure, resulting in a stable and high-quality print output. And secondly, this is done to meet the spatial needs of the system. If the OD is larger it means that the roller surfaces are closer to each other, and in this system, they need to be close enough to be able to come into contact. The shape of the 2 DOF flexure mechanism (seen in the following section) informed the diameter of the impression roller. Hence, the impression roller is designed with twice the OD of the print roller.

3.05 Advanced 2 DOF Flexure Design

Each end of the print roller is linked to a motion stage, i.e. the central controlled motion element of a flexure mechanism. To understand how a monolithic mechanism may enable the desired motion while constraining undesired motion, it is best to analyze the structure as if it was made up of separate components. Figure 17 aims to illustrate this point.

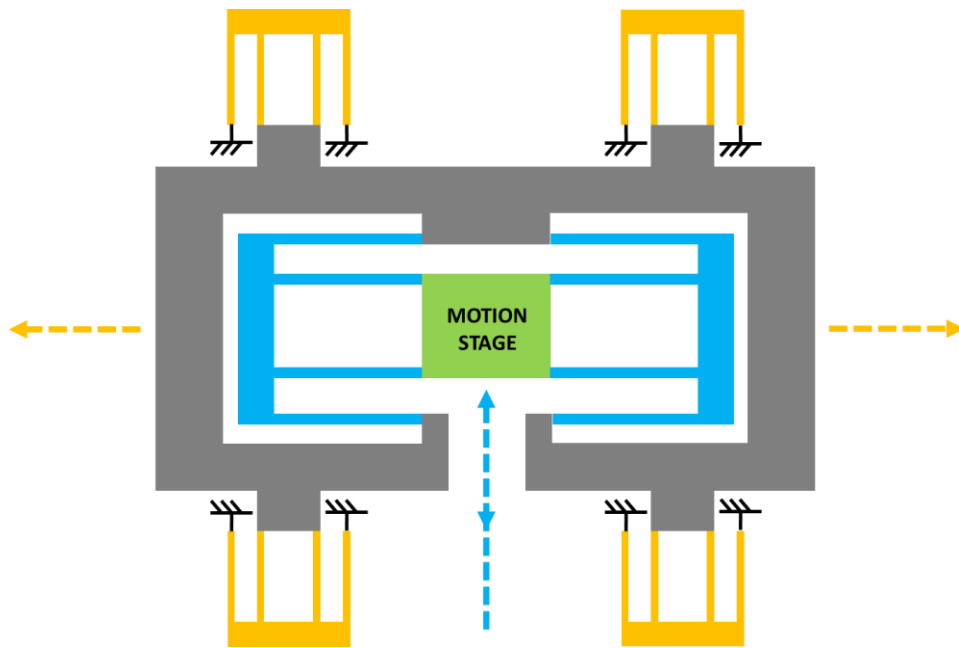


Figure 17. Bisymmetrical 2 DOF flexure with highlighted elements: (green) central motion stage, (blue) compound P-joints allowing vertical translation, (gold) compound P-joints allowing horizontal translation.

The motion stage itself is constrained by compound parallelogram joints that, as we established previously, permit translational motion in 1 DOF. This entire compound double parallelogram mechanism is housed within a rigid frame. This rigid frame itself acts as a second larger motion stage, which is constrained by another set of compound P-joints. These P-joints permit motion in the second DOF. The difference between “rigid” and “compliant” elements of the mechanism is due to the length and width of the beams. The entire structure is the same thickness (1.5”) throughout, which gives it high stiffness in the z-plane (normal to the page/screen that you are reading this on). Traditionally, in the design of

compliant mechanisms, the stiffness of the rigid elements is defined as being at least 50 – 100 times greater than the stiffness of the compliant motion elements (in the DOF direction) [47]. These beam length and widths are selected via analysis of the stiffness using the FEA method.

The stiffness of flexural beams/sheets may also be calculated [52] using the following formula:

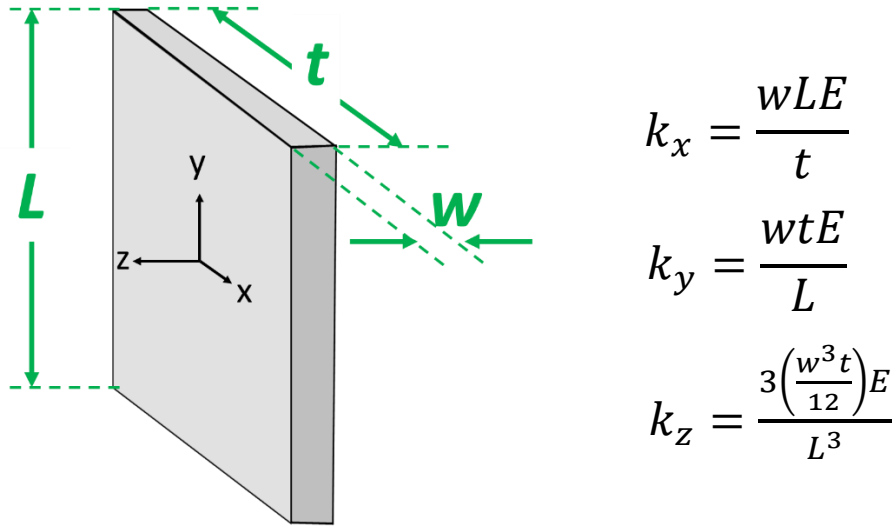


Figure 18. How to calculate stiffness in 3 DOFs for simple sheet flexure. L, w, and t are dimensions, and E is the elastic modulus of the flexure material.

When the stiffness is known, one can determine the slope of the linear (elastic range) portion of the force/displacement curve. When multiple beams are combined into a structure such as a P-joint, one can model them as a set of springs in parallel or series for the stiffness calculations. FEA method is employed for this complex design, both to save time and also to perform accurate failure analysis.

Back to the 2 DOF flexure design: the example shown in Figure 17 is an ideal design because of its bisymmetrical structure (2 axes of symmetry) which minimizes parasitic movements. The CUHK mechanisms [1] used this structure for their compact R2R system. However, spatial constraints prevent us from employing this layout as the frame would need to be significantly larger to support the heavier print roller, and the impression roller has to be mounted on the standing breadboard which would cause

it to interfere with the upper part of the proposed mechanism. Therefore, a truncated mechanism that has bilateral symmetry (1 axis of symmetry) is more suitable for this design.

One might raise an interesting question concerning the positioning stages: if two flexure mechanisms are coupled by the print roller shaft connection, then does that mean that they are constrained to only move together/simultaneously? And if so, does that disallow real-time tilting/adjustment of the print roller via the motion stages, thus defeating the purpose of the mechanism? The answer is yes if we assume a rigid connection between the shaft and the flexures – however there is a way around this. If the shaft is connected to the motion stage via a non-contact bearing with a certain amount of radial gap tolerance, then the two mechanisms may be controlled independently to tilt the roller. The maximum tilt angle then becomes a function of the tolerance gap of the bearings and the distance between the ends of the roller – which can be calculated using trigonometry. Therefore, the air bushings used to hold the shaft in place without contacting it directly are critical to the operation of the printhead mechanism. More detail is provided on these components in *Chapter 4.03 – Air Bearings for Frictionless Rotation*.

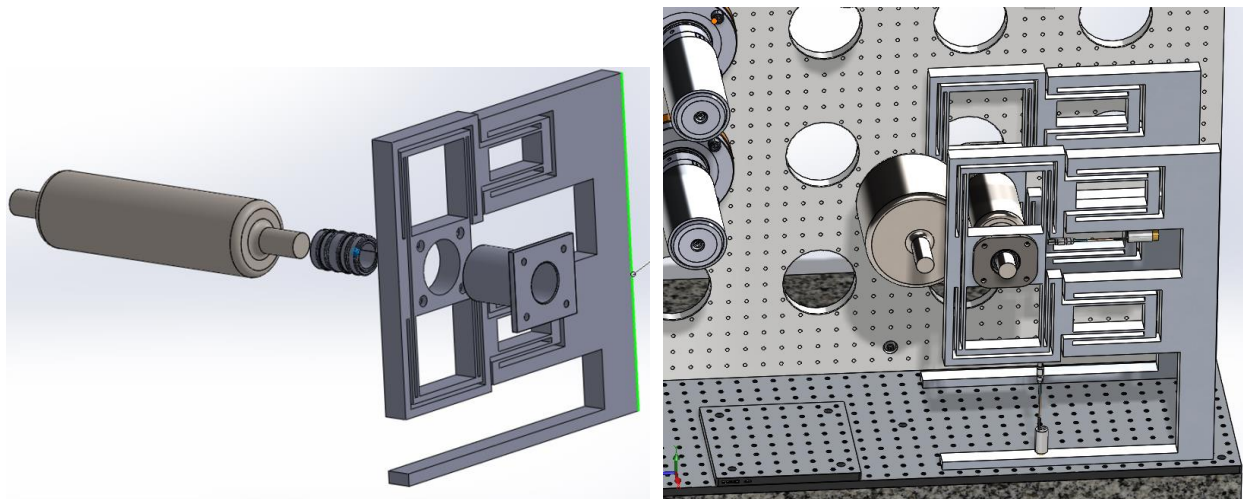


Figure 19. An early design concept for the flexure positioning stage, showing the print roller and air bearing connection.

The R2R system layout is also important in designing the flexures because it determines the intended approach direction of the print roller to the impression roller, which could either be horizontal or vertical. Early in the design phase, the plan was to use a similar layout to the MIT R2R system which had been used since 2014 onwards (designed by Libert [45]). This setup uses a horizontal approach direction, which does not mesh well with the space constraints of our current setup. Figure 19 shows an early design concept that was considered for the flexure, before it was established that a vertically symmetrical mechanism which approached from below would be more robust, require less material, and would fit more easily on the lab table.

The design for the first prototype mechanism to be fabricated is shown in Figure 20.

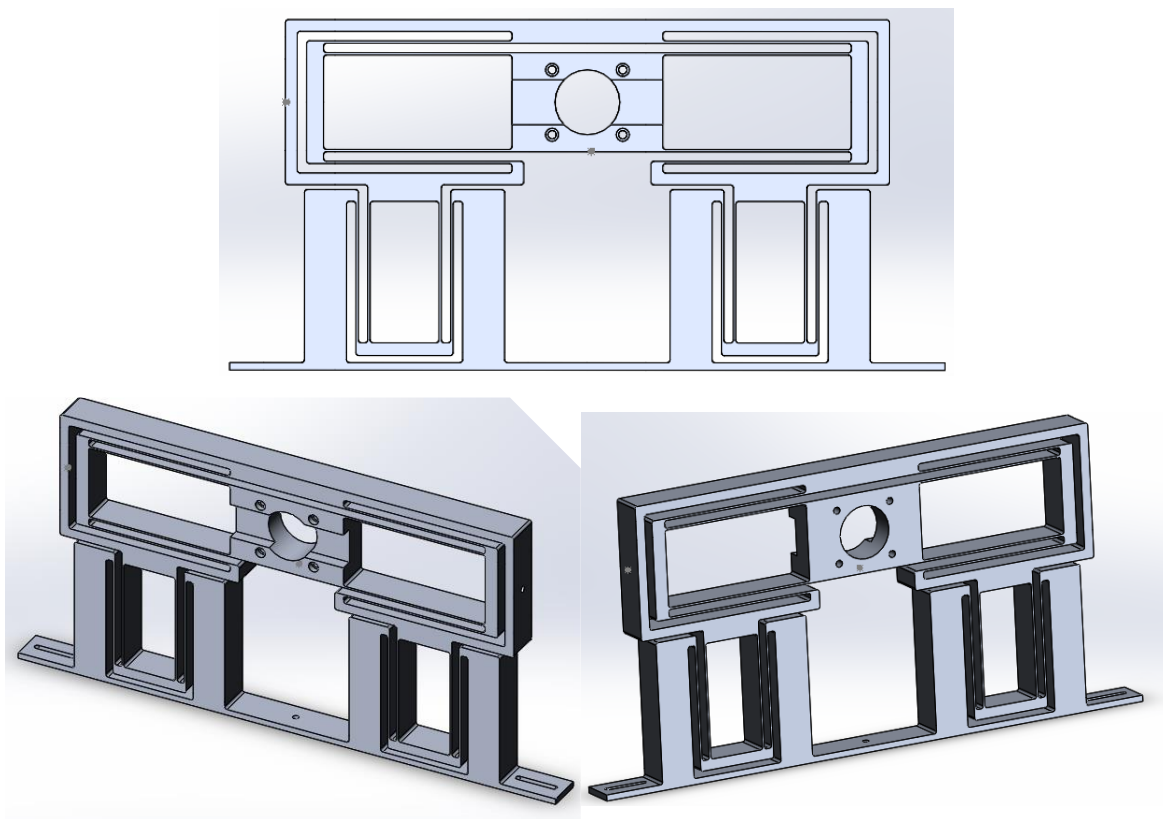


Figure 20. First prototype of new 2 DOF flexure design, showing three different views.

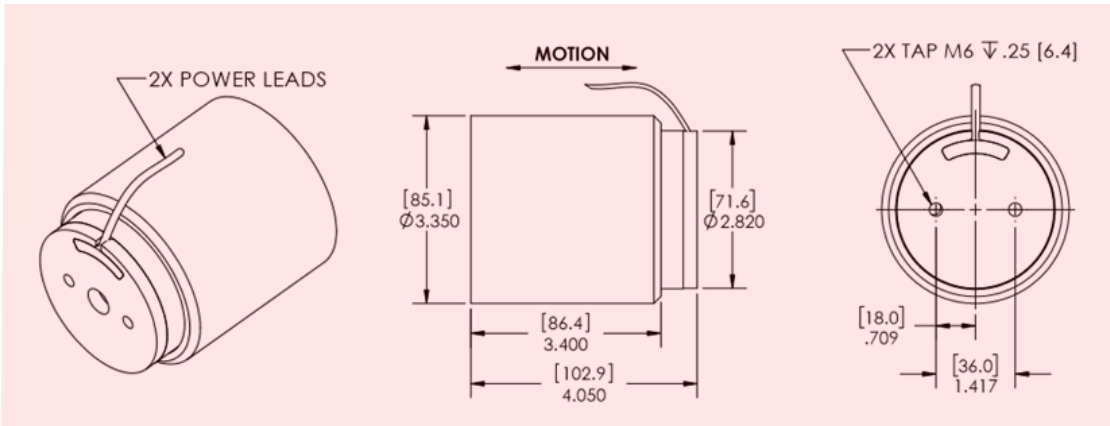
This model was designed to be as adaptable as possible, so that it could fit within our spatial constraints and meet the requirements for ROM, yield strength, and dynamic performance. Note the slots (width: 0.25”) built into the base to allow adjustable attachment to the lower breadboard via bolts. Also note the notch in the motion stage; this is to allow enough room for the air-fittings (connected to air pump) to attach to the air bushing mount once it is installed in the system.

3.06 Actuation

Of course, the compliant mechanisms are only there to guide and constrain the motion; they are of no use without an external supplier of force. Finding and procuring suitable actuators was one of the initial tasks of this thesis work. The actuators must fulfill the following requirements:

- Must fit within the structure of the printhead mechanism – this goes back to the first objective of the design (see *Section 3.01*).
- Maximum continuous force or holding force of the actuator must be sufficient to move the motion stage through the desired ROM.
- The weight of the actuators must not be an impediment to the system.
- Need to be controllable using LabView interface.

Considering all these factors led to the decision to use voice coil actuators (VCAs) for our system, for their simplicity, cost-effectiveness, and compatibility with the current control system setup. Figure 21 shows the specifications of the chosen VCAs. Linear stepper actuators would also have been a viable option, but the cost is higher, and the force/weight ratio is typically lower. However, for future systems we may consider steppers due to their holding force which saves energy (no need for continuous power) and gives them inherent positioning stability.



MOVING COIL NON-COMM ACTUATOR SPECIFICATIONS		
Motor P/N	NCC08-34-350-2H	
Stroke	0.80"	20.3 mm
Radial Clearance	0.015" per side	0.38 mm per side
Bearing Type	None Provided	
Moving Mass	1.0 lbs	0.46 kilograms
Total Mass	7.4 lbs	3.35 kilograms
Resistance @ 20C	6.25 ohms	
Inductance @ 20C	5.0 mH	
Electrical Time Constant	0.80 msec	
Motor Constant	4.98 LBS/SQRT(Watt)	22.6 N/SQRT(Watt)
Force Constant	12.8 LBS/Amp	56.9 N/Amp
Back EMF	1.4 V/ips	56.9 V/m/sec
Continuous Force	30 LBS	134 N
Max Power @ 100% Duty	36 Watts	
Peak Force	90 LBS	401 N
Max Power @ 10% Duty	330 Watts	

MOVING COIL NON-COMM ACTUATOR SPECIFICATIONS		
Motor P/N	NCC03-15-050-2X	
Stroke	0.25"	6.4 mm
Radial Clearance	0.015" per side	0.38 mm per side
Bearing Type	None Provided	
Moving Mass	0.13 lbs	60 grams
Total Mass	0.70 lbs	320 grams
Resistance @ 20C	3.75 ohms	
Inductance @ 20C	1.30 mH	
Electrical Time Constant	0.35 msec	
Motor Constant	1.38 LBS/SQRT(Watt)	6.14 N/SQRT(Watt)
Force Constant	2.7 LBS/Amp	11.9 N/Amp
Back EMF	0.3 V/ips	11.9 V/m/sec
Continuous Force	5.0 LBS	22.3 N
Max Power @ 100% Duty	13 Watts	
Peak Force	15.0 LBS	66.8 N
Max Power @ 10% Duty	118 Watts	

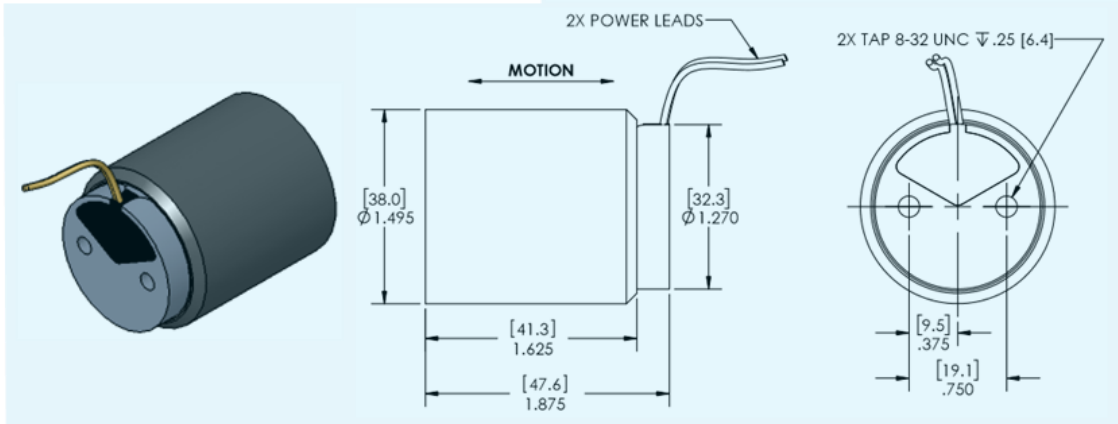


Figure 21. Specifications and diagram of the two H2W actuators (dimensions given in mm and in). Red – larger actuator; blue – smaller actuator. Source company: H2W Technologies.

3.07 Load Simulation & Calculations

To conclude this chapter, this section will summarize the results of the static and dynamic analyses of the flexure mechanism and print roller assembly. Finite Element Analysis (FEA) is a numerical method used for solving boundary value problems involving mathematical or engineering models; it is commonly used for structural analysis of mechanisms with complex geometry. It does this by dividing the model into a finite number of discrete elements, forming what is called a mesh, and then applying the forces and constraints acting on the system across every element in the mesh to calculate a solution.

In SolidWorks simulation software, each element is triangular, and the side length approximately defines its size. Using smaller elements yields more accurate results but also makes the simulation take longer to solve. Therefore, a mesh control system was applied to this model so that the flexure joint faces and the edges around them used the smallest available elements (3.63mm side length) while the rigid components used larger elements (14.52mm). The mesh, shown in Figure 22, is used for all analyses of this structure.

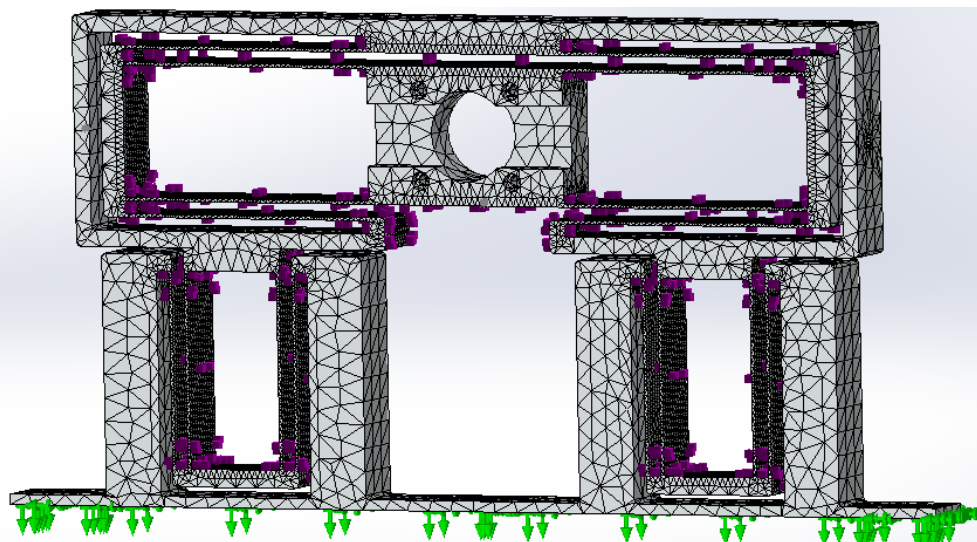


Figure 22. Mesh used for FEA of the flexure prototype mechanism. Note that the element size is smaller around the compliant i.e. moveable sections. This increases the accuracy. Green arrows represent fixed geometry, a constraint.

Frequency analysis revealed five modes of vibration for the flexure, two of which are useful for the purpose of the printhead. This is shown below, in Figure 23, with exaggerated displacement.

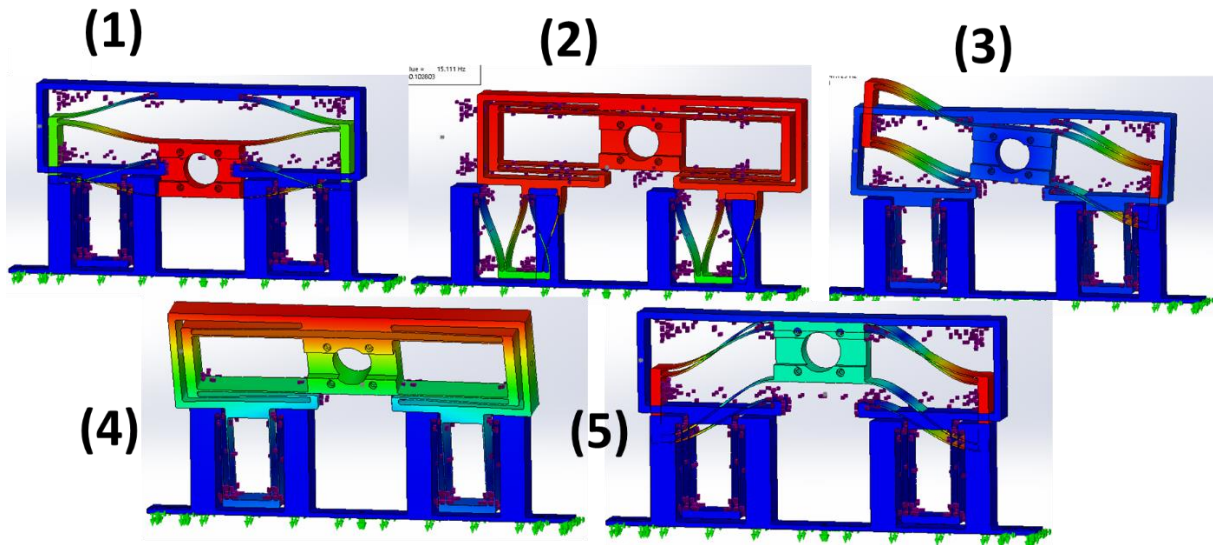


Figure 23. Five modes of vibration for the flexure. Modes (1) and (2) are intended DOFs of the mechanism.

The natural frequency of vibration for each of these modes is found to be: 15.11 Hz, 17.44 Hz, 47.72 Hz, 48.31 Hz, and 56.83 Hz, respectively. There is a 213% increase in vibrational frequency between the average of the first two modes (DOFs) and the average of the remaining three. This is due to the increased stiffness in those undesired directions of motion. While useful for understanding the dynamic behavior of the mechanism, the vibrational frequency is not linearly related to the stiffness, so this does not tell us the exact relation. For that, static force analysis is used to obtain an estimate.

In the static force analysis, we use the same mesh and constraints, but this time apply a force of 22.3 N (5.0 lbf) to surfaces of the mechanism to simulate actuator/external force. First this force is applied below the central motion stage (to achieve vertical motion as in mode 1), and the observed displacement is found to be 2.00 mm. Next the same force is applied to the side of the upper frame, simulating the horizontal translation as in mode 2, and 0.85 mm displacement is observed. Lastly, 22.3 N force is applied directly on the front face of the central motion stage to achieve out-of-plane movement as in mode 3,

and the displacement at the center of the stage is observed to be 0.076 mm. This demonstrates that the equivalent stiffnesses are:

$$k_x = 26200 \text{ N/m} \quad k_y = 11100 \text{ N/m} \quad k_z = 293000 \text{ N/m}$$

This is using the definition of x , y , z axes seen earlier in this thesis, where x is horizontal, y is vertical, and z is normal to the page. This shows that the stiffness in the z direction is one order of magnitude higher than the stiffness in the DOFs. Ideally this would be two orders of magnitude higher, but this would require the flexure mechanism to be thicker (3" or more). If the granite table were larger this would be a good improvement to make, however with the current setup there is no room for additional thickness in the z direction.

Lastly, an attempt was made to simulate the behavior of the coupled mechanisms with the print roller assembly in place. This analysis required more approximations and simplifications in place to be able to run – these were mostly related to the air bearing models, which were treated as frictionless in the axial rotation direction. This on its own is a near enough approximation to the real behavior, but the difficulties were in defining the bonded contact surfaces of the bearings without restricting the rotational DOF. As a result, not all modes of vibration were able to be analyzed by this method, as some yielded bizarre and incorrect results.

Figure 24 shows the three modes of vibration that were analyzed for the coupled system. Vibration in the vertical and horizontal DOFs had natural frequency of 17.46 Hz and 20.37 Hz, respectively. This is close to the estimates from the previous study which looked at the flexure mechanisms independently. For the out-of-plane vibration mode, the frequency was found to be 38.72 Hz, which is lower than the estimate from before. This could mean that the out-of-plane vibration is affected by the greater mass of the print roller in the coupled system. It also might be due to the fact that the coupled

system is 6.7 times wider in the z direction than the flexure by itself, and that causes the flexure thickness of 1.50" to behave like a thin compliant beam whereas before it was more rigid. However, the results could also be inaccurate for this mode, as the animation shows the print roller shaft breaking contact with the air bushings which disregards the reality of the physical connections. It is difficult to interpret the result without a more thorough understanding of the simulated system.

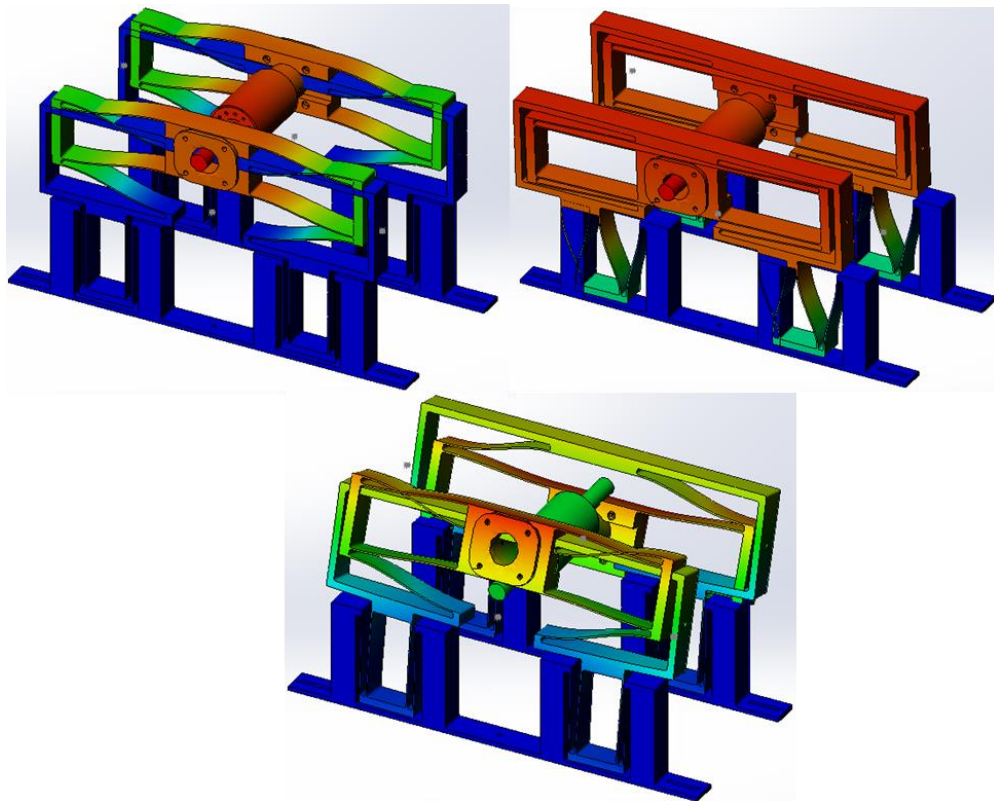


Figure 24. FEA result showing three modes of vibration of print roller system; ROM exaggerated.

Lastly, the results allow us to verify that the maximum stress on the flexure joints is below the yield and fatigue strength limits of the material. This leads to the material choice being Al-7075 alloy due to its fatigue strength of 159 MPa. With the maximum possible load from the actuator (130.95N) placed on the motion stage, the stress reaches 93.68 MPa, which is only 58.91% of the fatigue limit and 18.62% of the yield limit (503 MPa). Al-1060, commonly used, would be insufficient as it yields at 103 MPa.

4 COMPONENTS FABRICATION AND ASSEMBLY

4.01 Fabrication of Flexures

Once the static and dynamic analyses were completed and the plan for the printhead assembly was laid out, the next step was procurement of raw materials for fabrication. Two plates of Aluminum-7075 alloy, chosen for its exceptionally high yield strength, were ordered online via McMaster-Carr. These plates were each 1.50" thick. If this dimension were any larger, the flexures would not fit with the other components on the limited width of the base breadboard.

Once acquired, the Al-7075 plates were brought to the UMass MIE workshop for waterjet CNC cutting. Waterjet is a top-down cutting process that can achieve high-precision results (tolerances of 0.001" are average) and has the added benefit of not applying heat to the material unlike other mechanical cutting processes such as milling. The application of heat – via friction or otherwise – can cause edge distortion on some metallic structures and limit the machine's cutting accuracy for small radii fillets and holes. While CNC milling was considered for the job, it was ultimately not chosen due to the nominal higher precision of waterjet and because the large area plate (12"×24") fit better in the bed of the waterjet machine. The plates were cut one at a time.

After waterjetting of the two plates was completed, the remaining features which were not accessible for cutting during the waterjet process (because the cuts were not on the front plane) were added. Firstly, the two slots for flexible mounting of the mechanism on the breadboard were milled onto the bottom surface. And next, two dowel pin holes were drilled at the vertical and horizontal actuation points. This was a difficult process because the entire mechanism had to be securely clamped to make these features accurate; clamping the large flexure with its compliant beams was not an easy task. This

was a major oversight in the initial design of the flexure, as the scope of this problem was unanticipated and could have been countered by altering certain features of the flexure.

Nevertheless, the task was eventually accomplished by the machinists without major loss of feature accuracy. This problem that arose is one that must be carefully considered for future optimized flexure designs. The 2020 design, recently finalized (see *Chapter 6.01 – Optimized Flexure Assembly*) greatly improves ease of fabrication by making the entire flexure fabrication process one step, as all the features may be machined onto one surface of the plate. This is expected to save a great deal of time in the construction of the future design.

4.02 Roller Fabrication, Assembly, and Smoothing

After the flexures, the rollers were the most difficult and time-consuming components to fabricate in the assembly. Since the rollers are not monolithic like the flexures, there are more steps required to complete the assembly. However, there were fewer problems with the design and most of the steps involved in the fabrication process proceeded as planned. Construction of the print and impression rollers occurred in the steps outlined below. Images of the rollers under construction are shown in Figure 25.

1) DESIGN:

- a. Sizing the components and planning the layout of the assembly (see *Chapter 3.04*).
- b. Performing strain analysis to ensure that thin walled structures act as rigid bodies during print action.

2) ACQUISITION:

- a. Choosing the most suitable material that is available for the tubes, shafts, disks, hubs.
 - i. The inner shafts are chrome stainless steel (already smooth).
 - ii. The tubes (outer cylinders) are grade 304 austenitic stainless steel.
 - iii. The positioning disks and disk hubs are low carbon steel.
- b. Ordering the raw materials on McMaster-Carr Supplier website.

3) CUTTING/DRILLING:

- a. Center pin holes are drilled into the ends of the steel shafts, so that they can be held precisely in position while the tubes and disks are placed on them for calibration.
- b. The positioning disks are cut to the correct shape out of the ordered steel sheets. This is done using the CNC (computer numerical control) operated mill.
- c. Holes for weight reduction are drilled into the disks and hubs, as per the design.

4) WELDING:

- a. Positioning disks and hub cylinders are welded to the tubes via Gas Tungsten Arc Welding process, which is effective for welding thin plates of steel.

5) O.D. GRINDING:

- a. The now assembled, but rough, rollers are brought to a private machine shop (JB Precision LLC, Hatfield MA) where the outer diameters are grinded down to meet the surface roughness requirements of 0.10" wall thickness ± 0.0001 " tolerance.
- b. The UMass MIE workshop is not equipped to carry out OD grinding, hence why the task was brought to an outside company.

6) INSTALLATION:

- a. Clean faces of outer cylinders with alcohol.
 - b. Slide the tubes onto the shafts, insert into R2R system, secure in place by tightening dowel pins (only enough to exert light pressure).
 - c. Make sure rollers are aligned with other idler rollers, motor rollers on the breadboard.
- Use the laser tool to align (see upcoming *Section 4.04*).



Figure 25. Print and impression roller parts prior to completion.

4.03 Air Bearings for Frictionless Rotation

The significance of using air bushings for this assembly was mentioned previously in *Chapter 3.05 – Advanced 2 DOF Flexure Design*. These components both permit near-frictionless rotation of the print roller and they create a slight gap tolerance which allows tilting of the shaft by a small fraction of a degree. Note that the terms bushing and bearing are treated as interchangeable in this thesis write-up, but bushings refer to a specific type of bearing that use sleeves, fitted over shafts, which allow axial sliding. A technical drawing of these sleeves – the air bushings – is shown in Figure 26.

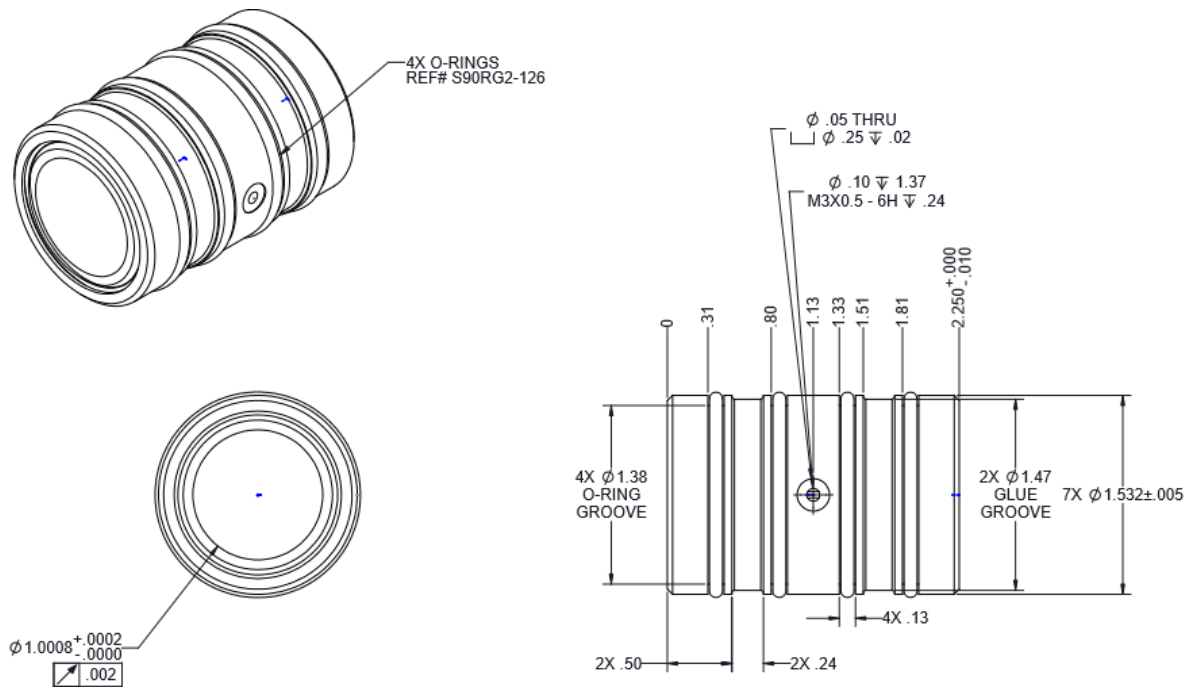


Figure 26. Technical drawing of the air bushing. Dimensions in inches. Source company: New Way Air Bearings.

The air bushings are tightly mounted inside these custom-made aluminum blocks, shown in Figure 27, which were fabricated in the MIE workshop via CNC milling. Note that the hole in the bushing for air inlet must be aligned with the corresponding hole in the mounting block.

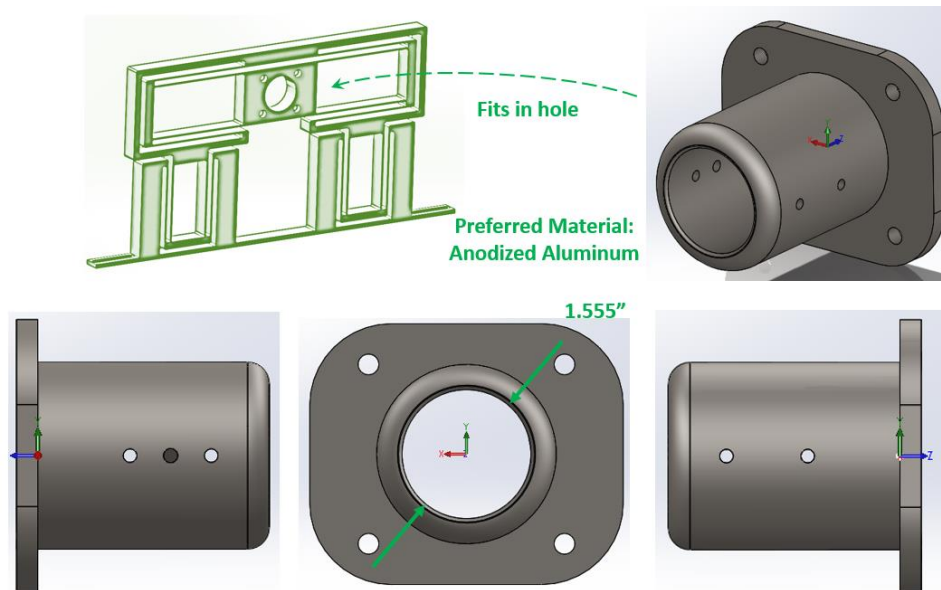


Figure 27. CAD drawing of custom mount designed to house the air bushing for the print roller.

The sleeves fit snugly over the ends of the 1.0" shaft, but when pressurized air flows in through the inlet valve then the shaft slides through with no contact. This is due to the approximately 0.002" increase in the inner diameter of the bushing when the air is turned on. The device specifications state that the air inlet pressure should be in the range of 60-80 psi. Polyurethane tubing is used to direct approximately 70 psi air from the ceiling pump in the lab to a brass T-connector, which divides the flow into two tubes, one for each air bushing. Each of these tubes attaches to another brass connector, which is threaded into the air inlet connection hole in the mounting block.



Figure 28. Brass air fittings and T-connectors ordered from same company.

4.04 Assembly & Alignment of R2R Components

With all the main components of the printhead design fabricated, the next step is to assemble them onto the table via the breadboard attachment. This requires careful precision to ensure that gaps or roughness between components do not misalign the initial position of the mechanisms. Before that, however, the motor rollers for wrapping/unwrapping and the idler rollers for guiding must be installed in the correct locations. The diagram in Figure 29 shows the correct positions for the main components of the R2R assembly.

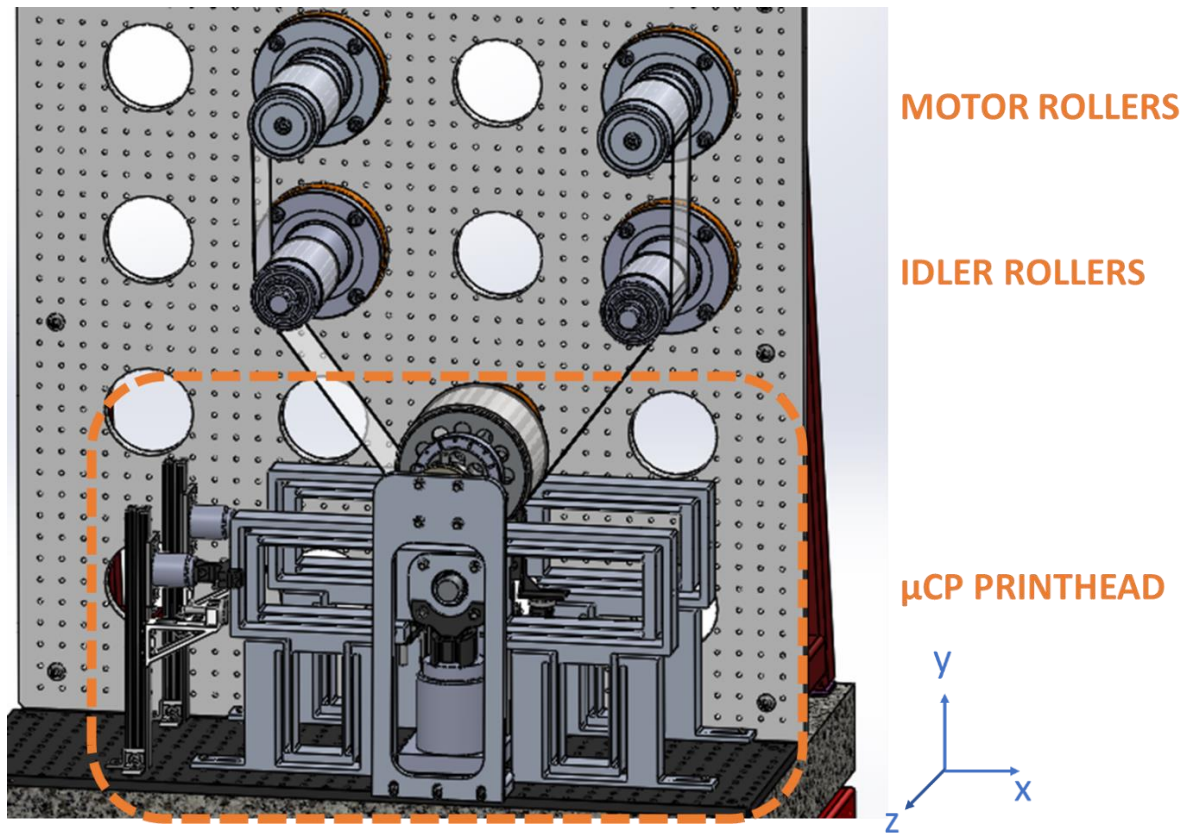


Figure 29. SolidWorks 3D model of the entire R2R assembly, minus the PDMS stamp.

Roller installation is as simple as bolting them onto the standing breadboard via their aluminum adapters, which were fabricated in the MIE workshop. However, this is not enough to ensure precise alignment in the horizontal and vertical planes. One can verify if the rollers are aligned in the same/parallel horizontal planes (meaning there is no up-down tilt) by using an electronic level that displays the tilt angle. The level is simply placed on top of the roller and the angular measurement is read. If the reading is non-zero, adjustments are made to the tightness of the adapter bolts, washers may be added, and thin sheets of copper foil or other materials may be fitted under or over the adapter to impose a slight angular change. Not an ideal solution, but it has proven effective. However, aligning the rollers in the vertical plane proves to be more challenging. As a separate project, several undergraduate students were attempting to solve this issue mechanically but could not come up with a feasible solution. Fortunately, our lab already had access to industry-grade precision laser alignment tools, shown in Figure 30, that are designed for

calibrating the alignment of mini rollers such as the ones in our system. These laser alignment tools are easily strapped onto the 3.0" diameter rollers and show the alignment of the laser line against the drawn lines on the opposite device. The maximum operating distance between the two devices is four feet, and the alignment precision specified is $< 0.001''/\text{ft}$, assuming correct usage [56].

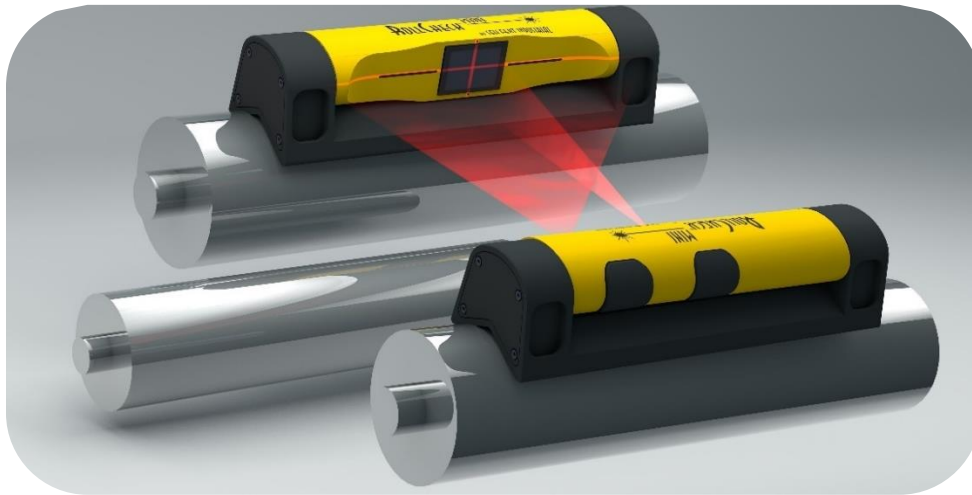


Figure 30. RollCheck® MINI devices for alignment of rollers. Each device is mounted using elastic belts. Source company: Seiffert Industrial. [56]

Using this method is simple and intuitive, allowing for near-simultaneous adjustment and checking of the alignment. The only drawback is that this method cannot directly be used to tell whether the rollers measured are perpendicular to the breadboard that they are mounted on. It can only be used to align the rollers with each other. A monolithic precision-engineered 3D post or strut of the correct diameter could be fabricated to accomplish this – an idea that is discussed later on in *Chapter 5.04 – Engineering Problems Encountered & Solutions*.

First the motor and idler rollers are aligned with each other two at a time. Next, the flexure mechanisms are loosely bolted to the frame via the slots (so they can slide in the x-axis) and the print roller is inserted through the air bearing holes. The laser measuring tool is used to align the print roller

with one of the other four rollers, such as the motor roller on the top left. When the print roller is aligned, the flexure connection to the breadboard is tightened in that position.

The impression roller is attached to the standing breadboard via the load cell's built-in clamp mechanism (see *Section 4.06* to see load cell structure). Before this, the load cell itself is mounted through the back of the breadboard using another adapter so it fits exactly centered in one of the large holes in the standing breadboard. Next the other half of the impression roller support frame is attached; this comprised of the second load cell and two aluminum frame pieces which are mounted to the table breadboard. These components also utilize slots instead of holes to allow flexible connection for angular adjustment in the X-Y plane. The complete impression roller frame is shown in Figure 31.

The reasons for using two frame parts (shown on the left side of the figure) instead of one simpler one that mounts directly onto the table breadboard are: (1) to provide flexibility for adjustment of the roller and (2) the table breadboard is not wide enough to accommodate this kind of frame, so it must be designed to partially hang off the edge of the table. In practice, with this design, aligning the impression roller proved to be a difficult and time-consuming process that requires at least two people, so one can check the calibration while the other adjusts the bolts in the slots. Can be improved on in future design.

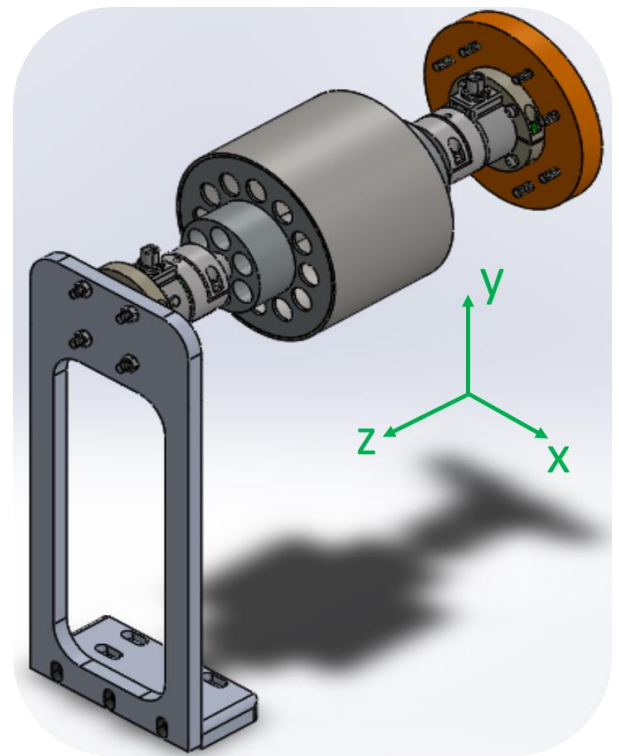


Figure 31. Impression roller frame assembly.

The impression roller is aligned to one of the motor rollers in the same way that the print roller was before it. Once the bolts are tightened, the top of the aluminum frame piece can be checked with a level to ensure that it is parallel with the table.

4.05 Actuator Setup & Linkages

The actuators need to be mounted securely to both the breadboard and the flexure mechanism with minimal gaps in the connections. Recall from the actuator specifications provided on page 33 that there are two actuators per flexure, one large and one small. The large VCA provides vertical force to push the motion stage and the print roller in the y-axis to bring the stamp in contact with the web. The small VCA provides horizontal force to push/pull the frame in the x-axis to make small adjustments to the alignment as needed during operation. Both actuators play a role in affecting the contact surface between the stamp and the web (backed by the impression roller), but the large VCA does the bulk of the work as it must lift the weight of the motion stage, air bearings, and steel print roller while inducing travel of 3mm against flexure resistance to raise the stamp surface up to the web and impression roller.

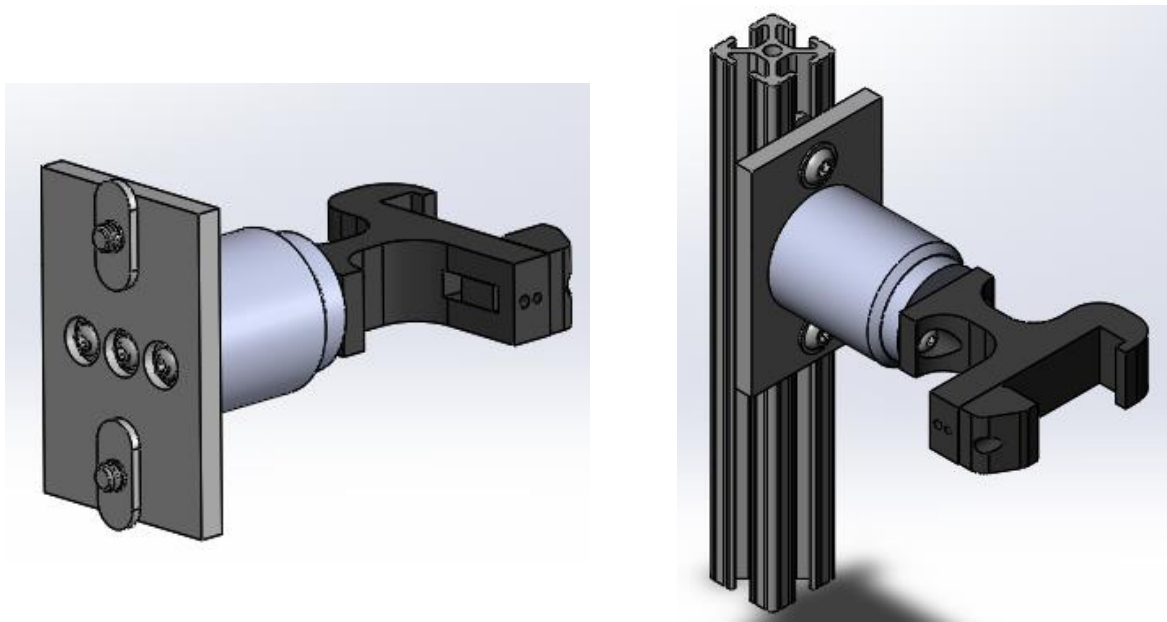


Figure 32. Horizontal actuator mount & connection.

Figure 32 shows how the small horizontally aligned VCAs are mounted. In the lab are an abundance of aluminum beams with this X-shaped cross section; useful for mounting and supporting many kinds of components. These may be easily mounted and aligned on the breadboard, so a simple

adapter was made to connect the actuator to the beam by its own threaded hole connections. To connect it to the flexure side surface, the black clamp piece was fabricated via 3D printing using the Markforged printer in ADDFab (Advanced Digital Design & Fabrication) facility in the UMass Life Science Laboratories. The black material is called Onyx: it is a blend of Nylon filament and chopped carbon fiber which gives it greater yield strength [57].

Weighing 3.35 kg, the large actuator requires a sturdier support base, so aluminum plates are milled to allow a strong and flexible table connection. These plates are shown in Figure 33.

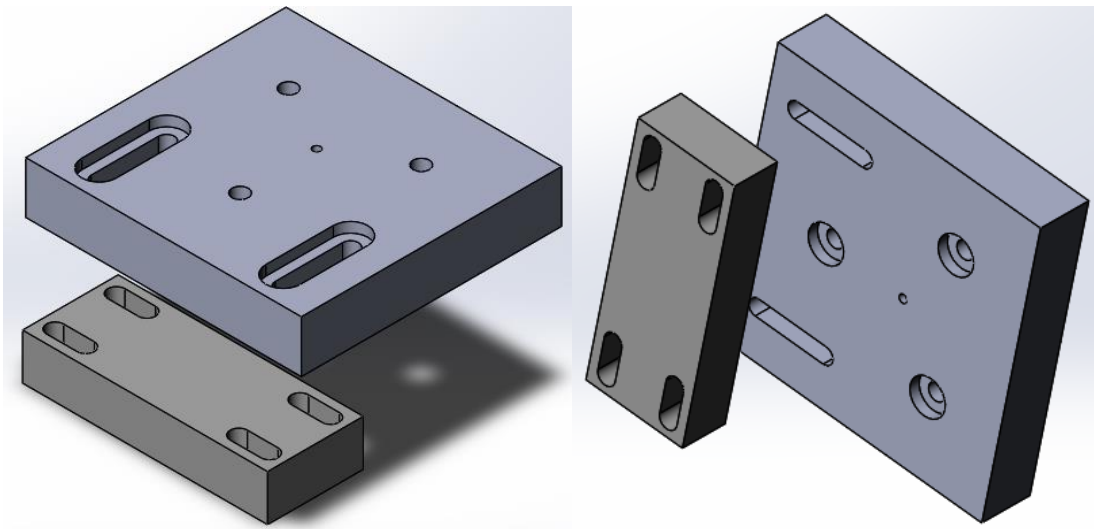


Figure 33. Aluminum plates designed to connect large VCA to table breadboard.

This connection is designed to allow flexibility with its slot connectors, which allow sliding in the x and z planes in case some adjustment is needed to center the VCA under the flexure motion stage. The VCA housing connects to the larger plate via the three holes, which have counterbores underneath to prevent the bolt heads from interfering with the connection between the plates and creating a gap. On the side without the slots, the large plate rests on the smaller frame component from the impression roller assembly which was shown in Figure 31.

The most difficult connection to design was the one between the large actuator and the motion stage. The reason for this is because this connection must allow free translation in the x direction to decouple the two actuators, while still being completely constrained in the y and z axes. If a rigid connection is made between the vertical actuator and the motion stage, then that connection will constrain the movement of the motion stage in the x axis and prevent the horizontal actuator from being able to do its job. This is an inherent flaw in this kind of compliant mechanism structure with perpendicular sets of P-joints, although it can be dealt with using engineering solutions. For example, in the CUHK design, the vertical actuator, which is much lighter, is housed into the flexure frame so that it moves horizontally along with the motion stage, while still being able to apply force. This is an elegant solution as it decouples the actuators completely, but it is impossible in our design because the heavy weight of our VCA would greatly affect the dynamic performance if it were suspended from the motion stage, and the flexure structure would have to be much more robust. Therefore, a different solution is employed where the VCA is fixed to the table and the connection itself allows movement. This is shown in Figure 34

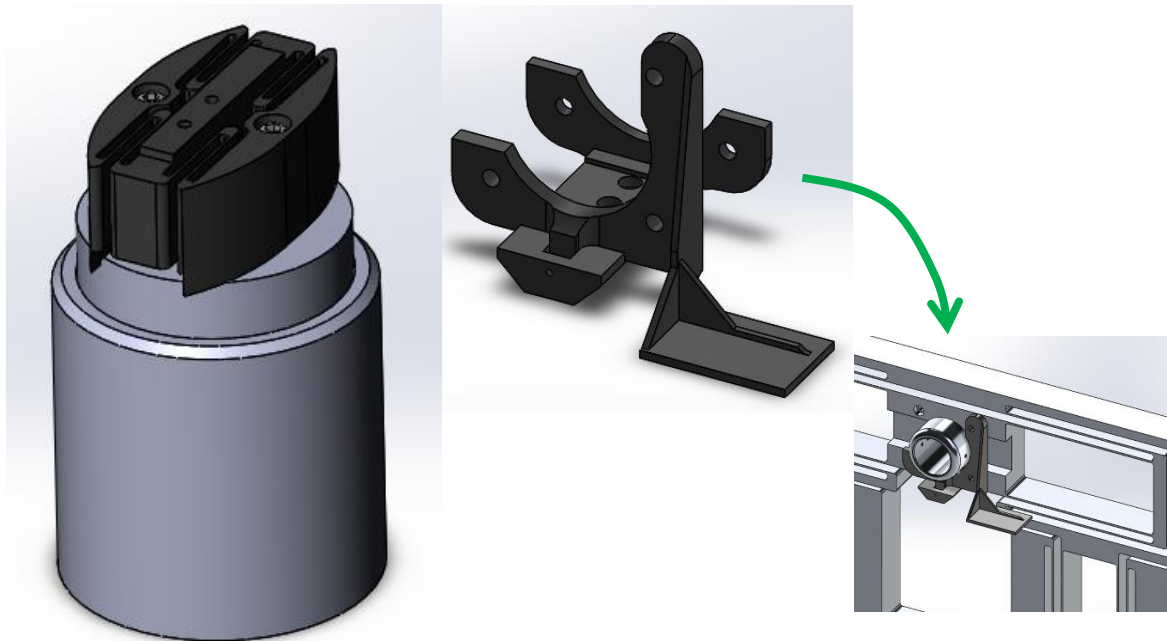


Figure 34. The two pieces of the vertical VCA and motion stage connection assembly.

The original thought was to purchase a linear slide bearing to allow near frictionless movement in the connection, and this is still viable to implement in the system, but because it was more accessible and quicker to fabricate, a printed mini-flexure was designed for the necessary decoupled connection. This part is also made of the same material, Onyx, as the previously shown connection pieces. The mini-flexure is analyzed through FEA simulation the same way the larger one was, and it was computed that it had a low stiffness of 4904.36 N/m in the x direction. This is only 18.7% of the stiffness k_x of the large flexure mechanism, which is not ideal, but it means that it will have only a small effect on the ROM of the larger mechanism. However, it complicates the dynamic model of the system which makes it very difficult to predict how it will affect the natural frequency of vibration in the horizontal DOF mode. Fortunately, quick response time is less important than positioning accuracy for the horizontal motion because the horizontal force theoretically should not have a significant dynamic relationship with the contact pressure on the stamp, unlike the vertical force.

The mini-flexure connection is linked using nut and bolt connections to the clamp-like piece, which connects to the motion stage via the same holes as the air bearing mount. Care is taken to ensure that there are minimal gaps or spaces in the assembly of these connectors which may introduce backlash into the system, although it is inevitable that some imprecisions are introduced. For the future printhead model, more work must be done to minimize the number of necessary components and design more precise linkages.

4.06 Sensors for Precision Control

Achieving microscale precision in the print pattern output of the machine requires careful calibration of the sensors in the printhead system. This thesis does not deal with the control aspect of printing, but the mechanical design of sensor mounts and connections plays an important role in the initial calibration which has a great effect on accuracy.

Capacitive sensors were chosen to measure the displacement change in the motion stage – and by extension – the ends of the print roller. If the sensors are calibrated to a balanced initial position, after the print roller alignment is verified by the laser tool, then the controller can ensure that the x and y position of one motion stage always corresponds to the x and y position of the opposite motion stage, therefore keeping the print roller level and aligned with the other rollers in the system. The main reason for choosing capacitive sensors over the other available types such as eddy current sensors was the nanometer scale resolution over short ranges of motion. Four capacitive probes were ordered, corresponding to the four actuators. The probe image and specifications are shown in Figure 35.

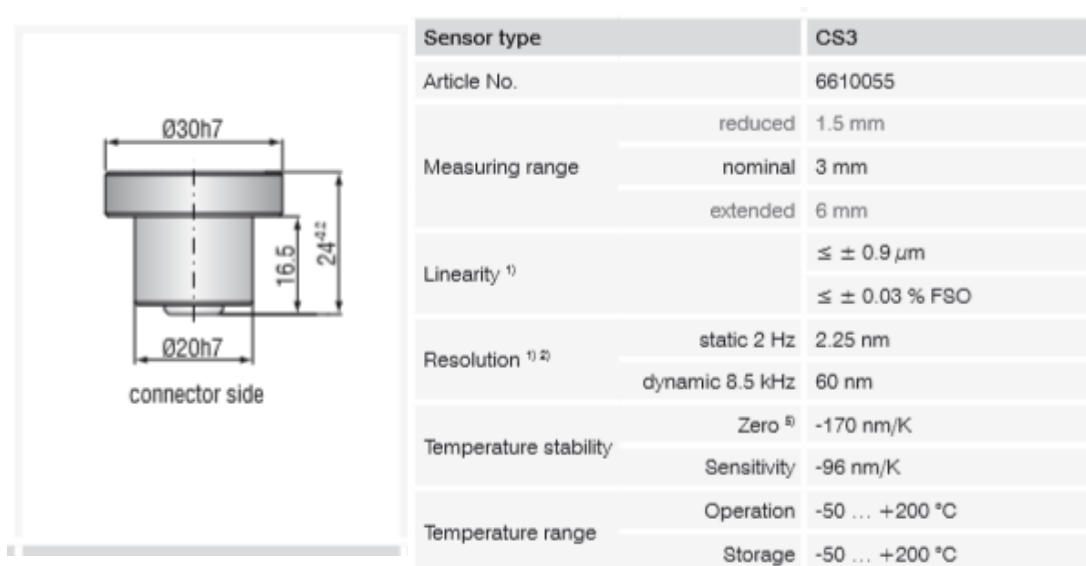


Figure 35. Capacitive sensor probe with 6 mm detection range. Source company: Micro-Epsilon America, LP.

The range of measurement for the probes is 6 mm, which is suited for this printhead set up since the flexure is designed for ± 3 mm ROM in the vertical axis, and ± 1 mm in the horizontal direction. The target surface being measured must be metallic and have a minimum radius of 27 mm. The important thing while mounting the sensors on the table is to ensure that the sensor and target faces are perfectly parallel to each other in either the vertical or horizontal planes. These probes are designed to be clamped, so more custom-shaped rigid components were 3D printed in order to create adjustable mounts, shown in Figure 36.

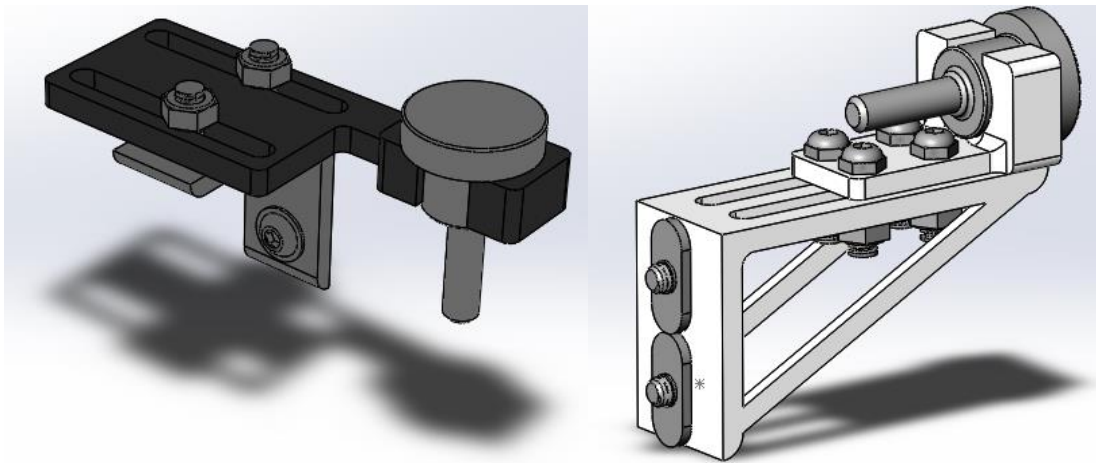


Figure 36. Sliding clamp mounts for the vertical (left) and horizontal (right) capacitive sensors.

The black piece is Onyx material while the white one is Nylon; the only reason for the difference is that a different printer was available for use at the time the latter pieces were fabricated, and the pre-loaded material was Nylon filament. The print density was increased by 20% to make up for any loss in strength. Each of these connectors shown was mounted on more spare aluminum beams of the type shown for the horizontal actuator mounts; in fact, the horizontal sensors are mounted below the actuators on the same beams. The vertical sensors are mounted on separate beams, as shown in Figure 37, and are positioned below the protruding face of the measurement surface built into the actuator connection piece. These measurement surfaces are coated with small aluminum foil sheets to allow the

sensors to detect them. The initial position is set by reading the distance measurement in real-time and adjusting the closeness of the sensors to the measurement surface until they are both 3 mm.

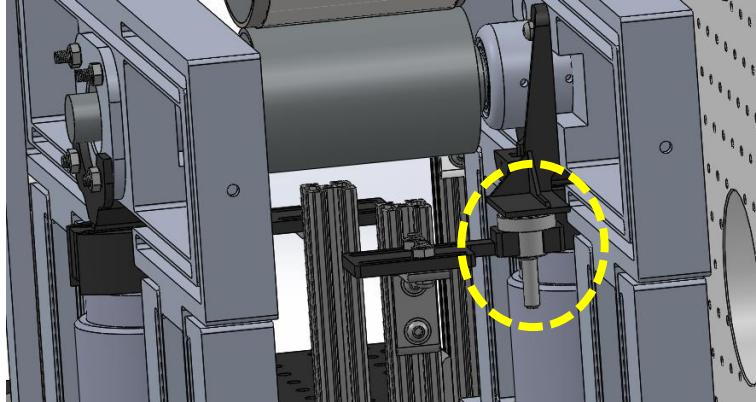


Figure 37. View of the printhead mechanism showing vertical capacitive sensor position (sensor is circled).

Reading the contact force or pressure on the stamp is far more difficult because the measurement methods are all indirect. Due to the successful print results achieved by the CUHK group, it was decided to purchase the same type of load cells that they used to measure the tension on the impression roller to within ± 0.05 N. The level of force control needed to generate prints on the sub- μm scale is estimated to be within this range, with contact forces of 3-20 N being the normal range for μCP in previously designed systems [1]. The load cells are mounted into the assembly using bolts and adapters, as shown previously in Section 4.04.

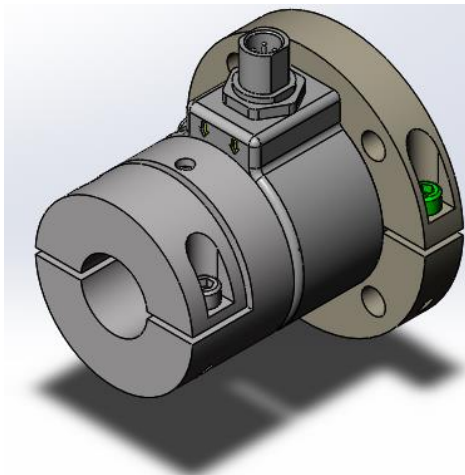
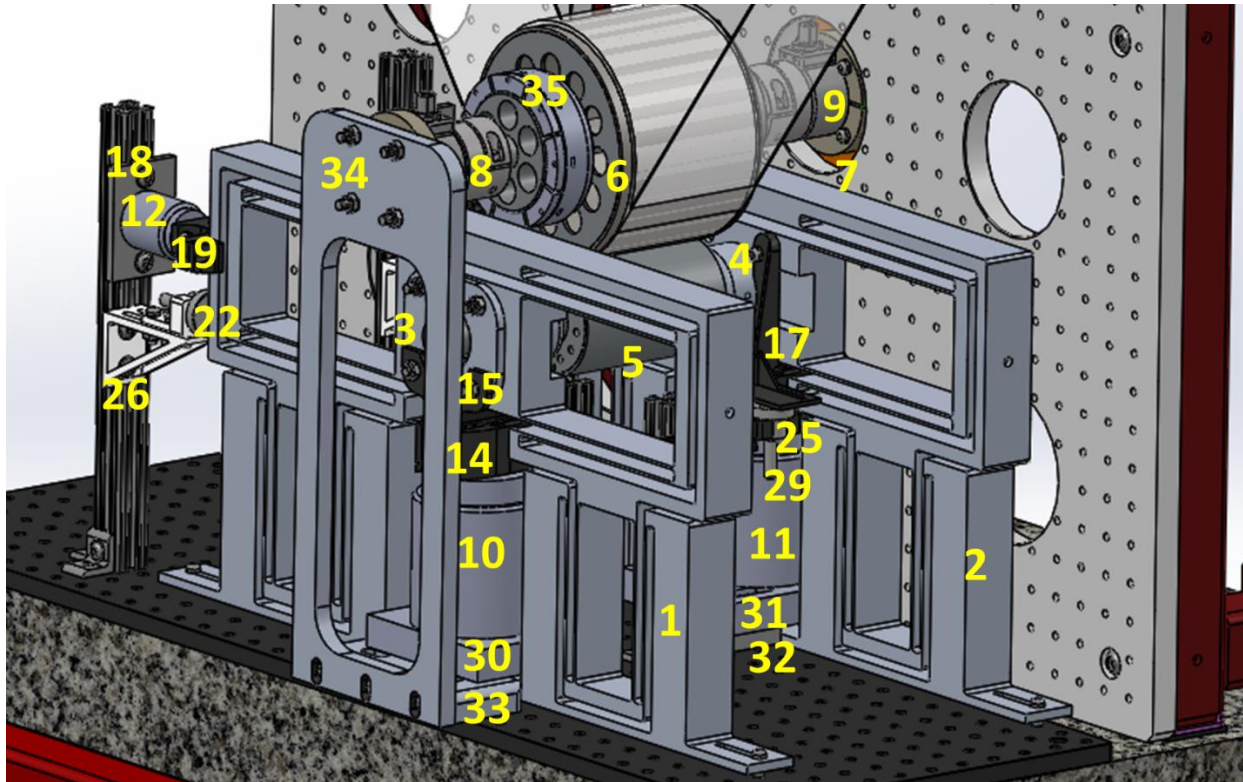


Figure 38. Load cell for tension measurement, featuring flanged shaft connection. Source company: MAGPOWR. Model: TS-25-FC EC12.

4.07 ASSEMBLY DRAWING WITH LABELLED COMPONENTS



COMPONENT LIST *blue text indicates parts that are not visible in drawing*

1) Flexure stage A	9) Load cell B	17) Large actuator clamp connection piece B	24) Capacitive sensor horizontal B	30) Large actuator support piece A
2) Flexure stage B	10) Large actuator A		25) Capacitive sensor vertical B	31) Large actuator support piece B
3) Air bearing holder A	11) Large actuator B	18) Small actuator plate attachment A	26) Capacitive sensor horizontal connection assembly A (2pcs)	32) Large actuator extra support piece B
4) Air bearing holder B	12) Small actuator A	19) Small actuator clamp connector A	27) Capacitive sensor vertical connection assembly A (2pcs)	33) Impression roller mounting piece 1
5) Print roller assembly (4 pcs)	13) Small actuator B	20) Small actuator plate attachment B	28) Capacitive sensor horizontal connection assembly B (2pcs)	34) Impression roller mounting piece 2
6) Impression roller assembly (6 pcs)	14) Large actuator flexure connection piece A	21) Small actuator clamp connector B	29) Capacitive sensor vertical connection assembly B (2pcs)	
7) Adapter load-cell to breadboard (orange part)	15) Large actuator clamp connection piece A	22) Capacitive sensor horizontal A		
8) Load cell A	16) Large actuator flexure connection piece B	23) Capacitive sensor vertical A		

red text indicates components that are pre-built e.g. actuators, sensors

Figure 39. Assembly drawing of R2R system, components labelled below.

	indicates assembly		indicates purchased part
Component no.	Material	Fab. Method	Nominal Fab. Tolerance (\pm)
1	Al-7075	Waterjet cutting	0.08 mm
2	Al-7075	Waterjet cutting	0.08 mm
3	Al-1060	CNC milling	0.03 mm
4	Al-1060	CNC milling	0.03 mm
5	Steel (assembly)	see Section 4.02	0.03 mm
6	Steel (assembly)	see Section 4.02	0.03 mm
7	Al-1060	Manual milling	0.03 mm
8			
9			
10			
11			
12			
13			
14	Onyx filament	3D printing	0.10 mm
15	Onyx filament	3D printing	0.10 mm
16	Onyx filament	3D printing	0.10 mm
17	Onyx filament	3D printing	0.10 mm
18	Al-6061	Manual milling	0.03 mm
19	Onyx filament	3D printing	0.10 mm
20	Al-6061	Manual milling	0.03 mm
21	Onyx filament	3D printing	0.10 mm
22			
23			
24			
25			
26	Nylon filament (assembly)	3D printing	0.10 mm
27	Onyx filament (assembly)	3D printing	0.10 mm
28	Nylon filament (assembly)	3D printing	0.10 mm
29	Onyx filament (assembly)	3D printing	0.10 mm
30	Al-6061	Manual milling	0.03 mm
31	Al-6061	Manual milling	0.03 mm
32	Al-6061	Manual milling	0.03 mm
33	Al-6061	Manual milling	0.03 mm
34	Al-6061	Manual milling	0.03 mm
35			
MAXIMUM FABRICATION ERROR (SUM)			1.52 mm

Table 4. List of all system components shown in Figure 39, with material info and fabrication tolerances provided.

5

EXPERIMENTAL TESTING AND RESULTS

5.01 R2R Setup in Lab

The first objective of this thesis was to assemble the μ CP printhead with all its components onto the current lab table with its restrictive spatial constraints. This proved to be successful despite difficulties with calibration and nonuniformity of certain fabricated components, as demonstrated in Figure 40 and Figure 41. There were no issues with fitting the components onto the breadboard.

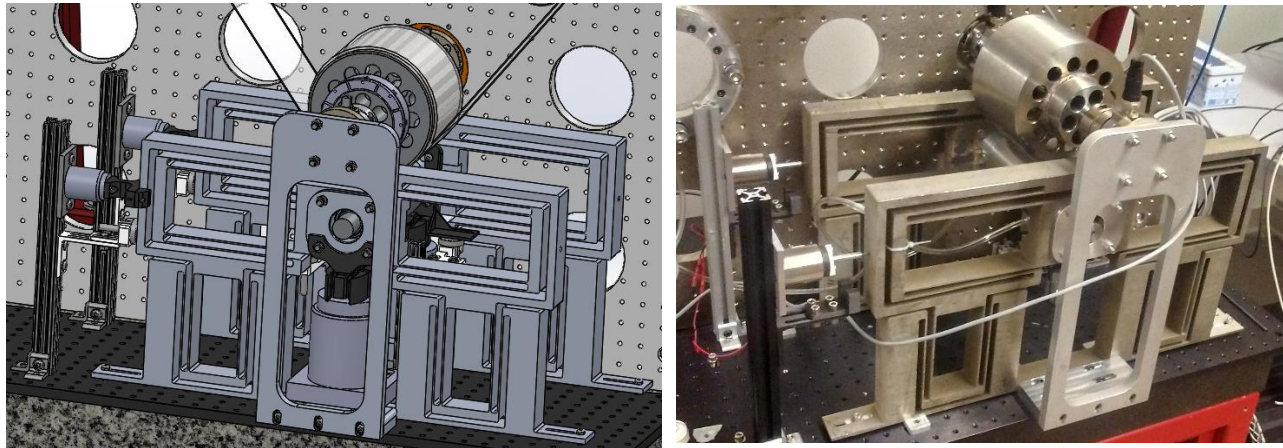


Figure 40. Microcontact printhead design (left) and real setup (right) but without vertical actuators, encoder, or web.

The aim of achieving large area prints, with resolution comparable to the best of the past MIT work and the CUHK system which achieved patterns with 300 nm linewidth on a 4-inch wide substrate, is still not completed. Before the system is ready to print, a patterned PDMS stamp must be generated and wrapped onto the print roller. The inking mechanism must also be considered: whether the stamp should be pre-soaked in thiol ink solution, or if a continuous inking system (i.e. ink bath interfacing with print roller during operation) should be implemented. And apart from the remaining mechanical parts to be optimized and designed, the coupled control issue of determining the appropriate relationship between force control and displacement control must be resolved.



Figure 41. R2R setup in action: running web tension experiment. Note that lower right idler roller has been swapped for tension measuring roller.

5.02 Dynamics Data from R2R Setup

The third objective for the R2R system is that it must be capable of controlling the position of the print roller and the contact force on the stamp using the actuation and sensory feedback. After being installed, the capacitive sensors were used to test the natural frequency of oscillation of the flexures individually. Figure 42 shows the oscillations observed in two different tests: (1) ambient vibrations with no disturbance and (2) vibrations with initial disturbance applied – a light tap from hammer.

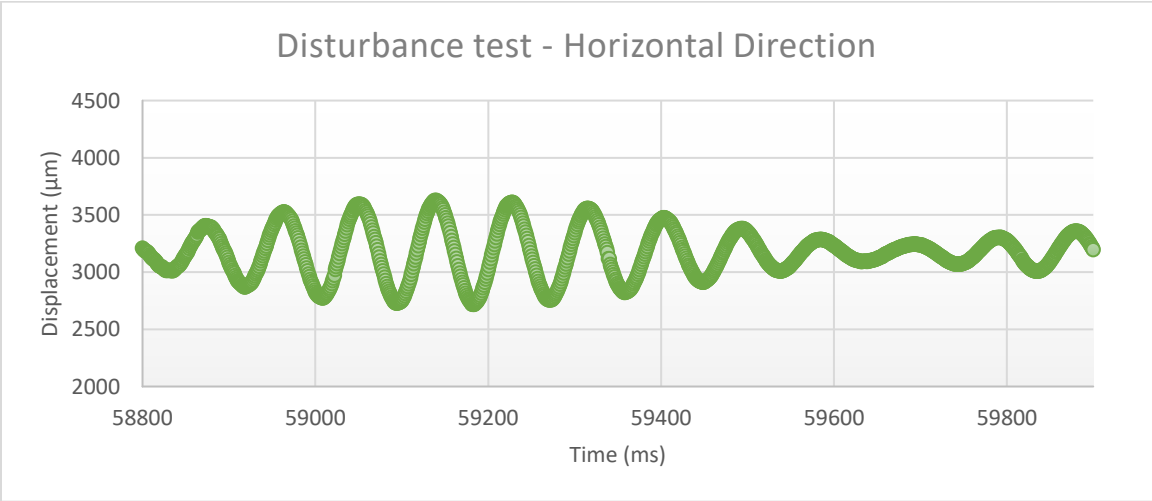
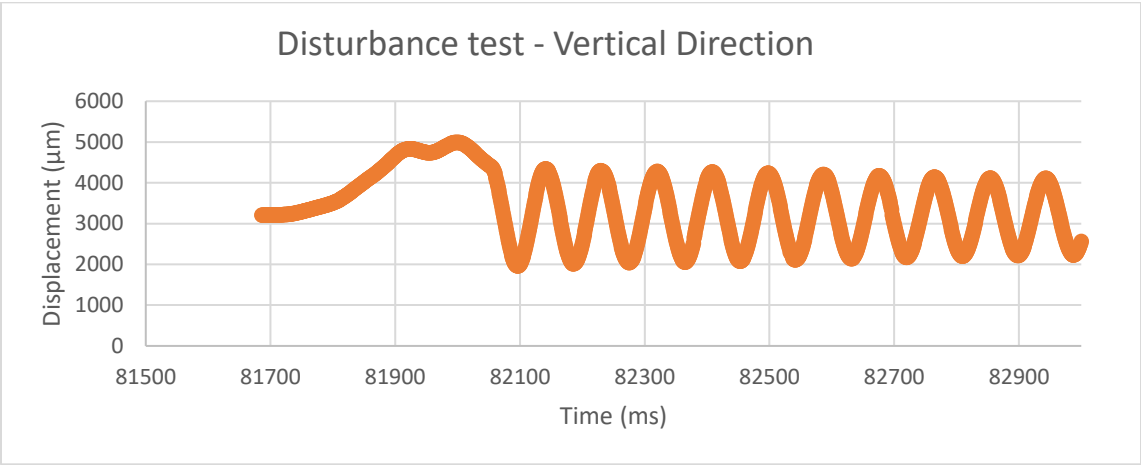
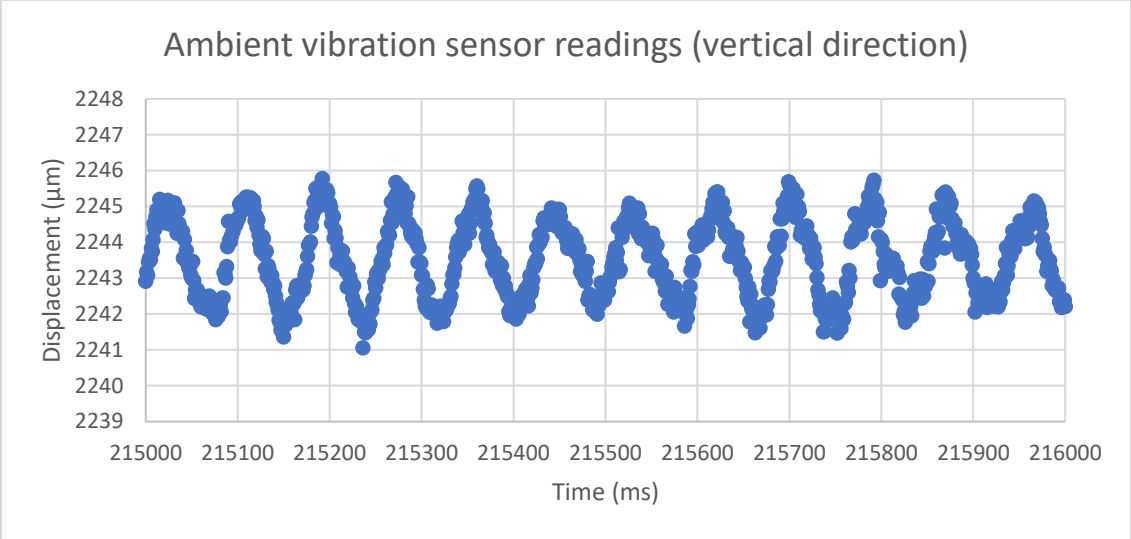


Figure 42. Vibration experiments on single flexure mechanism.

The ambient environmental vibrations in the horizontal DOF were rough and non-discernable. But for the three charts shown, the natural frequency (estimated by counting the peaks) is found to be 12.0 Hz, 11.3 Hz, and 11.7 Hz, respectively. This shows that the natural frequency of the flexure in both DOFs is approximately the same, between 11-12 Hz.

This is not far off the simulation estimates of the flexure natural frequency without the actuator clamp attachments. This was calculated to be 14.8 Hz for both horizontal and vertical DOFs (the mode was simultaneous vibration). The decrease seen in the experimental value is most likely due to differences between the dimensions in the drawing compared to the real flexures. The beam widths of several of the lower P-joint beams shows variation of ± 0.7 mm from the drawing. These joint structures were formed during the waterjet cutting phase: the two flexures were machined by waterjet separately, which is most likely the main cause of the dimensional errors. Other fabrication errors can be related to the difficulties in clamping the flexures while machining the slots and holes for actuator and table connections in the correct places (discussed in *Chapter 4.01*).

Unfortunately, further planned experiments on the coupled system were postponed due to the altered lab schedule since the closure of UMass Amherst campus in late March 2020.

5.03 Positioning & Force Control/Sensor Operation

The results of the force sensing experiment with the load cells were equally inconclusive, but they did reveal more about possible calibration and alignment errors. For this experiment, the coupled mechanism with print roller and all actuator connections were in place, making it accurate to real printing conditions with the system. The actuators apply upward force on the impression roller with a non-patterned PDMS stamp wrapped around the print roller – which simulates the forces at play in the printing

process. The goal was to balance the system so that both load cells gave the same reading and observe the asymmetries in the input forces from the vertical actuators on both sides. If the system is balanced, then equal upward forces on both sides would result in equal force sensor readings. This data could then be used to balance the system if it were misaligned. The results were far from balanced.

To begin with, a circuit model [58] of the VCA, shown in Figure 43, is used to accurately determine the upward force generated for a given input voltage. The parameters used for solving the equations are found in the actuator datasheet provided earlier. These include the resistance, inductance, time constant, and force constant. Knowing the input voltage (which is entered into the LabVIEW interface) and these other parameters makes it easy to calculate the steady-state current, which is then multiplied by the force constant to get the motor force.

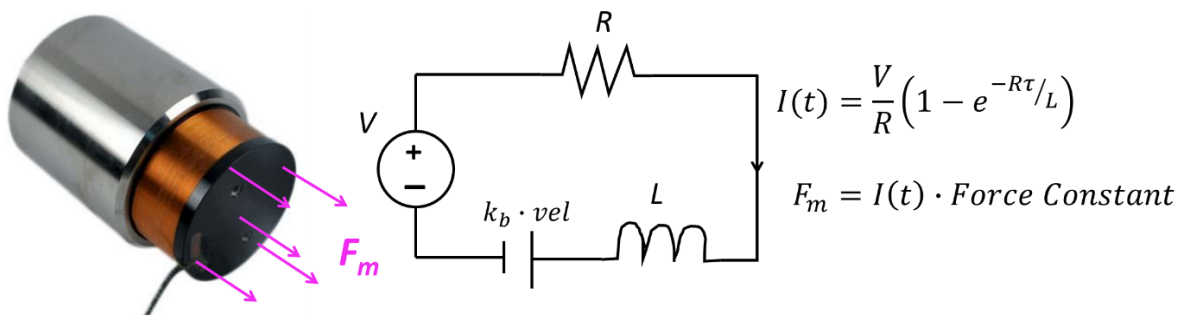


Figure 43. Circuit model and equations for the VCA.

This relation from the VCA circuit model provides the missing information to check if the system is unbalanced. The diagram in Figure 43 shows the system with the input voltages, motor forces, and load cell readings displayed for an initial position with nearly-balanced contact force between the print roller (with stamp) and the impression roller. The weight of the roller, bearings, and motion stage is also represented as a force in the diagram. The error/inconsistency in the load cell readings is approximately ± 0.1 N, which is about twice the nominal resolution of the sensors.

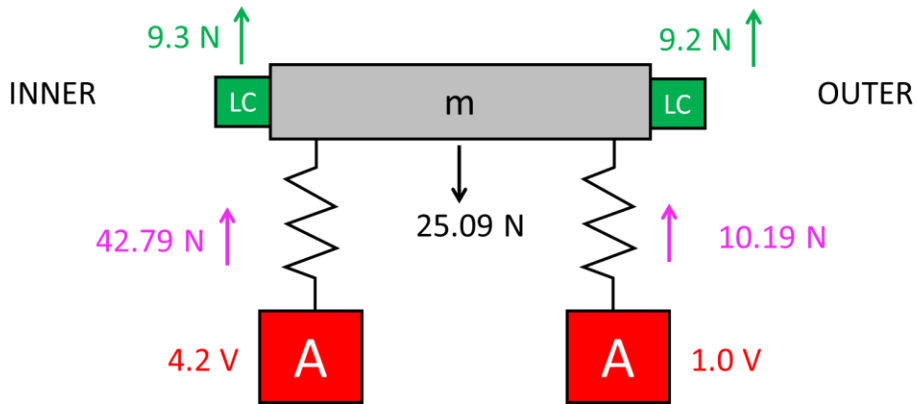


Figure 44. Simplified model of the print roller mechanism. The purple text indicates the force generated by the VCAs.

As is shown from the model, the VCA forces are wildly unbalanced while the load cell forces are the same (within the margin of error). The plots in Figure 45 emphasize this by showing the compiled data from another experiment, which has three stages of motion. In stage 1, the rollers are contacting with balanced force readings from the load cells. Stage 2 sees the actuators apply equal force steps on both sides, compressing the stamp and increasing contact pressure. In stage 3, the rollers break contact.



Figure 45. Plots from load cell calibration experiment. Tables display force data from both sides' VCAs.

The level of imbalance in the input force while the load cell readings are much closer in value indicates some form of misalignment in the system, fault in the calibration, or both. There is a high chance that the problem is largely due to the impression roller not being centered on its shaft – it is closer to the inner breadboard than the opposite side frame by about 25 mm. Given that the impression roller, minus its inner shaft, weighs a substantial 2.87 kg (6.32 lbs), it may very well be imposing a moment on the inner load cell that requires a greater push from the inner VCA-powered mechanism to compensate. Verification of this theory is necessary. Asymmetry in the frame of the impression roller most likely contributes to this effect. For future designs, the impression roller frame, particularly on the outer end, will need to be examined closely to ensure it is balanced.

5.04 Engineering Problems Encountered & Solutions

Many engineering problems arose during assembly and calibration of this R2R system, all of which proved to be useful learning experiences, as they became points of consideration while designing the optimized second version of the printhead.

To start with, the flexure height was deliberately made slightly too short to allow the motion stage to reach the level that it needed. The reason was that the flexure was one of the first components to be designed, so it was decided to leave some tolerance in case the impression roller assembly would hang lower than anticipated. This necessitated elevating the flexure by placing small 0.25” plates between it and the table. This solved the problem without difficulty, however in future it is better to avoid this by knowing the exact constraint from the beginning and designing for that. This is because any plates added to elevate the flexure may be non-uniform or rough enough to create a small misalignment of the mechanisms. Since the flexure is the component designed with the tightest tolerances, it is better to just use its own bottom surface as the base of support.

The next issue is with the alignment of the motor rollers and idler rollers. This was brought up previously in Chapter 4.04, but there is no way to accurately gauge whether the rollers are aligned perpendicular to the standing breadboard, even using the laser alignment tool. A method that was devised but not yet tested is to use a monolithic lightweight piece designed to be bolted onto the frame with a perfectly right-angled configuration. The laser alignment tool can be strapped to it and used to correct the alignment of other rollers. So far this has not been tried, but the design for the component is shown in Figure 46.

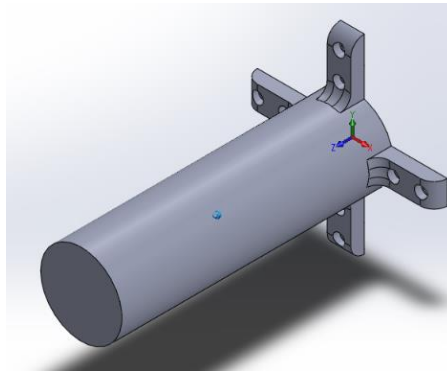


Figure 46. SolidWorks drawing of unused asset – roller alignment post.

Several times while running the machine, the air bushings hissed loudly due to air leakage, and the friction on the print roller increased significantly. When thread locking tape was added to the air fittings before reattaching them to the mounting block, the problem was solved.

A major problem discovered late in the project was that the table breadboard is slightly misaligned with the standing breadboard. This is due to errors in setting up the granite table and frame for the standing breadboard, which was done before the start of this thesis work. Because these errors would have required complete re-assembly of the table and removal of the granite to fix, it was instead decided to re-align the bottom breadboard by making some small adjustments. The aluminum breadboard was brought to the MIE machine shop and the four holes for the granite table connections were widened into

slots to allow adjustment. The breadboard was re-mounted on the table and adjusted by hand, while using calipers to confirm that the distance from the standing breadboard was equal on both left and right sides.

The last point to note is regarding the horizontal actuator mount. Currently, the aluminum column that it is mounted to has been observed to experience vibration during operation of the actuator. This is evidence that the component requires a more stable support. A simple plan (shown in Figure 47) was devised to fix this problem by using another one of these beams and more of the connector pieces.

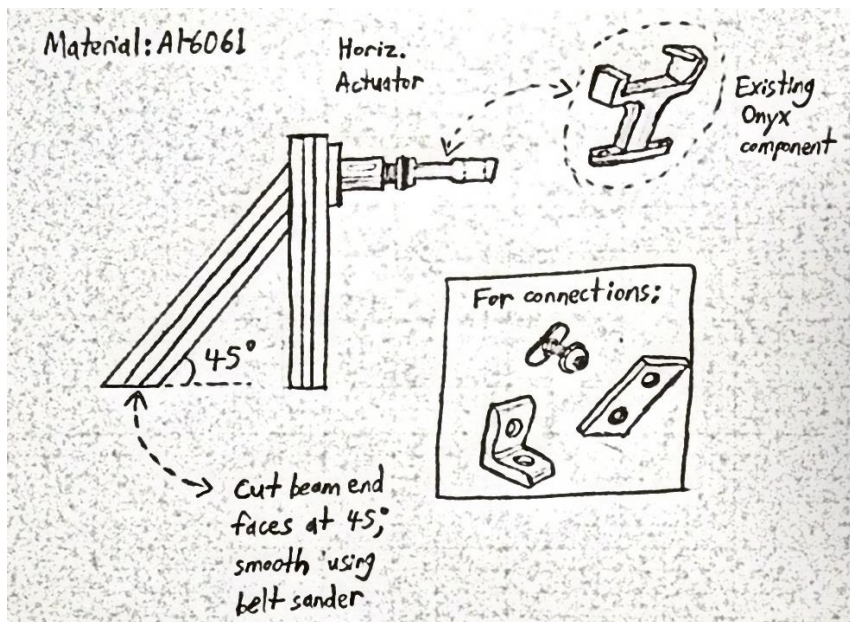


Figure 47. Sketch of improved mount for small VCA.

The faces of the beam could be cut at a 45° angle in the MIE workshop using the band saw with a right-triangular shaped block, and then smoothed using the belt sander. Following this, the beams could be easily linked together using the same kind of connection pieces that are readily available in the lab. Implementation of this plan was forestalled by the closure of the MIE workshop.

5.05 Work on PDMS stamp / Validation of Test Prints

Lastly, a small portion of the work was focused on learning the PDMS curing process for generating stamps, analyzing stamp microfeatures using interferometry, and performing compression testing on lab-generated samples of PDMS. The reason for this work is that the machine is incomplete without the stamp and gaining understanding of the stamp's mechanical properties could be useful for characterizing the dynamic behavior of the print system. Therefore, a diagram and images of the compression test experiment are shown in Figure 48 below. The method was simple: using this setup, the PDMS was compressed between sheets of sandpaper (to impede any sliding) and the resultant stress-strain curve was obtained. The slope of the linear portion represents the modulus; using this method, the value came out to be 15.81 MPa, which is unusually high compared to online estimates of 3-5 MPa for PDMS. A hypothesis is that the modulus of compression for a very thin (~1mm) sheet of PDMS, such as the stamp that was tested, is significantly higher than the commonly referenced figures which rely on tensile testing of cross-sectionally larger samples. Waiting on further experimentation to confirm accuracy of results.

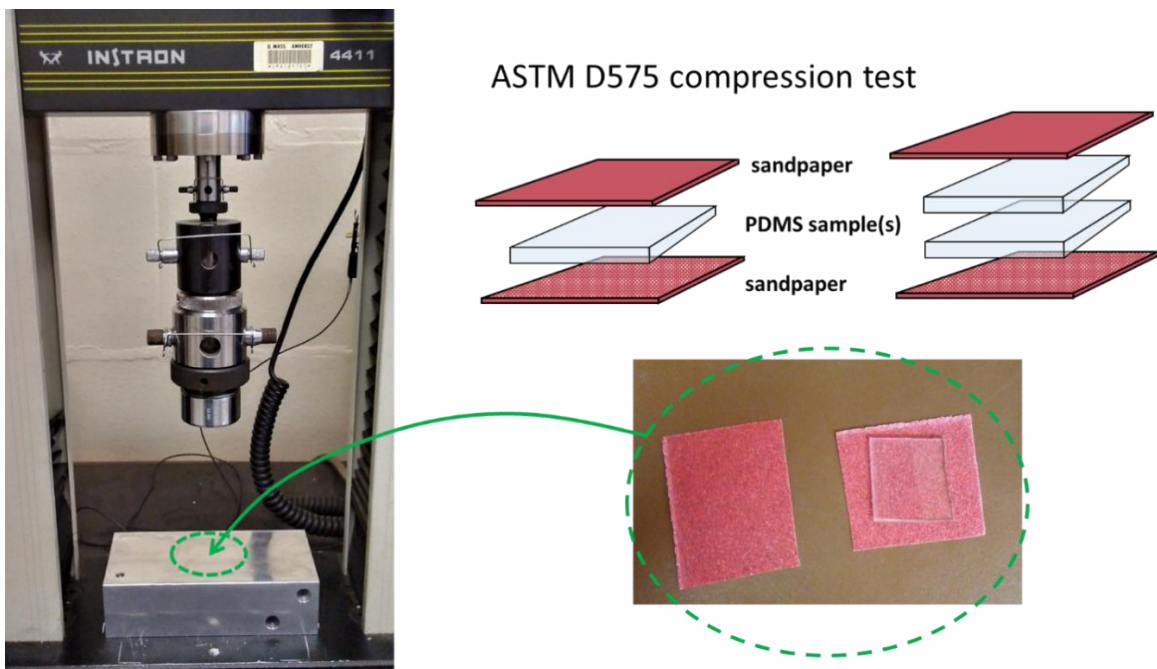


Figure 48. Compression testing procedure for PDMS stamp pieces (cut from larger stamp).

6.01 Optimized Flexure Assembly

With the knowledge and understanding gained from fabrication, assembly, and testing of the prototype R2R print system and all the weaknesses of that design, μ CP Printhead version 2.0 is set to vastly outperform its predecessor in precision of motion, bandwidth, manufacturability, and ease of assembly and calibration. At the core of the design improvements been made in the last six months has been the development of an entirely new, compact, and optimized flexure mechanism.

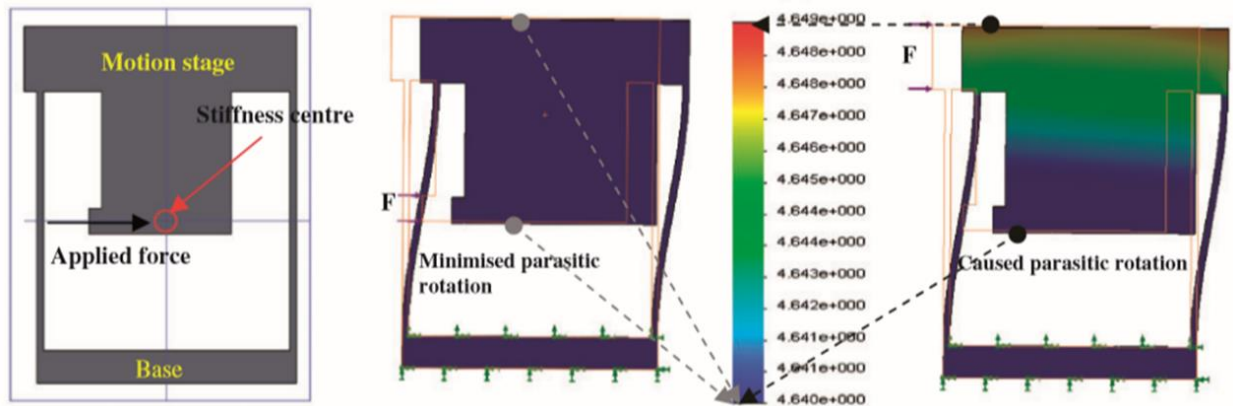


Figure 49. Method for applying force to a parallelogram joint with minimal parasitic rotation. [59]

Most of the issues with the previous mechanism design are due to the excess of interface components for connection with other parts of the system. The most egregious fault is the actuator clamp connectors, with the awkward decoupling mechanism to prevent the actuators from interfering with each other (see Figure 34 and the rest of *Chapter 4.05*). This mini-flexure decoupling mechanism increases the asymmetry of the compound P-joint structure for allowing horizontal displacement of the motion stage, creates parasitic motions that interfere with the movement precision, and it has difficult-to-analyze negative effects on the dynamic model of the system. Therefore, a crucial aim of the new flexure design

is to achieve decoupled actuation within the core mechanism itself, negating the need for external bearings or other non-rigid connections.

After careful study and analysis, a method for accomplishing this goal was determined based on exploiting a compliant mechanism motion principle known as the center of stiffness (see Figure 49). In a 2014 Journal of Mechanical Engineering Science paper by Dr. Guangbo Hao, it is explained how the parasitic rotation inherent to asymmetrical P-joint structures may be countered by changing the force application point [59]. By repositioning this point in line with the stiffness center of the mechanism (defined by shape) one can achieve translation of the motion stage with effectively minimized parasitic rotation. This idea is implemented in the novel flexure design, shown in Figure 50.

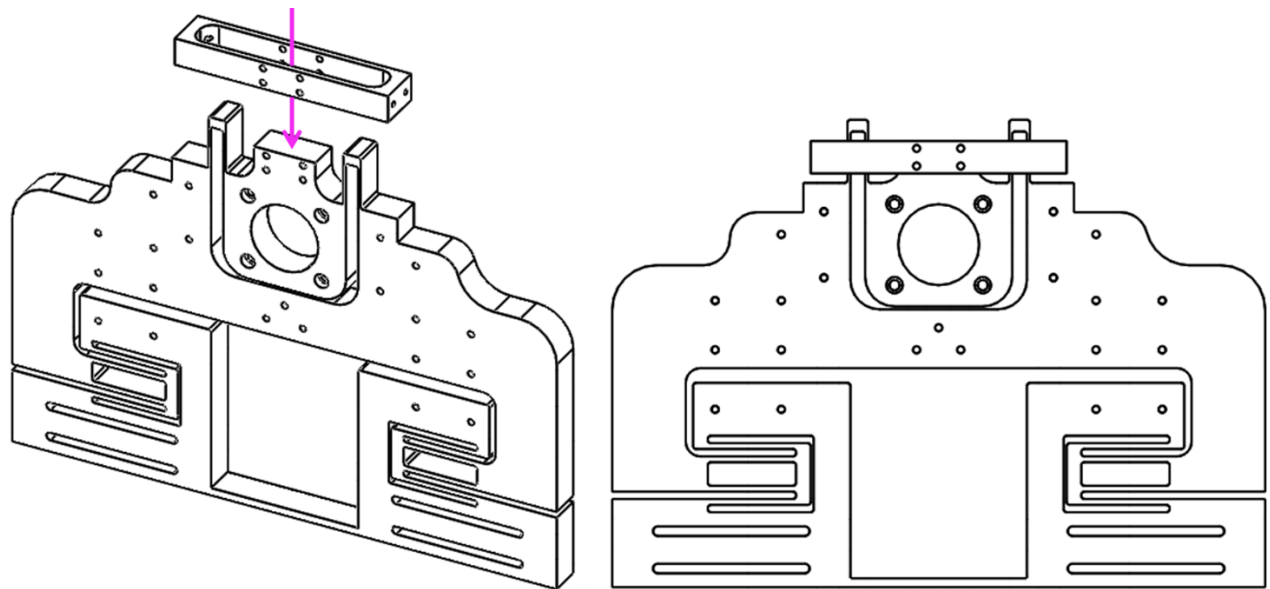


Figure 50. New flexure design, 2 pieces, polycarbonate

Instead of being mounted to the table, the small VCA can be mounted on the shoulder of the new mechanism via a simple, secure holder. From this position the actuator can apply force directly in line with the stiffness center of the newly designed compound P-joint, producing horizontal translation of the motion stage. This action is completely decoupled from the vertical motion produced by the large actuator

which is mounted securely to the table and linked to the flexure via another rigid, precise connector. A counterweight to the VCA can be placed on the opposite shoulder using the same connection type, to offset any asymmetries that would affect the dynamic behavior.

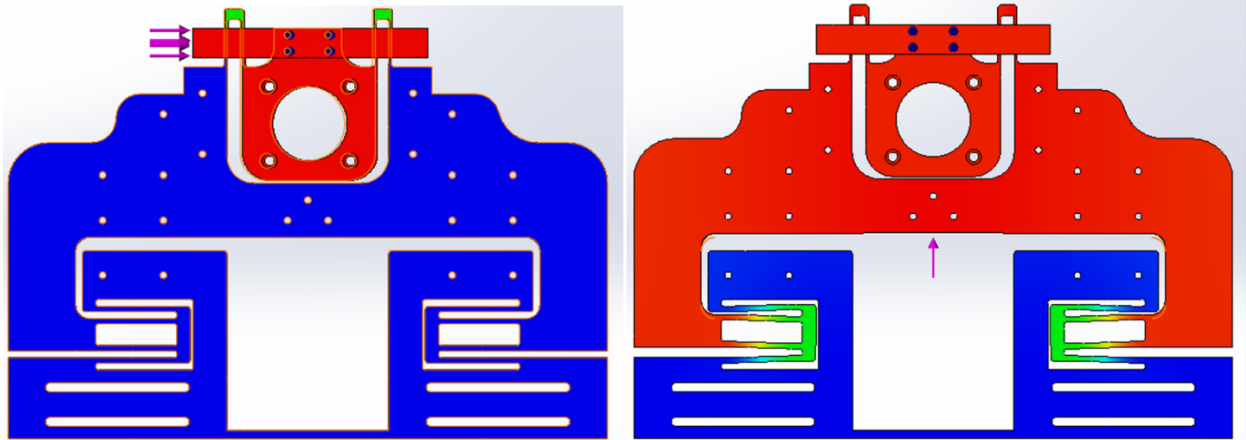


Figure 51. FEA simulated actuation force resulting in translation in horizontal and vertical DOFs.

Instead of aluminum alloy, this flexure is fabricated out of polycarbonate sheets which have a far lower stiffness. This allows the new design with its more compact structure to achieve the necessary ROMs in both dimensions without requiring stronger actuators. As shown in Figure 51, the translation achieved is with minimal parasitic rotation – solid colors indicate uniform displacement. The maximum stress to the beams under full load from the VCAs is within the factor of safety for polycarbonate (yield strength: 62 MPa).

Despite the change to a more compliant material, frequency analysis reveals that the natural frequency of oscillation in the vertical DOF is 24.03 Hz which is a 59% increase over the previous design's simulated result. This demonstrates the improved dynamic performance of the new mechanism. Other advantages of using polycarbonate are (1) the transparency makes it easier to monitor the system in action with the eye or with camera/vision systems, (2) the weight of the flexures is reduced from 6.04 kg to 2.23 kg and (3) machining the softer material via CNC milling and other methods is easier and less likely

to result in thermally-induced warping of edges, radii, etc. The consequence is that with a more compliant material, the flexure is more susceptible to deformation in the z-plane. This could be easily countered by doubling the sheet thickness, however that poses difficulties given the spatial constraint of the table. The expected stress experienced by the mechanism in the z-plane during print operation is still lower than the amount needed to produce significant out-of-plane displacement, but vibrational effects must still be analyzed and anticipated before fabrication.

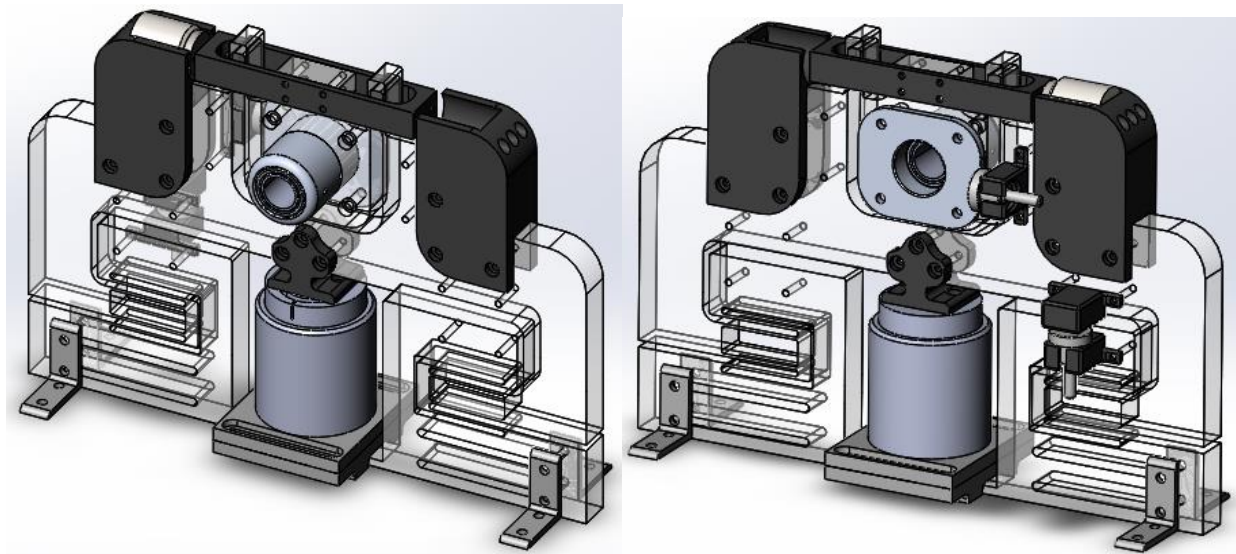


Figure 52. New printhead mechanism assembly design, front and back, featuring capacitive sensors and VCA connectors built into mechanism. Nuts/bolts omitted from drawing.

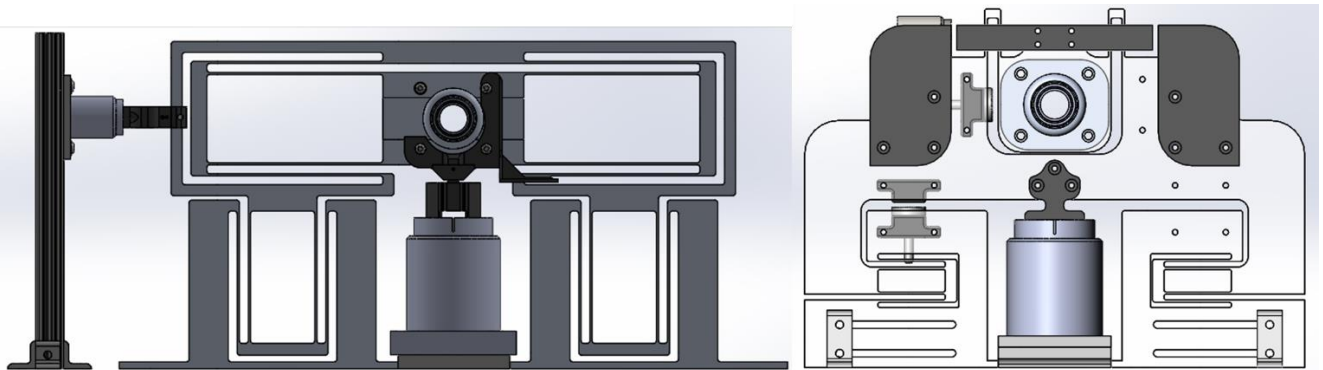


Figure 53. Same scale comparison between versions of printhead mechanism, including actuation and sensing components.

6.02 Redesigned Lightweight & Transparent Rollers

Since the idea for using polycarbonate as the material for the new flexures, recent experimentation has focused on the feasibility of redesigning the printhead rollers (print and impression rollers) out of polycarbonate as well. Just as rough steel tubing was easily acquired from McMaster-Carr, polycarbonate tubing of the same dimensions may be brought in, machined to the precise OD and wall thickness, and processed so that the surface roughness is reduced to the necessary levels. Polycarbonate components may be glued together securely via an inexpensive solvent welding process, which means that the assembly of polycarbonate rollers should be far less challenging and time-consuming than it was for the steel ones. Importantly, the smoothing of polycarbonate surfaces is performed via vapor polishing, which can reduce the surface finish to $32\mu\text{in}$, or under $1\mu\text{m}$.

The density of polycarbonate ($\sim 1.20\text{ g/cm}^3$) is only 15% of the density of stainless steel ($\sim 8.00\text{ g/cm}^3$). If one imagines a simplified theoretical system consisting of a motion stage supported by a double P-joint mechanism, then according to Hooke's Law and the simple harmonic motion equation, decreasing the mass of the motion stage to 15% of the original would result in a 258% increase in the natural frequency of the system. This is a drastic improvement in the bandwidth of the system without even accounting for changes in the flexure mechanism at all, only reducing the weight at the center.

Lastly, the use of clear rollers is advantageous due to the potential for real-time visual monitoring of the print product via optical instruments placed over/under the impression/print roller. This would permit for another layer of control, visual feedback, to be added to the system to allow observing of pattern fidelity, linewidth, and other quality metrics for the printed micropatterns.

6.03 Cylindrical PDMS Stamp Fabrication

Earlier in *Chapter 2.03*, it was discussed how one of the MIT works [35] included a novel patterned PDMS stamp that was generated in a cylindrical shape, as opposed to the typical flat stamp. This design is advantageous because it negates the issue of wrapping the stamp on the roller and having a seam that affects the concentricity of the roller and the micropattern distortion of the print result. A cylindrical stamp may simply be slid onto the roller while being expanded by compressed air, as is the case of the MIT design. However, there were many faults with their design method being that it was expensive, inflexible, and generated a pattern with undesired distortions. They used a robotic mechanism to laser-etch the pattern on the inside of a drum, and then used the drum as the mold for their stamp. Because of the limited space inside the drum, and the rotational travel path of the laser, the etching resolution was poorer than it would have been on a flat surface.

An alternative method, in some ways the inverse of the one previously described, has been proposed by the author. Although the idea is only in the early concept stages and still requires refinement, it has the potential to achieve much higher resolution than those before it. Figures 53 – 55 attempt to illustrate the basic concept of the idea to the reader.

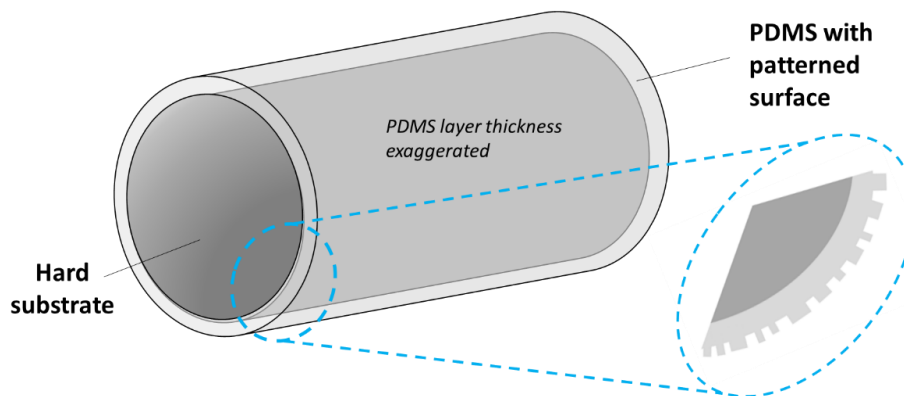


Figure 54. Desired cylindrical PDMS stamp with outward facing pattern.

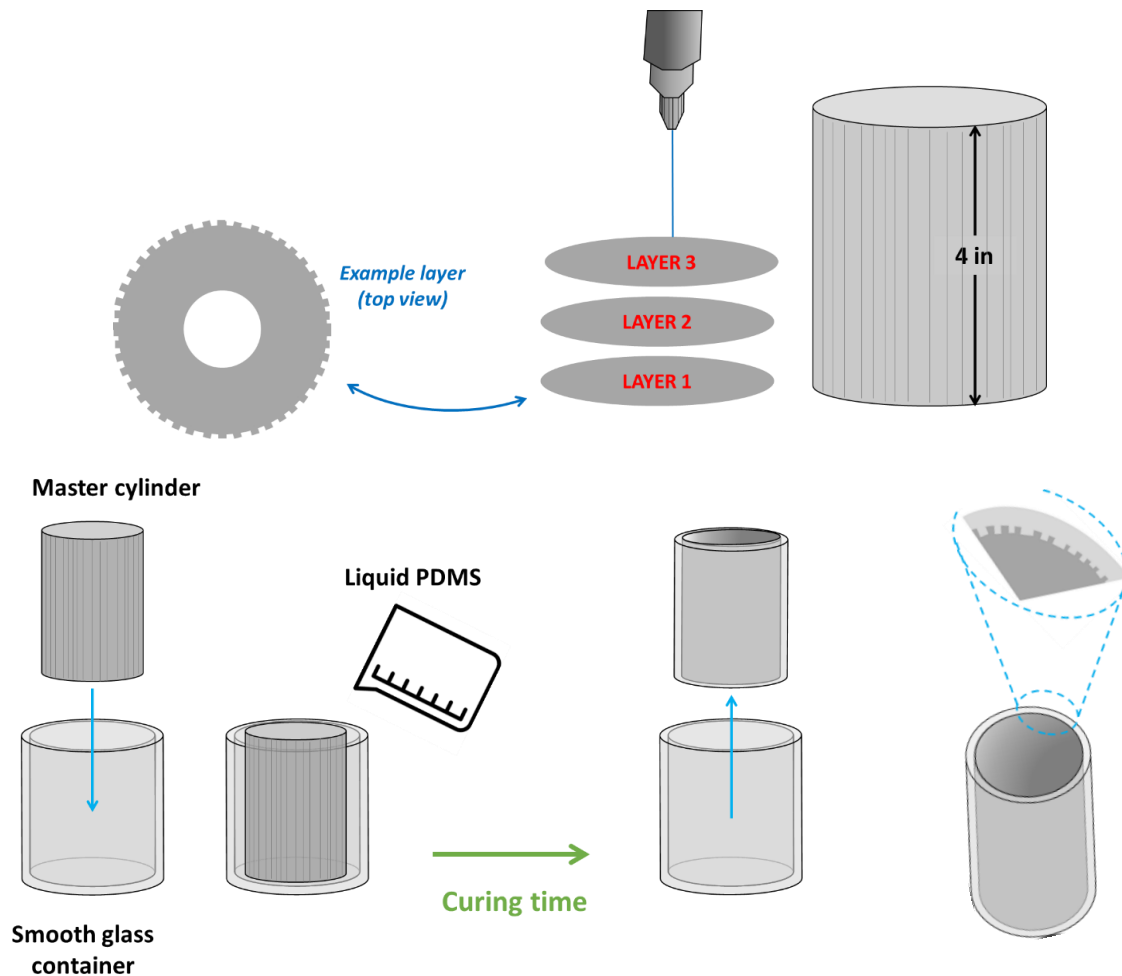


Figure 55. Diagram showing fabrication of patterned master cylinder, which is used in the mold to create a PDMS stamp of uniform thickness. The catch is that the pattern is on the inside of the cylinder rather than the outside.

Once this patterned stamp is generated with the pattern on the wrong side, it must be reversed to achieve the desired outcome (see Figure 54). This could possibly be accomplished by using controlled airflow using a specially designed instrument that channels compressed air in such a way to “unwrap” the stamp from the master cylinder and flip it inside out. A crude concept sketch of this idea is shown in Figure 56. Since the MIT work demonstrated that controlled airflow could be used to expand the diameter of the stamp in order to slide it onto the print roller, it seems possible that a similar method could be used to invert it: perhaps in combination with another mechanism.

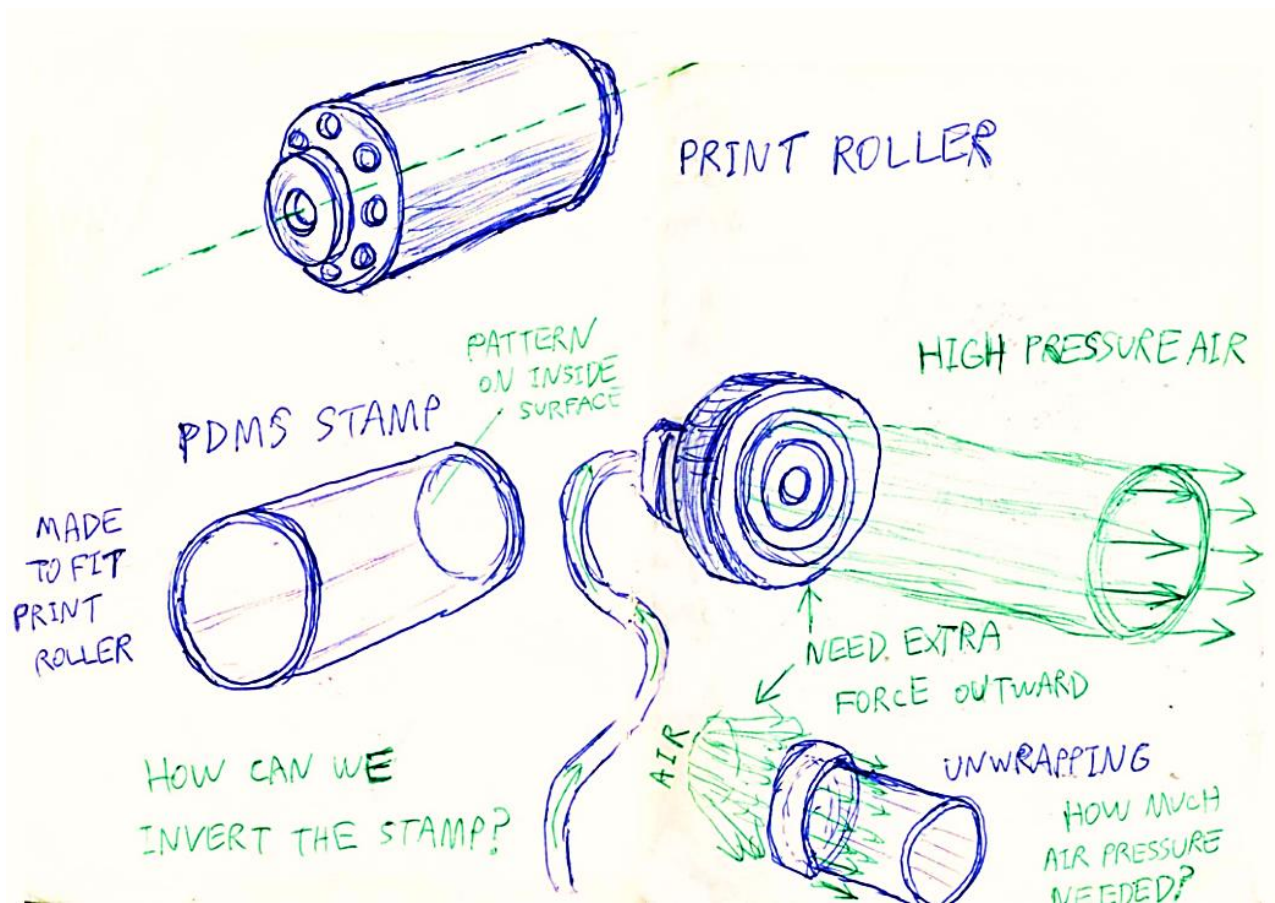


Figure 56. Sketch from notes about idea for reversing/unwrapping PDMS stamp.

If this fails to work, other ideas for inverting the generated stamp have been under development as well, including a method of using the R2R system itself to align the stamp on the print roller. This is shown in Figure 57.

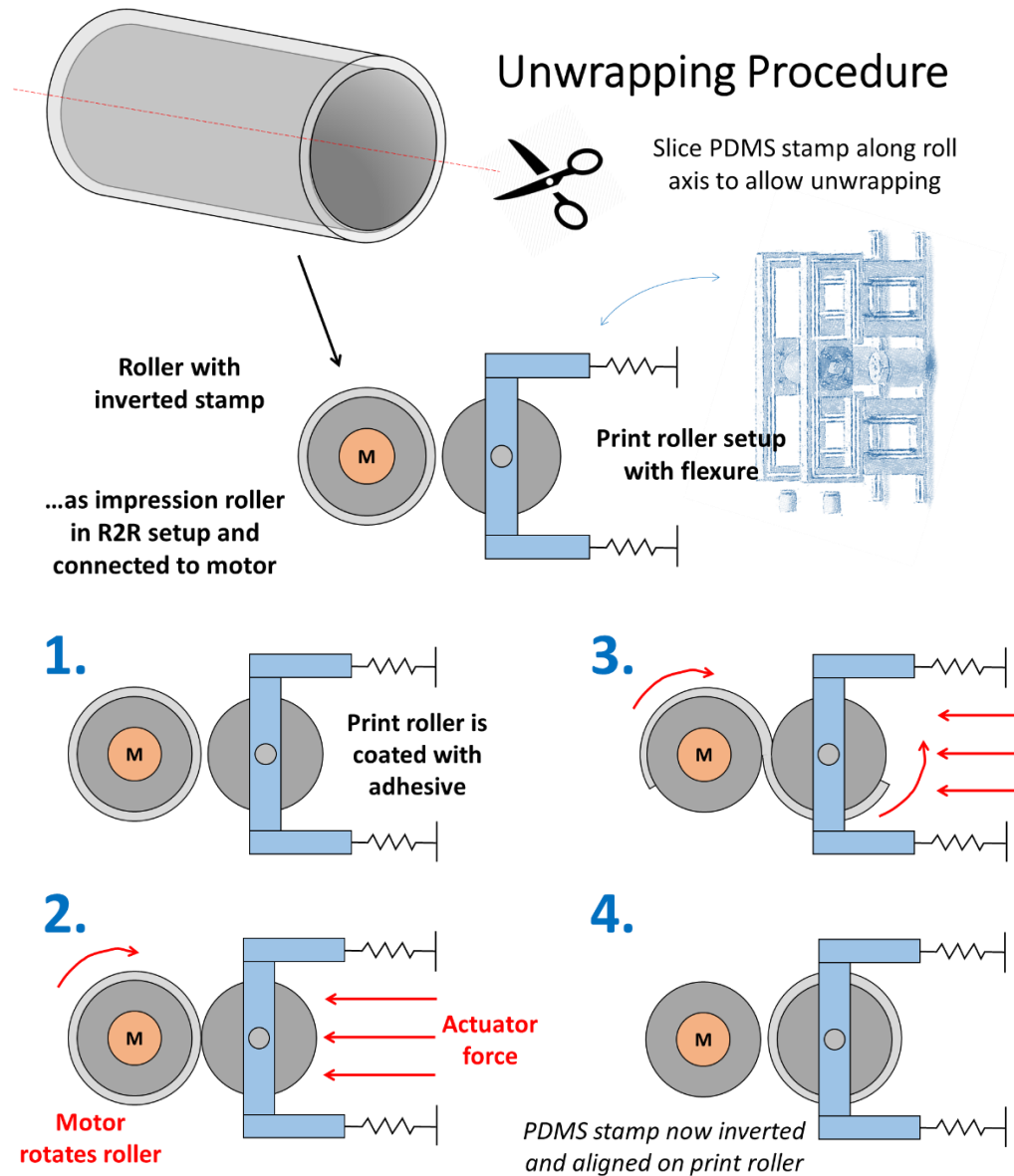


Figure 57. Alternative method of using the R2R system to invert the stamp from the master. Note that in this case, the master itself is set up in the position of the impression roller (where the imp. roll. would be in the normal setup).

While work is being done on fabrication of the new flexures and printhead assembly, finalizing these design concepts for the cylindrical stamp will become top priority. With this last piece, the design for the enhanced R2R μ CP printer will be finalized and ready for testing.

7.01. Synopsis of Work/Accomplishments

Although the experimental printhead design prototype has not reached the point where it is ready to achieve the high-print resolution targets that are the aim of this work, it has paved the way for an optimized version of the system that corrects many of the faults of its predecessor to be made (see *Chapter 6*). 33 individual pieces were designed and fabricated for the current assembly, not counting parts such as the actuators, sensors, or bolts, etc. The key components to this novel design are the print & impression rollers and the flexure mechanisms, which were designed analytically to determine the ROM, natural frequency of oscillation, and whether the stress concentrations would exceed yield/fatigue strength. Despite engineering problems that arose during the assembly and calibration of the mechanisms, the devices' ROM and dynamic performance closely matched the analysis results. With improvement of the linkages' designs and streamlining of the assembly components, the original objective of achieving high resolution control of the contact force, to the order of ± 0.01 N, and of the printhead alignment, to the order of 500 nm, may potentially be within reach.

7.02. Unresolved Issues

As anticipated, there several significant issues and gaps in the currently installed system that remain to be addressed. Future work must answer these problems with design solutions for the R2R μ CP device to attain print resolution comparable to the cutting-edge systems developed by MIT and CUHK labs.

The first concern is finding a reliable method of achieving accurate centering of the axial position of the print and impression roller cylinders on their shafts. If these cylinders, which make up a large portion of the weight of their respective rollers assemblies, are not exactly centered on the shafts, then the resulting asymmetry in the z axis will throw off load cell readings and create an unbalanced system where one motion stage requires more actuation force applied than the other in order to balance the tilt. This not only throws off the calibration of the sensors, it also negatively impacts the dynamic performance of the mechanism due to the asymmetry.

Exact calculation of the center of mass location for both rollers has already been achieved in simulation, but a method for determining this information for the real assemblies has yet to be found. Even small material inconsistencies such as weld beads and the dowel pin holes can throw off the symmetry of the roller assembly. Currently the best solution seems to be rethinking the design, and possibly the material choices (see *Chapter 6.02*) for the rollers themselves. If these can be made with fewer parts/connections, that makes it less difficult to analyze the geometry and determine the mass center experimentally, and thus align the rollers in the z axis.

A minor issue related to this one is that a mechanism for constraining axial sliding of the print roller shaft in the z axis has yet to be built. However, ongoing work includes a design for a simple, lightweight, 3D printed thrust bearing to be attached to the flexure outside the air bearing mounts that constrains the motion to $\pm 200 \mu\text{m}$ travel in the z direction. The precision is limited by that of the fabrication medium, so other options are also up for discussion. Simply using C-clips placed by hand would also constrain the motion as is done for most air-bushing applications, but this is insufficiently precise for our system beyond the initial tests prints.

The air bushings installed allow near-frictionless rotation of the print roller, but the ends of the impression roller must be clamped to the load cells for them to return the necessary force readings. This,

combined with the increased inertia of the heavier impression roller, means that there is an imbalance in friction for the two rollers – both static friction and rolling friction. Currently this has not seemed to present any challenges to system operation as the impression roller still freely rotates without difficulty, but it is unknown if this imbalance has any effect on the contact pressure between the stamp and printhead assembly. This must be studied further during the late-stage testing of the future system.

Lastly, there is the concern regarding the accuracy of indirect contact force measurement using load cells. Improved understanding of the system dynamics and material properties of components will help us understand the relationship between the measured force on the impression roller shaft and the actual contact force. No past R2R system has employed a truly direct means of measuring contact pressure on the stamp, but that does not mean it cannot be done using cutting-edge methods. For example, one option being considered is to use a pre-printed flexible pressure sensor (wrapping it directly onto the impression roller) to measure the contact force. Flexible pressure sensors for medical applications have already been developed and tested with impressive results [32, 60, 61, 62, 63], and so far only cost seems to be the prohibitive factor for implementation in our system.

7.03. Conclusion

This thesis has reviewed the prior art for R2R μ CP systems, outlined the design methodology for the assembly of an in-house flexure-controlled R2R system, described the fabrication techniques involved in creating the components and analyzed the faults of the prototype system through examination of the experimental results. This work has led to the development of an experimentally functioning lab setup that is ripe for further improvements in the performance. Completion and calibration of this augmented R2R system will, in future, enable UMass Amherst in-house production of large-area flexible electronics which may be used in a wide range of applications, including medical sensors, solar cells, displays, and

more. In addition to microcontact printing, this R2R system may integrate other compatible printing technologies such as nanoimprint lithography, screen-printing, and inkjet printing. Future work must focus more on regulating the stamp contact pressure as well as studying the effects of stamp microfeature deformation on the print process.

References

- [1] X. Zhou, H. Xu, J. Cheng, N. Zhao and S.-C. Chen, "Flexure-based Roll-to-roll Platform: A Practical Solution for Realizing Large-area Microcontact Printing," *Scientific Reports*, vol. 5, p. 10402, 2015.
- [2] M. R. Bageant, "Precision Control of Continuous Microcontact Printing," Doctoral Dissertation: Massachusetts Institute of Technology, Boston, USA, February 2018.
- [3] C. A. Harper, *Electronic materials and processes handbook*, McGraw-Hill, 2003, p. 7.3 and 7.4.
- [4] Falconer Electronics, ""History of Circuit Boards Through the 20th Century"," 2017.
- [5] T. E. French and C. J. Vierck, *A manual of engineering drawing for students and draftsmen: 9th Edition*, New York: McGraw-Hill Book Company, 1960.
- [6] A. S. Brown, "Flexible electronics could transform the way we make and use electronic devices," *Penn State News*, 08 April 2013.
- [7] Desi Aleksandrova, Marketing Communications Manager, "Five benefits of flexible electronics for displays and sensors," FlexEnable Ltd., 17 February 2020. [Online]. Available: <https://www.flexenable.com/blog/five-benefits-of-flexible-electronics-for-displays-and-sensors/>.
- [8] A. C. Arias, J. D. MacKenzie, I. McCulloch, J. Rivnay and A. Salleo, "Materials and Applications for Large Area Electronics: Solution-Based Approaches," *Chemical Reviews*, vol. 110, pp. 3-24, 2010.
- [9] G. E. Moore, "Cramming more components onto integrated circuits," *Electronics*, vol. 38, no. 8, 1965.
- [10] M. Pagliaro, R. Ciriminna and G. Palmisano, "Flexible Solar Cells," *ChemSusChem*, vol. 1, no. 11, 14 November 2008.
- [11] J. Szlufcik et al, "High-efficiency low-cost integral screen-printing multicrystalline silicon solar cells," *Solar Energy Materials & Solar Cells* , vol. 74, p. 155–163, 2002.
- [12] Dechan Angmo et al., "Roll-to-Roll Inkjet Printing and Photonic Sintering of Electrodes for ITO Free Polymer Solar Cell Modules and Facile Product Integration," *Advanced Energy Materials*, vol. 3, no. 2, pp. 172-175, 2012.
- [13] E. Brandon, W. West, L. Zhou, T. Jackson, G. Theriot, R. A. Devine, D. Binkley, N. Verma and R. Crawford, "Flexible electronics for space applications," *Materials Research Society (MRS)* , vol. 814, 2004.
- [14] A. Chaturvedi, "NASA-ISRO satellite to open a new chapter in Indo-US space partnership," *Geospatial World*, 2017.

- [15] N. Kooy, K. Mohamed, L. T. Pin and O. S. Guan, "A review of roll-to-roll nanoimprint lithography," *Nanoscale research letters*, p. 320, 2014.
- [16] Y. Zhou, "Direct Printing/Patterning of Key Components for Biosensor Devices," Doctoral Dissertation: Univ. of Massachusetts Amherst, MA, USA, 2019.
- [17] Robert Abbel et al., "Industrial-scale inkjet-printed electronics manufacturing—production up-scaling from concept tools to a roll-to-roll pilot line," *Transl. Mater. Res.*, no. 015002, 2014.
- [18] J. Donoghue, J. Herbert and P. Stack, "Remote Non-Intrusive Patient Monitoring.," Tyndall National Institute, Cork, Ireland, 2020.
- [19] S. Khan, S. Ali and A. Bermak, "Recent Developments in Printing Flexible and Wearable Sensing Electronics for Healthcare Applications," *Sensors (Basel)*, vol. 19, no. 5, p. 1230, 11 March 2019.
- [20] C. G. Núñez, W. T. Navaraj, E. O. Polat, and R. Dahiya, "Energy-Autonomous, Flexible, and Transparent Tactile Skin," *Adv. Funct. Mater.*, vol. 27, no. 1606287, 2017.
- [21] Z. Lou, L. Li, L. Wang, and G. Shen, "Recent Progress of Self-Powered Sensing Systems for Wearable Electronics," *Small*, vol. 13, no. 1701791, 2017.
- [22] F. –R. Fan, Z. –Q. Tian, and Z. L. Wang, "Flexible Triboelectric Generator!," *Nano Energy*, 2012.
- [23] Z. Lin et al., "Triboelectric Nanogenerator Enabled Body Sensor Network for Self-Powered Human Heart-Rate Monitoring," *ACS Nano*, no. no. 11, pp. 8830-8837, 2017.
- [24] Sílvia Manuela Ferreira Cruz, Luís A. Rocha and Júlio C. Viana, "Printing Technologies on Flexible Substrates for Printed Electronics," in *Flexible Electronics*, S. Rackauskas, Ed., IntechOpen, 2018, p. Chapter 3.
- [25] Sanchez-Romaguera et al., "Towards inkjet-printed low cost passive UHF RFID skin mounted tattoo paper tags based on silver nanoparticle inks," *Journal of Materials Chemistry*, p. 6395, 2013.
- [26] K. Y. Mitra, S. Kapadia, M. Hartwig, E. Sowade, Z. Xu, R. R. Baumann and R. Zichner, "Process Development of Large Area R2R Printing and Sintering of Conductive Patterns by Inkjet and Infra-Red Technologies Tailored for Printed Electronics," in *NIP & Digital Fabrication Conference, Printing for Fabrication*, 2018.
- [27] W.-Y. Chang, T.-H. Fang, H.-J. Lin, Y.-T. Shen and Y.-C. Lin, "A Large Area Flexible Array Sensors Using Screen Printing Technology," *J. Display Technol.*, vol. 5, no. 6, pp. 178-183, 2009.
- [28] D. Numakura, "Advanced Screen Printing Practical Approaches for Printable & Flexible Electronics," in *3rd International Microsystems, Packaging, Assembly & Circuits Technology Conference*, Taipei, 2008.

- [29] W. J. Hyun, E. B. Secor, M. C. Hersam, C. D. Frisbie and L. F. Francis, "High-Resolution Patterning of Graphene by Screen Printing with a Silicon Stencil for Highly Flexible Printed Electronics," *Advanced Materials*, vol. 27, pp. 109-115, 2015.
- [30] [Online]. Available: <https://www.murakami.co.jp/english/about/index.html>.
- [31] Xuan Cao et al., "Screen Printing as a Scalable and Low-Cost Approach for Rigid and Flexible Thin-Film Transistors Using Separated Carbon Nanotubes," *American Chemical Society*, vol. 8, no. 12, p. 12769–12776, 2014.
- [32] Su-Jeong Woo et al., "A Thin All-Elastomeric Capacitive Pressure Sensor Array based on Micro-Contact Printed Elastic Conductors," *Journal of Materials Chemistry*, vol. 2, pp. 4415-4422, 2014.
- [33] Mäkelä T, Haatainen T., & Ahopelto J., "Roll-to-roll printed gratings in cellulose acetate web using novel nanoimprinting device," *J. Microelectron Eng*, pp. 2045-2047, 2011.
- [34] S. Rigo, "Surfaces with Dual Functionality through Specific Coimmobilization of Self-Assembled Polymeric Nanostructures," *Langmuir*, vol. 35, no. 13, p. 4557–4565., October 2018.
- [35] J. E. Petrzela, "Contact region fidelity, sensitivity, and control in roll-based soft lithography," Doctoral Dissertation: Massachusetts Institute of Technology, Boston, USA, June 2012.
- [36] J. L. Wilbur, "Microcontact printing of self-assembled monolayers: applications in microfabrication," *Nanotechnology*, 1996.
- [37] Luminite Manufacturers, "Flexo Printing vs Gravure Printing: Pros and Cons," Luminite, 3 February 2020. [Online]. Available: <https://blog.luminite.com/blog/flexo-printing-vs-gravure-printing>.
- [38] Ethan B. Secor et al., "Gravure Printing of Graphene for Large-area Flexible Electronics," *Advanced Materials*, vol. 26, no. 26, pp. 4533-4538, 2014.
- [39] S. Kim, H. Sojoudi, H. Zhao, D. Mariappan, G. H. McKinley, K. Gleason and A. J. Hart, "Ultrathin high-resolution flexographic printing using nanoporous stamps," *Science Advances*, vol. 2, no. 12, 7 December 2016.
- [40] A. Vena, E. Perret and S. Tedjini, Chipless RFID based on RF Encoding Particle, ISTE Press - Elsevier, 2016.
- [41] A. Stagnaro, "Design and Development of a Roll-to-Roll Machine for Continuous High-Speed Microcontact Printing," MS Dissertation Defense: Massachusetts Institute of Technology, Boston, USA, August 2008.
- [42] P. Baldesi, "Design and Development of High Precision Five-Axis Positioning System for Roll-to-Roll Multi-Layer Microcontact Printing," MS Dissertation: Massachusetts Institute of Technology, Boston, USA, September 2009.

- [43] M. Hale, "Manufacturing Conductive Patterns on Polymeric Substrates: Development of A Microcontact Printing Process," Doctoral Dissertation: Massachusetts Institute of Technology, Boston, USA, June 2013.
- [44] S. T. Nill, "Integrated Hardware, Software, and Sensor Design for Control of a Scalable, Continuous Roll-to-Roll Microcontact Printing Process," MS Thesis Dissertation: Massachusetts Institute of Technology, Boston, USA, June 2014.
- [45] A. M. Libert, "Precision Control of Cylindrical Stamp Contact in a Continuous Roll-to-Roll Microcontact Printing Machine," MS Thesis Dissertation: Massachusetts Institute of Technology, Boston, USA, June 2014.
- [46] X. Zhou, D. Wang, J. Wang and S.-C. Chen, "Precision design and control of a flexure-based roll-to-roll printing system," *Precision Engineering*, vol. 45, p. 332–341, March 2016.
- [47] L. L. Howell, *Compliant mechanisms*, John Wiley & Sons, 2001.
- [48] X. Du, "Intelligent Sensing Lab," Univ. of Massachusetts Amherst, 31 August 2018. [Online]. Available: <https://blogs.umass.edu/xiandu/>.
- [49] G. Hao and X. He, "Designing a monolithic tip-tilt-piston flexure manipulator," *Elsevier, Archives of Civil and Mechanical Engineering (ACME)*, April 2017.
- [50] V. Bagad, *Mechatronics*, Technical Publications, 2009.
- [51] Guangbo Hao et al., "Design and analytical analysis of a large-range tri-symmetrical 2R1T compliant mechanism," *Microsystem Technologies*, April 2017.
- [52] D. L. Blanding, *Exact Constraint: Machine Design Using Kinematic Principles*, New York: ASME Press, 1999.
- [53] FlexSys Inc., "Joint-less Stapler".
- [54] M. Riza and G. Hao, "A Flexure Stage System for Light Beam Control," *Springer, Microsystem Technologies*, vol. 25, pp. 3185-3191, October 2018.
- [55] Dion and Ryan, "Independent Study Report: 3D Printing for Application," UMass Amherst MIE Dept., Amherst, MA, 2018.
- [56] Seiffert Industrial, "RollCheck MINI Laser Roll Alignment Tools," [Online]. Available: <https://www.seiffertindustrial.com/product/rollcheck-mini/>.
- [57] Markforged, "Onyx Filament".
- [58] V. Annadurai, J. An, J. Ahn and H. Kim, "System modeling and identification of a balance type checkweigher compensated by voice coil actuator," *Advances in Mechanical Engineering*, vol. 11, 2019.

- [59] G. Hao, "A 2-legged XY parallel flexure motion stage with minimised parasitic rotation," *Journal of Mechanical Engineering Science*, vol. 228, no. 17, pp. 3156-3169, 2014.
- [60] C. Hou, T. Huang, H. Wang, H. Yu, Q. Zhang, and Y. Li, "A Strong and Stretchable Self-Healing Film with Self-Activated Pressure Sensitivity for Potential Artificial Skin Applications," vol. 3, no. 3138, 2013.
- [61] T. Someya, T. Sekitani, S. Iba, Y. Kato, H. Kawaguchi, and T. Sakurai, "A Large-Area, Flexible Pressure Sensor Matrix with Organic Field-Effect Transistors for Artificial Skin Applications," *Proc. Natl. Acad. Sci. USA*, vol. 101, no. 27, pp. 9966-9970, 2004.
- [62] B. C.-K. Tee, C. Wang, R. Allen, and Z. Bao, "An Electrically and Mechanically Self-Healing Composite with pressure- and Flexion-Sensitive Properties for Electron Skin Applications," *Nature Nanotechnology*, vol. 7, pp. 825-832, 2012.
- [63] G. Schwartz, B. C.-K. Tee, J. Mei, A. L. Appleton, D. H. Kim, H. Wang, and Z. Bao, "Flexible Polymer Transistors with High Electric Pressure Sensitivity for Application in Electronic Skin and Health Monitoring," *Nature Communications*, vol. 4, no. 1859.